Final scientific /technical report:

Optical fiber chemical sensor with sol-gel derived refractive material as transducer for high temperature gas sensing in clean coal technology

(Project ID number: DE-FC26-04NT42230)

Report period covered: October 1, 2004—December 31, 2006
Date of report: February 1, 2007

Dr. Shiquan Tao

Institute for Clean Energy Technology
Mississippi State University
205 Research Blvd., Starkville, MS 39759
Tel: 662-325-7631; Fax: 662-325-8465
e -mail: tao@icet.msstate.edu

Disclaimer

Abstract:

The chemistry of sol-gel derived silica and refractive metal oxide has been systematically studied. Sol-gel processes have been developed for preparing porous silica and semiconductor metal oxide matrerials. Micelle/reversed micelle techniques have been developed for preparing nanometer sized semiconductor metal oxides and noble metal particles. Techniques for doping metal ions, metal oxides and nanosized metal particles into porous sol-gel material have also been developed.

Optical properties of sol-gel derived materials in ambient and high temperature gases have been studied by using fiber optic spectroscopic techniques, such as fiber optic ultraviolet/visible absorption spectrometry, fiber optic near infrared absorption spectrometry and fiber optic fluorescence spectrometry. Fiber optic spectrometric techniques have been developed for investigating the optical properties of these sol-gel derived materials prepared as porous optical fibers or as coatings on the surface of silica optical fibers. Optical and electron microscopic techniques have been used to observe the microstructure, such as pore size, pore shape, sensing agent distribution, of sol-gel derived material, as well as the size and morphology of nanometer metal particle doped in sol-gel derived porous silica, the nature of coating of sol-gel derived materials on silica optical fiber surface. In addition, the chemical reactions of metal ion, nanostructured semiconductor metal oxides and nanometer sized metal particles with gas components at room temperature and high temperatures have also been investigated with fiber optic spectrometric methods.

Three classes of fiber optic sensors have been developed based on the thorough investigation of sol-gel chemistry and sol-gel derived materials. The first group of fiber optic sensors uses porous silica optical fibers doped with metal ions or metal oxide as transducers for sensing trace NH_3 and H_2S in high temperature gas samples. The second group of fiber optic sensors uses sol-gel derived porous silica materials doped with nanometer particles of noble metals in the form of fiber or coating for sensing trace H_2, NH_3 and HCl in gas samples at for applications ambient temperature. The third classes of fiber optic sensors use sol-gel derived semiconductor metal oxide coating on the surface of silica optical fiber as transducers for selectively sensing H_2, CH_4 and CO at high temperature. In addition, optical fiber temperature sensors use the fluorescence signal of rare-earth metal ions doped porous silica optical fiber or the optical absorption signal of thermochromic metal oxide materials coated on the surface of silica optical fibers have also been developed for monitoring gas temperature of corrosive gas.

Based on the results obtained from this project, the principle of fiber optic sensor techniques for monitoring matrix gas components as well as trace components of coal gasification derived syngas has been established. Prototype sensors for sensing trace ammonia and hydrogen sulfide in gasification derived syngas have been built up in our laboratory and have been tested using gas samples with matrix gas composition similar to that of gasification derived fuel gas. Test results illustrated the feasibility of these sensors for applications in IGCC processes.

Content

1. Executive summary

In this project, sol-gel techniques have been developed for preparing porous silica and semiconductor metal oxide materials. In addition, nanometer particles of noble metals have been prepared with micelle/reversed micelle techniques. Nanocrystalline semiconductor metal oxide materials have also been prepared with sol-gel techniques. Metal ions, metal oxides and nanocrystalline semiconductor metal oxides have been immobilized into porous silica materials via doping a silica sol solution with metal salt solution or co-hydrolyzing a metal alkyloxide to obtain a mixed sol solution. Nanometer metal particles have been immobilized into porous silica through the combination of a sol-gel technique with micelle/reversed micelle techniques. A patented technique has been employed for fabrication of porous silica fibers for designing fiber optic sensors.

The prepared materials have been investigated with electron microscopes. SEM has been employed to observe the microstructure and morphology of sol-gel derived porous silica materials, semiconductor metal oxides, the coating of sol-gel derived porous materials on the surface of optical fibers, and sol-gel derived porous silica optical fibers. TEM has been employed to observe the microstructure and morphology of nanometer metal particles and measure the distribution of particle size.

The optical properties of the prepared porous materials have been investigated with fiber optic spectrometric methods. Active core fiber optic spectrometry has been employed to investigate the optical properties of sol-gel derived porous silica optical fibers. Fiber optic EW spectrometry has been employed to investigate the optical properties of the porous materials as coatings on the surface of silica optical fibers. The optical absorption and fluorescence emission properties of these materials in the wavelength region from 200 nm to 2.1 μm have been investigated. These materials have been exposed to gas samples of different compositions at different temperatures, and the response of these materials to different gas composition at high temperature has been investigated.

Fiber optic sensor techniques have been developed based on the comprehension of the microstructure and optical properties of these materials exposed to gas samples of varied composition at different temperatures. Fiber optic temperature sensor techniques using sol-gel derived refractive thermochromic materials can be used for monitoring temperature up to 1000 ^{o}C. Fiber optic gas sensors developed in this project include an ammonia sensor using silver nanometer particle immobilized porous silica material for monitoring trace ammonia at ambient temperature down to 61 ppb, a CuCl2 doped porous silica fiber sensor for monitoring trace ammonia at high temperature down to 0.3 ppm, a CdO doped porous silica fiber sensor for monitoring trace hydrogen sulfide at high temperature down to sub-ppm level, and a SnO2 coating based fiber optic sensor for selectively monitoring hydrogen gas at high temperature down to ppm level. All these sensors are reversible, can be used for continuous monitoring industrial processes. The sensors for high temperature gas and temperature sensing are corrosion resistant, applicable in corrosive gas environment encountered in IGCC processes.

Based on the foundation knowledge built up in this project, sensor technologies for monitoring other gas components exist in coal-derived syngas can be developed. In addition, the fiber optic spectrometric techniques developed in this project are also useful in investigating the catalyzed high temperature chemical reactions used syngas reforming and cleaning.

Experimental

1.1. Material preparation

1.1.1. Preparing porous silica materials using sol-gel processes

The preparation of a porous silica material involves the hydrolysis of an ester of a silicic acid to generate a silica sol solution, gelatinization of the silica sol solution in a special container to form a silica gel, drying the silica gel to form a porous silica material. Depending on the application purpose, treatment procedures could be applied to the prepared materials in order to improve the optical properties and change the microstructure of the materials.

The procedural details used for preparing a pure porous silica material with hydrochloric acid as a catalyst are as follows. First, 2 mL tetraethylorthosilicate (TEOS), 1 mL de-ionized water, and 40 μL 0.1M HCl were mixed and stirred in a baker until homogenized. The resulting solution was stored in the small baker, which was covered with a parafilm. The silica sol solution was gelatinized inside the baker and the formed gel was air dried inside the baker. The gelatinization and drying processes usually takes tow weeks.

1.1.2. Preparing metal ions doped porous silica materials with the developed sol-gel techniques

In praparing a metal ion doped porous silica material, an aqueous solution of the metal chloride was mixed with a silica sol solution prepared according to the precedure descirbed above using TEOS as a precursor. The mixed solution was sealed inside a baker for gelatinization and drying. Porous silica materials doped with Cd^{2+}, Co^{2+}, Cu^{2+}, Eu^{3+}, Fe^{3+}, Ni^{2+}, Pd^{2+}, Zn^{2+} have been prepared with this method.

2.1.3. Preparing metal oxide doped porous silica matrials by adding an ammonium salt of metaloxo meta acid to a silica sol solution

Vanadium oxide, molybdenum oxide and tungsten oxide doped porous silica materials were parepared as examples of metal oxide doped porous silica materials. In preparing a vanadium oxide doped porous silica material, a solution of ammonium vanadate was mixed with a TEOS silica sol solution. The obtained solution was stored in a baker for gelatinization and drying.

Similar procedure has been used for preparing a molybdenum oxide doped porous silica material and a tungsten oxide doped porosu material.

2.1.4. Preparing semiconductor metal oxide doped porous silica materials by co-hydrolyzing a metal alkyloxide with TEOS.

A semiconductor metal oxide can also been immobilized into a porous silica material through co-hydrolyzing an alkyloxide of the metal with TEOS or TMOS. Through this method, porous silica composite materials (TiO2-SiO2, ZrO_2-SiO_2, V_2O_5-SiO_2, Mo_2O_5-SiO_2, and WO_3-SiO_2) have been prepared.

The procedural details used for preparing a TiO_2-SiO_2 material are as follows: 2 drops 2M HNO_3 was dropped in 8ml ethanol. Then 1ml tetraethyl orthosilicate (TEOS) was added. During stirring, titanium isopropoxide was added according to titanium isopropoxide (TIP) to TEOS molar ratio 1:2. After the solution was stabled for 10min, 0.5 ml H_2O was added drop by drop while stirring. The obtained sol solution was sealed in a baker for gelatinization and drying.

Similar procedure has been used for preparing ZrO_2-SiO_2, VO_2-SiO_2, Mo_2O_5 and WO_3-SiO_2 composite materials. The metal alkyloxide used for preparing these materials are zirconium(VI) isopropoxide ($Zr(i\text{-}OC_3H_7)_4$, vanadium(III) triisopropoxide oxide ($VO(i\text{-}OC_3H_7)_3$, molebdenium(V) isopropoxide ($Mo(i\text{-}OC_3H_7)_5$, and tungsten(V) isopropoxide ($W(i\text{-}OC_3H_7)_5$).

2.1.5. Preparing noble metal nanoparticles with micelle/reversed micelle techniques and immobilizing noble metal nanoparticles into porous silica materials via sol-gel techniques

Nanometer particles of a noble metal can be prepared through reducing a metal complex with a ligant dissolved in an organic solvent, which is distributed in water as micelles by using a surfactant. The nanoparticles of noble metals can also be prepared through reducing metal ions in an aqueous solution, which is distributed in an organic solvent as reversed micelles. If the micelle technique is used, the metal complex was first dissolved in an organic solvent. The obtained solution is then distributed into water by using a surfactant. A reducing agent in an aqueous solution is then added into the micelle solution. Part of the reducing agent molecules participated into the micelles to reduce the metal complex in the micelles to form metal atoms. The formed atoms in individual micelles aggregate to form metal particles with size in nanometer range. If the reversed micelle technique is used, a metal salt is first dissolved in an aqueous solution. The obtained solution is then distributed into an organic solvent by using a surfactant. A reducing agent in an aqueous solution is then added into the reversed micelle solution and distributed into the reversed micelles. Metal ions in the reversed micelles are reduced to metal atoms in the micro water pools. The formed atoms aggregate to form metal particles with size in nanometer range.

If a micelle solution is used, the solution of nanometer metal particles in micelles is then mixed with a silica sol solution obtained from the hydrolysis of TEOS. With the gelatinization of the silica sol solution, the metal particles are immobilized inside the porous silica to form a hybrid material. The organic solvent used for forming the micelle solution was evaporized during the drying process. With this method, porous silica materials doped with nanometer particles of Au, Ag, Pd, and Pt have been prepared. The procedural details for preparing a Pd nanoparticles doped porous silica material by using Pd-2, 4-pentadionate in 2, 4-pentadionate solution as a Pd nanoparticle precurser are as follow: First, 12 µl Pd-2,4-pentadionate in 2, 4-pentadionate solution (2×10^{-3} M) was mixed with 2 ml Trion X-100 aqueous solution at its critical micelle concentration (CMC, 0.3 mM) at room temperature with rapid stirring. One drop of 9 M hydrazine hydrate ($N_2H_4\cdot xH_2O$) was added to the mixture as a reducing agent. 4 ml of TEOS was added to the above mixtures after nanosized palladium formed with stirring. The pH values of the mixtures were adjusted to around 2 by adding 2 M HNO_3. The pH-adjusted mixture was then stired until a clear solution was obtained. The obtained solution was kept in a baker and allowed to gelatinization for one week.

In order to immobilize nanometer metal particles prepared in a reversed micelle solution, an aliquot of a sol-gel silica precursor (TMOS or TEOS) solution is added into the reversed micelle solution. The precursor molecules participated into the water pools in the reversed micelles and hydrolyzed in the water pools. After the silica sol solution gelatinized, the metal particles are immobilized in the formed porous silica material. The technique has been used to preparing Ag, Au and Pd doped porous silica materials by

using $AgNO_3$, $HAuCl_4$ and $PdCl_2$ as the precursors of metal particles. TEOS, TMOS are used as the precursor of porous silica. The procedural details for preparing a silver nanoparticles immobilized porous silica material using the reversed micelle technique are as follows: 2×10^{-5} M silver nitrate solution (PH=1.5), water, Igepal CO-520 and 5ml cyclohexane were used to get a total 10ml solution with w_0=8 (for Igepal CO-520). The mixtures were stirred until a stable and clear solution was got. One drop of 9M $N_2H_4 \cdot xH_2O$ was added to the solution. After stirring for 30 min, TEOS was added to the solution according to the ratio V_{H2O}/V_{TEOS}=2 and vigorously stirred for 24 hours to get the final products. 2M HNO_3 was added until the pH value arrive 2.

Instead of using surfactant, a mercapto-siliane can be used as a stabilizer for preparing nanometer particles of noble metals. In this method, a metal is first mixed with the mercapto-silane compound compounds in an organic solution. A reducing agent is added to the mixture solution. Metal particles formed from the reduction of the metal compound were surrounded by the mercapto-silane molecules and stabilized in the solution. The mercapto-silane is then hydrolyzed together with another precursor of silica to form a silica sol solution and the metal particles are immobilized inside the silica gel after the gelatinization of the formed sol solution. The procedural details for preparing a silver nanoparticles using 3-mercaptopropyltrimethoxysilane (MPTS) as a stabilizer are as follow: 5 ml 1×10^{-3} M $AgNO_3$ methanolic solution was mixed with 0.092 ml MPTS. The mixture was vigorously stirred. Then, 5ml 4×10^{-3} M $NaBH_4$ methanolic solution was added to the above solution in an ice-bath drop-by-drop. In order to immobilize the formed silver nanoparticles into a porous silica composite, 2.5 ml DI water and 5 ml Tetramethoxysilane (TMOS) were added to the silver nanoparticle solution obtained above, one drop 2M HNO_3 was added to the mixed solution for catalyzing the hydrolysis of TMOS. A yellowish solution was obtained after stirring the mixed solution for 2 Hours. The prepared sample is referred as Ag-SH-SiO_2 later. This method has also been used for preparing Au-SH-SiO_2, Pd-SH-SiO_2 and Pt-SH-SiO_2.

2.1.6. Preparing semiconductor metal oxide vial sol-gel techniques and coating the semiconductor metal oxide on the surface of silica optical fiber

Semiconductor metal oxides, such as SnO_2, TiO_2, ZrO_2, have been prepared through hydrolyzing an alkyloxide of the metal ion, and gelatinization of the obtained metal oxide sol solution. This procedure was used for preparing metal oxide sol solution for coating the metal oxide on the surface of a silica optical fiber.

2.2. Fabrication of porous silica optical fibers with a sol-gel derived material as composite by using a patented sol-gel technique

The sol-gel fiber fabrication technique developed in our previous work [1,2] has been employed for preparing porous silica optical fibers with the sol-gel derived silica materials (pure or doped) as composites. The procedural details for preparing a cupper ions doped porous silica optical fiber using a sol-gel derived silica sol solution doped with CuCl2 are as follows: First, The $CuCl_2$-doped silica sol solution was filled into varying lengths of 1.0 mm ID/0.22 mm OD Tygon tubing (Cole-Parmer, Vernon Hills, IL). Once filled, both ends of the tubing were sealed with parafilm and the tubing was fixed in a vertical position for 24 h. Next, the parafilm in one end was removed and the tubing placed in a horizontal position until a transparent gel was formed inside the tube.

Then, water was injected through the Tygon tube to push the gel fiber out of the tube. The fiber gel was air-dried.

Similar procedure was used in preparing porous silica optical fibers doped with other metal ions, metal oxide and naometer metal particles.

2.3. Heat-treatment of the sol-gel derived materials

The sol-gel derived materials were heat-treated by using the split tube furnace with the programmable controller. During the treatment a dried sol-gel derived material (monolith, fiber or coating on the surface of a silica optical fiber) was placed inside the gas flow cell. The gas flow cell with the materials was then inserted into the tube furnace. The furnace was heated with the programmable controller from 25 °C to 600 °C over an 18 h period (100 °C increase every 3 h) and then held at 600 °C for 4 h. Upon completion of the heat treatment, the fibers were removed from the furnace and cooled to room temperature. Air gas or a specific gas was flown through the quartz cell during the heat treatment process.

2.4. Investigating the microstructure of sol-gel derived materials by using electron microscopes

Sol-gel derived materials prepared in this work have been investigated with a scanning electron microscope (SEM, Leo Stereoscan 360 scanning electron microscope, Leo Electron Microscopy, Thornwood, N. Y.) and a transmission electron microscope (TEM, JEOL JEM-100CX II operated at 80 KV). The SEM has been used to observe the morphology of sol-gel derived porous silica material, sol-gel derived hybrid materials, porous silica optical fibers, the coating of sol-gel derived silica material and semiconductor metal oxide materials. Some of the sol-gel derived material samples have been coated with gold by using a sputter coater before SEM observation in order to increase the electron conductivity. For the TEM studies, the samples were prepared by dropping the freshly made sol solution onto a FormVAR film coated copper grid and dried in air. The TEM has been employed to observe the morphology and shape of noble metal nanoparticles, measure particles size.

2.5. Investigating the optical properties of sol-gel derived materials by using fiber optic spectrometric methods

Three fiber optic spectrometric methods have been used to investigate the optical properties of the prepared materials. These are active core fiber optic absorption spectrometry (ACF-OAS) [1-5], optical fiber evanescent wave absorption spectrometry (OF-EWAS) [5-7] and active core fiber optic fluorescence spectrometry (ACF-OFS) [5]. The principle and instrument structure of these methods are briefly described below.

2.5.1. Active core fiber optic absorption spectrometry [1-5]

The ACF-OAS is similar to traditional optical absorption spectrometry. However, a specially prepared optical fiber is used as a sample cell in this technique. A diagrammatic graph of the concept of ACF-OAS is shown in Fig. 2.1. In this method, a piece of specially prepared optical fiber is connected with two conventional optical fibers with glue or a specially designed connector. A light beam from a light source is focused into the free end of one of the conventional silica optical fiber, then guided through the specially prepared optical fiber, fed into the second conventional silica optical fiber. The light emerged from the free end of the second conventional optical fiber is detected with an optical fiber compatible optical spectrometer. With this method, the optical absorption

signal of the specially prepared optical fiber is observed. The optical absorption signal of this method can be described by using the Lambert-Beer law described by follow equation:

$$A = \text{Log}\,(1/T) = \varepsilon CL \qquad (2.1)$$

In this equation, A is the absorbance; T is the transmittance; ε is the absorption coefficient of the analyte compound inside the fiber; C is the concentration of the analyte inside the fiber; L is the length of the interaction, which is decided by following equation:

$$L = l/(1-\sin^2\theta_0)^{1/2} \qquad (2.2)$$

where l is the length of the optical fiber transducer, and θ_0 is the incident angle of light beam to the active core optical fiber.

In this work, the specially prepared optical fiber is a porous silica optical fiber prepared with the sol-gel techniques described above.

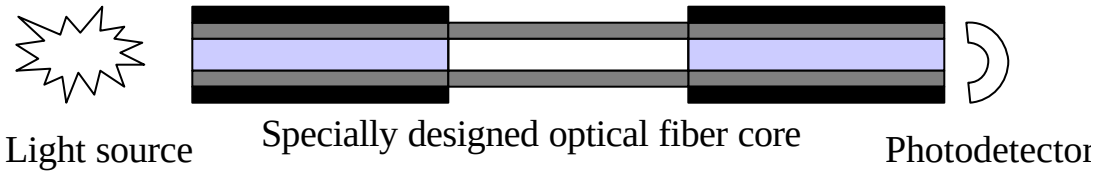

Fig. 2.1. A diagrammatic structure of an active core fiber optic chemical sensor. In this sensor, the interaction of light guided inside an optical fiber core (the red colored part) with a chemical species inside the fiber core is detected as a sensing signal.

2.5.2. Fiber optic evanescent wave absorption spectrometry

The OF-EWAS is different from traditional optical absorption spectrometry. In this method, a conventional optical fiber, which has a coating on the surface of the optical fiber core, is used. The optical fiber core is used for sensing light from a light source to a sample, which is the cladding coated on the surface of the fiber core. This specially coated fiber is connected with a light source and an optical fiber compatible optical spectrometer. The optical absorption signal of the material coated on the surface of the optical fiber core is observed. A diagrammatic graph of OF-EWAS concept is shown in Fig. 2.2. The optical absorption signal of OF-EWAS can be described by using the Lambert-Beer law described by follow equation [4,5]:

$$A_{EW} = \text{Log}(1/T) = \gamma\varepsilon C(d_p / n_2\sin\theta/a(n_1^2-n_2^2\sin^2\theta)^{1/2}) \qquad (2.3)$$

In this equation, γ is the ratio of optical power flowing in the cladding over total light power guided through the optical fiber. ε is the absorption coefficient of the analyte compound in the coating, and $d_p / n_2\sin\theta/a(n_1^2-n_2^2\sin^2\theta)^{1/2}$ is the absorption path length, which is equal to the penetration depth (d_p) times the number of total internal reflections.

The number of total internal reflections is calculated as $l\ n_2\sin\theta/a(n_1^2-n_2^2\sin^2\theta)^{1/2}$, as light travels a length of l inside the optical fiber.

In this work, the materials coated on the surface of conventional silica optical fibers are the sol-gel derived silica materials and semiconductor metal oxide materials prepared with the sol-gel techniques described above.

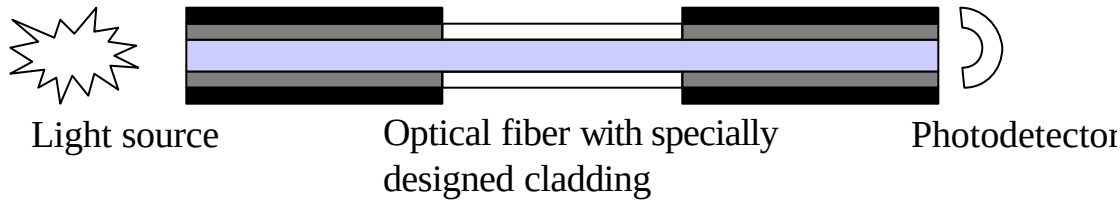

Fig. 2.2. A diagrammatic structure of a fiber optic EW absorption chemical sensor. In this sensor, the interaction of light distributed into the cladding (the red colored part) of the fiber with a chemical species exist inside the cladding layer is detected as a sensing signal.

2.5.3 Active core fiber optic fluorescence spectrometry

The ACF-OFS technique used in this work is different from traditional optical fluorescence spectrometry. A diagrammatic graph of the ACF-OFS concept is shown in Fig. 2.3. In this method, a piece of specially prepared optical fiber is connected with two conventional optical fibers with glue or a specially designed connector. The excitation light from a light source is focused into the free end of one conventional silica optical fiber, then guided through the specially prepared optical fiber. Part of the excitation light is absorbed by the fluorophores inside the specially prepared fiber. The resulted fluorescence light and the un-absorbed light is fed into the second conventional silica optical fiber and detected with an optical fiber compatible optical spectrometer. The fluorescence signal of this active core fiber fluorescence technique can be expresses by follow equation:

$$F = K\phi I_0 \varepsilon C L \qquad (2.4)$$

In this equation, K is a constant; ϕ is the quantum efficiency of the fluorescent analyte compound inside the fiber; I_0 is the incident light intensity. ε is the absorption coefficient of the analyte compound inside the fiber; C is the concentration of the analyte inside the fiber; L is the length of the active core optical fiber.

In this work, the specially prepared optical fiber is a porous silica optical fiber prepared with the sol-gel techniques described above.

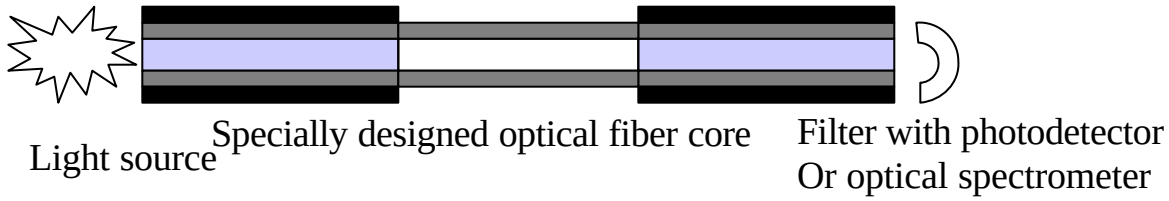

Fig. 2.3. A diagrammatic structure of fiber optic sensor using active core fiber fluorescence spectrometry. In this sensor, a fluorophore inside an optical fiber core (the red colored part) is excited by light guided inside the fiber core. This fluorescence signal is used as a sensing signal.

2.6. Observation of optical properties of sol-gel derived materials at high temperature with fiber optic spectrometric methods

In order to investigate the optical properties of the sol-gel derived materials at high temperatures using the fiber optic spectrometric methods described above, a special testing system has been designed and built up for this project. The diagrammatic structure of this testing system is shown in Fig. 2.4. This system consists of a temperature control sub-system (a split tube furnace with a programmable controller, special gas flow cell), and an optical fiber spectrometric sub-system (optical fibers with a specially designed connector and fiber holder for deploying a porous silica optical fiber into the gas flow cell). A picture of this testing system is shown in Fig. 2.5.

For testing a sol-gel derived porous silica optical fiber by using active core fiber optic spectrometry, the sol-gel derived material to be tested was deployed into the gas flow cell with a specially designed connector and a specially designed holder as shown in Fig. 2.6. Because the materials will be tested at high temperatures, the fibers used to connect a porous fiber with the light source and spectrometer are gold jacketed optical fibers (AFS400/440G, core/cladding/jacket diameter: 400/440/510 μm) from Fiberguide Industries, Inc. (Stirling, NJ). This optical fiber has silica as a fiber core, porous silica as a cladding and a thin layer of gold on the top of the cladding as a jacket for mechanical protection. This fiber can work at temperature up to 800 ^{o}C.

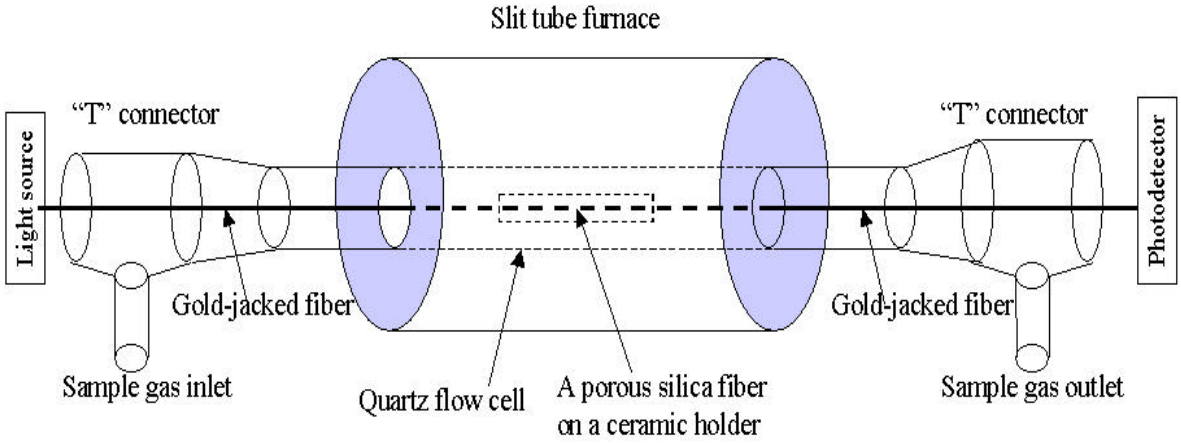

Fig. 2.4 A diagrammatic structure of a gas testing system for investigating the reactions of coal gas components with sol-gel derived silica optical fibers in a high temperature environment using finer optic spectroscopic techniques.

Fig. 2.5. A picture of the testing system for investigating the optical properties of sol-gel derived silica optical fibers. The testing system consists of three sub-systems: a programmable split furnace with a temperature controller (A&B); a dynamic gas calibrator for mixing up to three gas components to make a gas sample and a gas flow cell housed inside the split furnace (C&D); a spectroscopic system for observing the optical transmission, absorption or fluorescence emission of the sol-gel silica fibers (E,F,G,H & I). A multi gas sensor (J) with the function of alarm was also used for monitoring possible toxic gas (CO, H_2S) leakage and air quality during the tests.

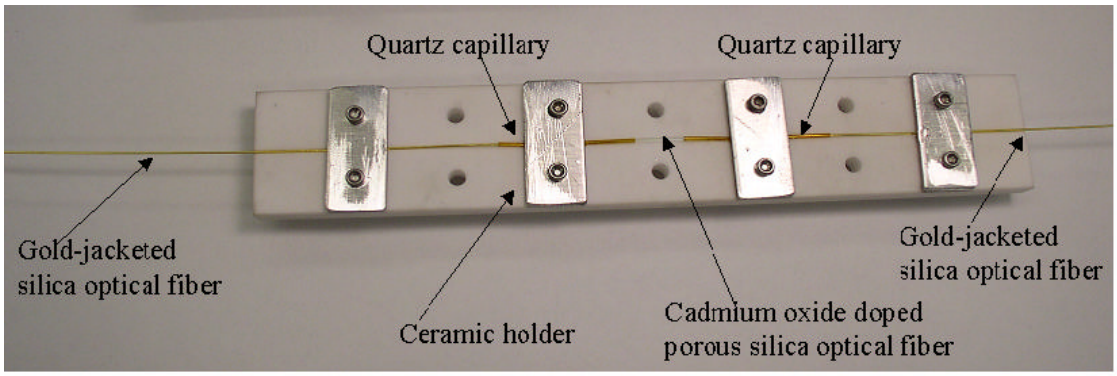

Fig. 2.6. A picture of a ceramic holder for assembling a porous sol-gel optical fiber with two gold-jacketed silica optical fibers in order to investigate the optical properties of the porous silica optical fiber by using active core fiber optic spectrometric methods.

A sol-gel derived porous silica optical fiber and the gold-jacketed silica optical fibers can be assembled with follow procedure. First, two gold jacketed silica optical fibers were prepared by etching the gold jacket from the fiber ends via aqua-regia (3:1 HCl:HNO_3). Next, one side of each gold jacked fiber was inserted into a 1 cm piece of 700 μm ID/850 μm OD fused silica capillary (Polymicro Technologies, Phoenix, AZ). The short porous silica fiber was then placed inside both pieces of fused capillary, forming a continuous fiber path. The resulting fiber assembly was placed in the groove of the ceramic optical fiber holder and stabilized using the holding plates and screws (Fig. 2.6). This setup allows light to travel from a light source through the porous silica optical fiber and to a detecting element without the use of any glue, which could break down under the high temperatures during the test. The ceramic holder/fiber assembly was placed inside the specially designed quartz flow cell, which served as the testing chamber. Next, the device was positioned inside the tubular furnace and appropriate gas lines were connected to the quartz flow cell. The free ends of the two gold-jacketed silica fibers were then connected to a light source and an optical fiber compatible spectrometer with SMA connectors, respectively.

If the material to be tested is in the form of coating on the surface of an optical fiber, the material was coated on the surface of the optical fiber core of the gold-jacketed optical fiber with the coating procedure described above. The sol-gel derived material as coating on the surface of an optical fiber was deployed into the gas flow cell by fixing the fiber with a rubber stopper as showing in Fig. 2.7.

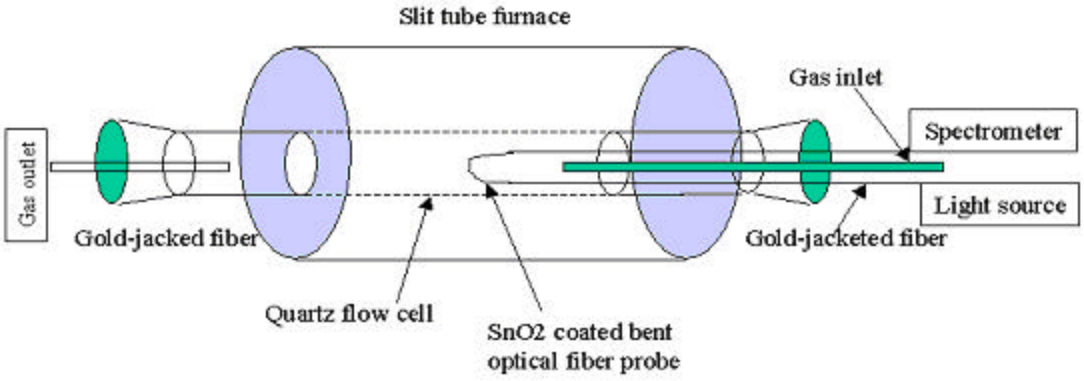

Fig. 2.7. A diagram of the laboratory set up for investigating the optical properties of a sol-gel derived material coated on the surface of an optical fiber core. During a test the coating is exposed to different gas samples inside the gas flow cell. If the material will be tested for high temperature application, a gold jacketed silica optical fiber was used for preparing the probe.

The structure of the fiber optic spectrometric sub-system for active core fiber optic spectrometry is shown in Fig. 2.8. This sub-system consists from an optical fiber compatible light source, a porous silica optical fiber connected with two gold-jacketed silica optical fibers, and an optical fiber compatible spectrometer. In this project, a deuterium/tungsten combo light source (Model DT-1000CE, Analytical Instrument Systems, Inc., Flemington, NJ), a NIR light source and light emitting diodes (LED) were used for providing light in the wavelength region from 200 nm to 2.1 μm. An optical fiber compatible UV/Vis spectrometer (Model SD 2000, Ocean Optics, Inc., Dunedin, FL) and an optical fiber compatible NIR spectrometer (NIR-512, OceanOptics, Inc.) were used for recording optical absorption spectrum and optical fluorescence spectrum.

During a test, the split tube furnace inserted with the quartz flow cell housed the assembled fiber unit or the coated bent optical fiber probe was placed inside a ventilation hood, which pull the exhaust gas from the experiment to outside air. The split tube furnace was initially heated to certain temperature at a programmed rump rate with compressed air flowing through the flow cell. The gas sample flow through the quartz cell was then switched to pure N_2. After the observed light intensity signal was stabilized, an analyte gas component was introduced into the gas sample by using the gas diluting system described below, and the optical signal (UV/Vis absorption, NIR absorption or fluorescence) of the porous silica fiber or the coated bent optical fiber probe was recorded with the optical fiber compatible spectrometer.

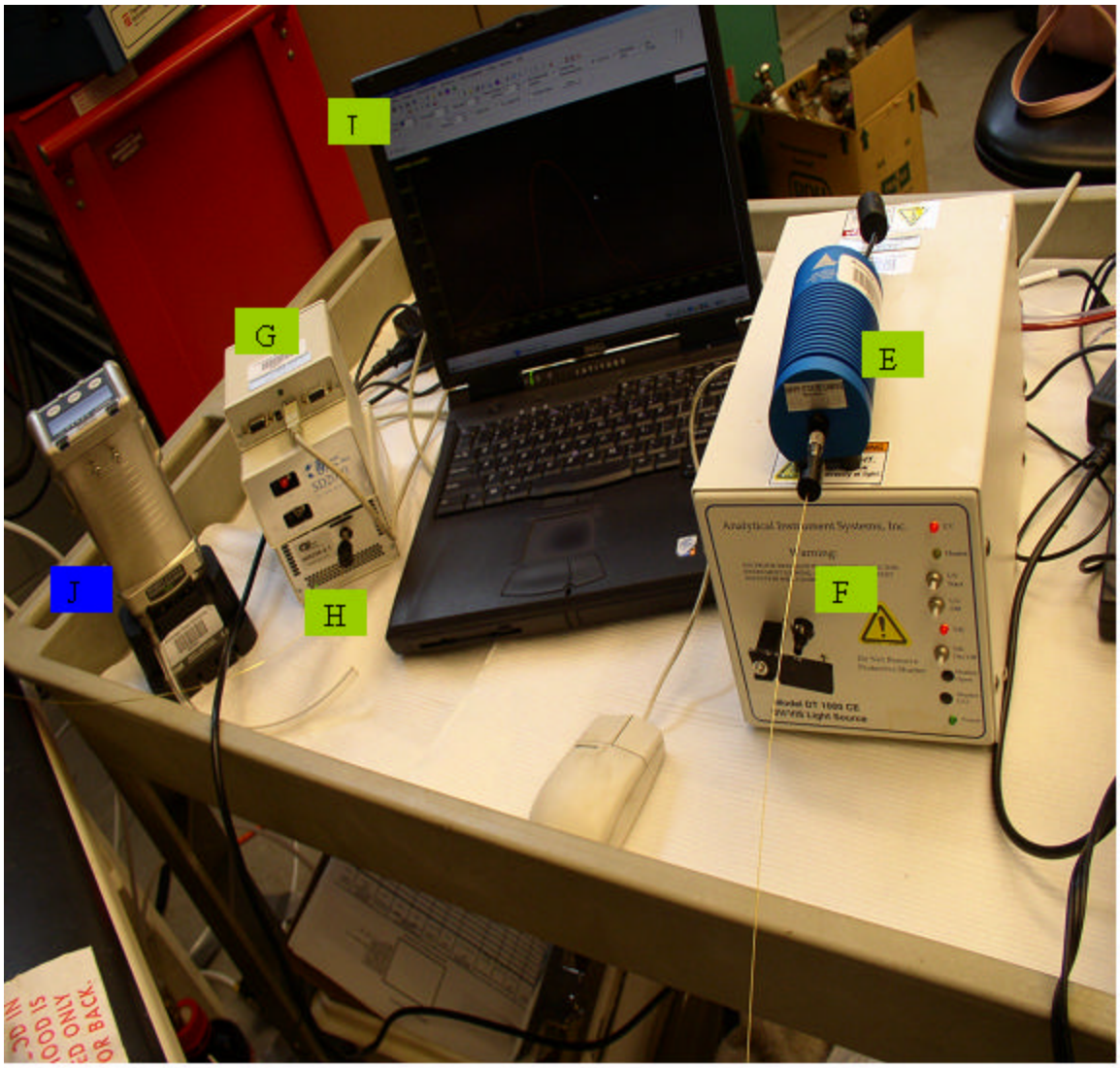

Fig. 2.8. A picture the spectroscopic system used in the investigation of the optical properties of the sol-gel silica fibers. This system includes a visible/NIR light source (E), a UV/is light source (F), a dual channel UV/Vis spectrometer (G), a NIR spectrometer (H), and a computer for data acquisition (I). All the light sources and the spectrometers are fiber compatible.

2.7. Preparing gas samples for testing the sol-gel derived materials

Gas samples (0.1%v H_2S-N_2, 1%v NH_3-N_2, 10%v H_2-N_2, 5%v CH_4-N_2, 10%v CO-N_2) obtained from AirGas Inc. (Marietta, GA) were used in this project for testing the response of the sol-gel derived materials. A gas sample of desired gas composition was prepared by mixing gas sample of high analyte concentration with another gas sample with a dynamic gas calibrator (Model 146, Thermo Environmental Instruments, Inc. Franklin, MA).

2.8. The features of the high temperature testing system guilt up for this project

The features of the system built up for this project for testing the optical properties of sol-gel derived materials at high temperatures are as follow:

- Gas sample temperature range: ambient to 900 ^{o}C;
- Gas flow rate: 0.01 L/min to 10 L/min;
- Gas composition: ppmv to tens percent;
- Wavelength range of optical properties observed: 200 nm to 2.1 mm;
- Optical properties being tested: UV/Vis absorption, NIR absorption and fluorescence emission.
- The form of the material to be studied: porous fiber, coating on the surface of silica optical fiber.

3. Results and Discussion

3.1. Development of sol-gel processes for making sol-gel derived material suitable for designing optical fiber chemical sensor

A sol-gel process is a low temperature wet chemical process for the synthesis of inorganic or composite organic/inorganic networks based on the hydrolysis of a molecular precursor and subsequent polycondensation. This is a versatile solution process for making ceramics, glasses, thermal isolating materials, catalysts for high temperature gas reaction, sorbents for gas storage, separation and water purification, bioactive materials for catalyzing biochemical reaction and separation, semiconductor materials for gas sensing, coating material for fiber optical sensing, etc.[8-10]. The chemistry of sol-gel processes includes the hydrolysis of a precursor, condensation of the hydrolysis product to form a sol solution, gelatinizing the sol solution to form a gel, drying the formed gel and heat treatment of the dried sol-gel material.

The precursor of sol-gel materials is usually a silicon alkoxide or a metal alkoxide. In some reports, silicate salts[4] and metal coordinating complexes[5] have also been used as the precursors. The hydrolysis and condensation of a silicon alkoxide to form a silica colloid sol solution can be expressed as follows:

$$(RO)_3Si\text{-}OR + H_2O == (RO)_3Si\text{-}OH \quad (3.1.1)$$

$$(RO)_3Si\text{-}OH + (RO)_3Si\text{-}OR == (RO)_3Si\text{-}O\text{-}Si(OR)_3 + ROH \quad (3.1.2)$$

$$(RO)_3Si\text{-}OH + (RO)_3Si\text{-}OH == (RO)_3Si\text{-}O\text{-}Si(OR)_3 + H_2O \quad (3.1.3)$$

Equation (3.1.1) shows the hydrolysis of an alkoxide group (OR) which is replaced by a silanol group (-OH) after the reaction. The hydrolysis reaction can continue until eventually all of the OR groups are replaced by silanol groups. Equations (3.21.) and (3.1.3) are condensation reactions, through which siloxane bonds are formed. The condensation reaction continues and oligomeric silanols are formed. Ultimately, the oligomeric silanols condense to silica colloid particles in nanometer size. These silica particles distributed in the water/alcohol solution form a silica sol solution.

The silica sol solution is an unstable system. The particles are further connected to each other through surface silanol dehydration condensation or through aggregation. These connected particles form a gel which is a porous material with solvent (water and alcohol) filled inside the pores. In the aging process, the reactions that caused the gelation continue on to produce a strengthening, stiffening and shrinkage of the gel network. In the same time, part of the solvent migrated out of the pores. In the drying process, the solvents in the pores are moved out of pores of the gel through evaporation or by using supercritical fluid techniques.

The optical properties and microstructure of a sol-gel material are determined by a number of parameters used in a sol-gel process, including precursor composition, solvent type and concentration for the hydrolysis and gelatinization, catalyst type and concentration, gelatinizing and drying process. In this project, the effect of precursor composition, catalyst composition and conditions for gelatinization and drying silica gel on the optical propterty of sol-gel derived silica was investigated and optimized sol-gel procedures for making sol-gel derived porous silica materials which are best suitable as constituent materials for designing optical fiber chemical sensors have been established.

3.1.1. Preparing porous silica materials with different precursors

Porous sol-gel silica materials can be prepared by using an ester of silicic acid as a procursor. Depending on the procursor used, the conditions for preparing a porous silica material are different. For example, the time needed to hydrolyze the ester varies with the procursor in the sequency: tetramethylorthosilicate (TMOS)< tetraethylorthosilicate (TEOS) < tetrapropylorthosilicate (TPOS). Usually with TMOS as procursor, the hydrolysis process can be finished within 10 minute. With TEOS as the procursor, it will needed more than four hours for hydrolysis. With TPOS, the time is more than 16 hours. Temperature can significantly affect the hydrolysis and gelatinization time. Because the hydrolysis is exothermic, the reaction proceeds faster at higher temperatures. In this project, TMOS and TEOS are used as precursors for preparing silica sol solution. TMOS was used when the obtained sol solution need to be used for form a gel in a short time (within two or three days), while TEOS was used when the obtained silica sol solution need to be stored for a longer time (several weeks) before gelatinization.

3.1.2. Preparing porous sol-gel silica materials with different catalysts

The hydrolysis of a silicon alkoxide is a slow process. This is true even for the most reactive silicon alkoxide, TMOS. Therefore, a catalyst is usually added to the mixture of a silicon alloxide and water to promote the reaction. In this work, two catalysts, HCl and NH_3 were compared for preparing porous silica materials through catalyzed hydrolysis of TMOS. A solution of 0.1 M HCl and a solution of 1% NH_3 were used as the catalyst, respectively. TMOS was hydrolyzed within several minutes (<10 min) with both of the catalysts. The obtained sol solutions gelatinized in a few hours when the solutions were exposed to air. When the sol solutions were sealed in glass vials, transparent silica gels were obtained after 3 days. Transparent glass materials were obtained after drying the silica gels gelatinized within the sealed glass vials. There is no visually observable crack in the dried silica monoliths. When the sol solution obtained with the HCl solution as a catalyst was gelatinized and dried in air, the silica material breaks into small pieces during the drying process. Each individual piece looks like a small piece of glass and is transparent. However, if the sol solution obtained with the NH_3 solution as a catalyst was gelatinized and dried in air, the obtained silica material breaks to many small pieces and the material has an opaque appearance.

These experimental results indicate that both an HCl solution and a NH_3 solution can be used to promote the hydrolysis of a silicon alkoxide. The speed of the hydrolysis reaction using an HCl solution or a NH_3 solution as a catalyst is comparable. However, the finally formed porous silica material is different. With an HCl solution as a catalyst, the obtained sol-gel silica is transparent even the sol solution was gelatinized and dried relatively fast. When a NH_3 solution was used as a catalyst, a transparent sol-gel silica material can only be obtained from well controlled gelatinizing and drying processes. These results are in agreement with observations reported by other scientists worked on sol-gel chemistry [11]. It was believed among sol-gel silica chemists that with an HCl solution as a catalyst, the silica particles in the obtained sol solution have a “curved wire” structure. During the gelatinizing process, the “curved wires” are interconnected to form a network. When a NH_3 solution is used as a catalyst, the silica particles in the obtained sol solution have a “ball” structure. The “balls” stick to each other in the gelatinizing and drying processes to form a porous silica material. Compared with the porous silica formed from “curved wires”, this porous silica material has more pores and larger pore

size. If the solvent inside the pores is rapidly vaporized, as in the case of drying the silica gel in air, this porous silica tend to break because the bond between the "balls" is not as strong as that between the interconnected wires. From the viewpoint of fiber optic sensor design, a gas sensor using a porous sol-gel silica fiber with more pores and larger pore size can have a faster response. Therefore, both catalysts could be used to prepare porous silica fiber. If NH_3 is used as the catalyst, well controlled gelatinizing and drying procedures must be followed in order to obtain transparent porous silica fiber.

3.1.3. Gelatinizing silica sol solutions at different temperatures

An experiment was carried out to compare the processes of gelatinizing a silica sol solution and drying the obtained silica gels at different temperatures. A silica sol solution was obtained by hydrolyzing a liquid TMOS using an 0.1 M HCl solution as a catalyst. The obtained solution was divided to two glass vials and sealed in the glass vials. One of the glass vials was kept at room temperature and the second vial was placed in a refrigerator. The sol solution kept at room temperature gelatinized in three days. However, it takes more than three weeks for the sol solution in the refrigerator to gelatinize. This feature of slower gelatinization at lower temperatures provides an opportunity for doping the sol solution with other chemical reagent for synthesizing hybrid porosu silica materials. A sol solution can be stabilized for a long time by storing in a refrigiritor before mixing it with aother solution to make hybrid materials.

The glass vials were opened after silica gels were formed inside the vials. The silica gel formed at room temperature was dried in air at room temperature and the silica gel formed in the refrigerator was kept in the refrigerator. A silica gel monolith in the shape of a glass rod was formed inside the glass vial after drying the gel at room temperature for about one week. When the gel was kept in the refrigerator, it took more than one month to dry the gel. When the sol-gel silica monoliths were examined with naked eyes, there is no observable difference between the materials gelatinized and dried at different temperatures.

3.2. Developing techniques for improving the quality of sol-gel silica fibers for designing fiber optic sensors

Porous silica optical fibers prepared with the procedure described in Section 2.2 have been observed visually as well as with SEM. Follow problems were found exist with the fibers prepared with this procedure. First, a silica gel inside the Tygon tube breaks to short pieces during the gelatinizing process. It is difficult to make a long porous silica fiber due to this problem. Second, a silica gel fiber tends to bend during the drying process. It is difficult to obtain a long straight fiber. Third, it was observed under the SEM (Fig. 3.2.1) that the sol-gel derived porous silica fiber has a very rough structure on its surface. Pores with diameter in micrometer level were observed on the surface of such a fiber, while the pore size within the fiber is in nanometer range. The rough structure on the surface of the sol-gel silica fiber scatters light out of the fiber. This severely limits the capability of the sol-gel silica fiber for guiding light.

It was believed that the break of a silica gel fiber inside a Tygon tube is caused by the shrink of the silica gel during gelatinizing process. The microstructure on the inner surface of the Tygon tube causes a friction between the Tygon tube wall and the newly formed silica gel fiber. During the gelatinizing process, the silica gel fiber shrinks. This shrink forms a force to pull the gel fiber to the center of the tube. However, the friction between the inner surface of the Tygon tube and the silica gel fiber inhibits the free

movement of silica gel fiber inside the tube. Therefore, the gel fiber breaks to short pieces. In order to solve this problem, a revised method was developed to make the silica gel fiber. After filling the silica sol solution into a Tygon tube, one end of the tube was sealed using a parafilm. The Tygon tube was then vertically fixed on a wall with the sealed end in the lower side. The tube was kept straight against the wall by fixing its two ends with tapes. During the gelatinizing process, the gravity of the material inside the tube helps the silica gel moving down while the gel is shrinking. With this improved method, a silica gel fiber with a length almost equal to that of the Tygon tube can be made.

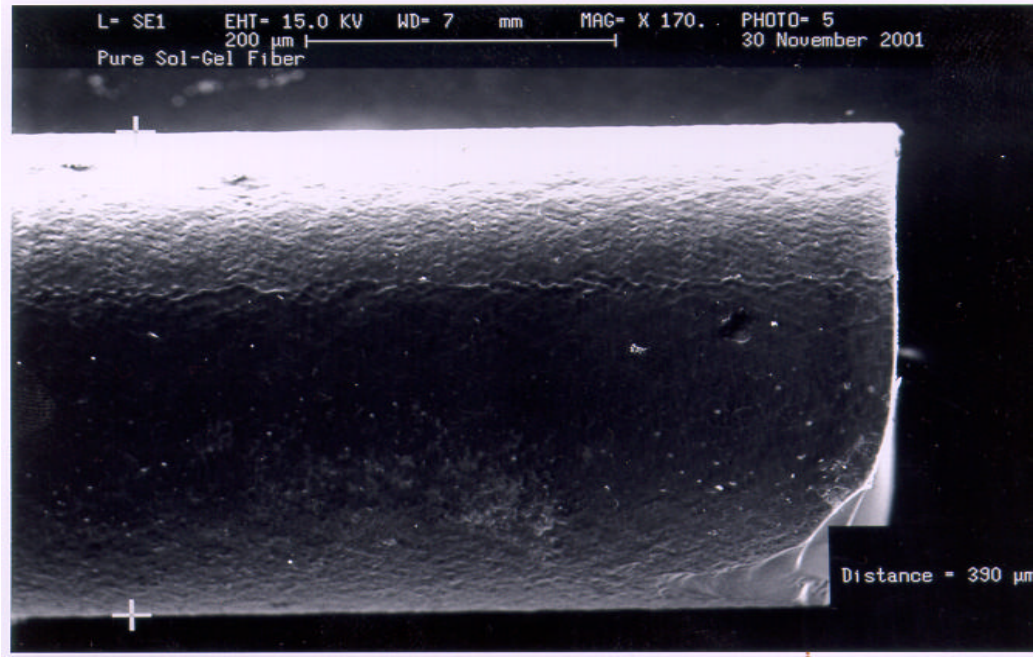

Fig. 3.2.1. A SEM image of a porous silica optical fiber prepared with the sol-gel techniques described in Section 2.2 of this report. Rough and uneven structure are observable on the surface of this fiber under the SEM. IT was believed that this rough structure on the surface of the fiber scatters light out of the fiber and attenuates the capability of the fiber for guiding light.

The bending of a silica gel fiber during drying process was observed. It was believed that the difference of solvent vaporization between the surface of the silica gel fiber in contact with air and the surface of the gel fiber in contact with the surface of a fiber holder causes the fiber to bend. The vaporization of solvent near the surface of the gel fiber in contact with air is faster than the vaporization of solvent near the surface of the gel fiber in contact with the holder. The vaporization of solvent from the gel fiber causes the fiber to shrink. Therefore, during the drying process, the shrinking tension build up near the surface of the gel fiber is different between the surface in contact with air and the surface in contact with the fiber holder. The gel fiber surface in contact with air shrinks faster than the fiber surface in contact with the holder. Thus, the fiber becomes bent in order to balance the difference between the shrinking tensions. One solution to this problem is drying the gel fiber inside the Tygon tube. In one of our experiments, a silica gel fiber formed from gelatinizing a sol solution obtained from

hydrolyzing TMOS was kept inside a Tygon tube. A long straight fiber was obtained after kept the gel fiber inside the tube for more than four weeks. The second solution to the bending problem is continuous rolling the gel fiber during an air-drying process. In a preliminary experiment, a reciprocal shaker (Model 3506, Lab-Line Instruments, Inc., Melrose Pork, IL) designed to shake flasks during solvent extraction was used to rolling silica gel fibers during the air-drying process. With the help of this machine, straight sol-gel silica fibers with length at around 10 cm were made (Fig. 3.2.2). It is expected that longer sol-gel silica fibers can be obtained if a rolling machine better fits this purpose is available.

A wet chemical procedure was developed to remove the rough microstructure from the fiber's surface. In this method, a dried sol-gel silica fiber with a rough surface was first soaked into a solution of 5% HF for several minutes. The fiber was then removed from the HF solution and rinsed with DI water. Through this process, the rough structure on the surface of the sol-gel silica fiber was removed and light scattering by a treated sol-gel silica fiber is reduced.

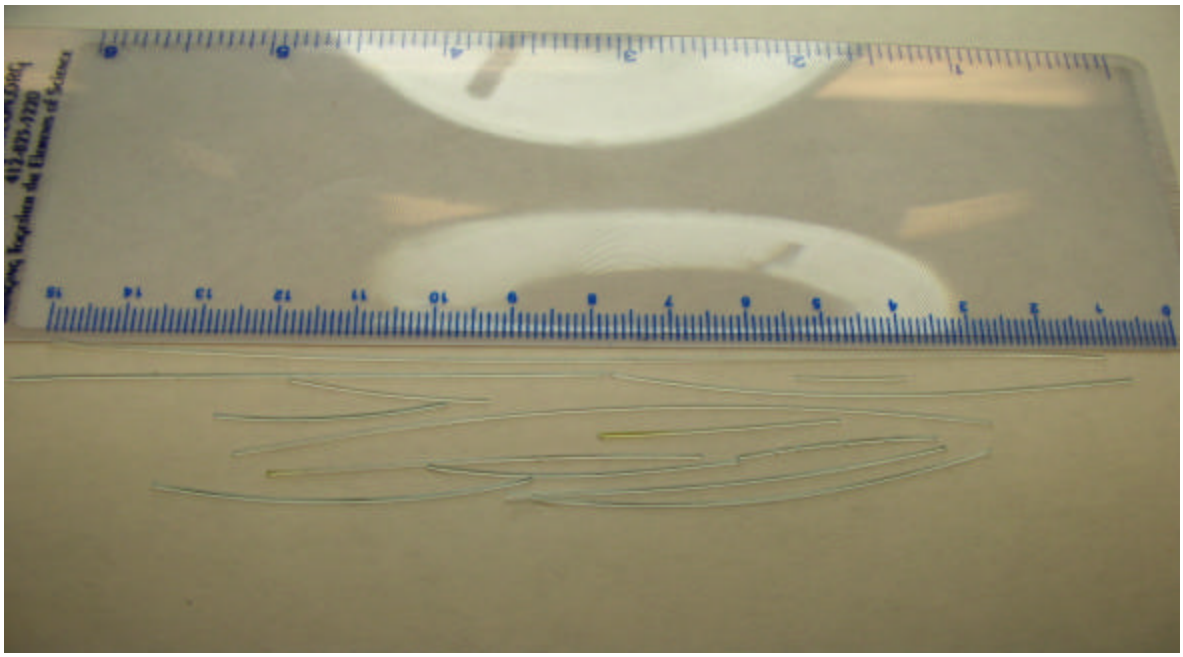

Fig. 3.2.2. Sol-gel silica optical fibers obtained by drying silica gel fibers in air. The original gel fibers were placed on the top of a reciprocal shaker. During the drying process, the fibers were rolled on the shaker to prevent the fiber to bend. A compound of blue color was doped into the fibers in order to take the picture of the fibers.

Figure 3.2.3 shows a comparison of two sol-gel silica fibers for guiding light. As showing in this picture, a light beam from a blue LED (470nm peak emission) was fed into a silica optical fiber. The light beam was splited to two beams in two optical fibers by using a optical fiber coupler. A sol-gel silica fiber was connected to each of the two branched optical fibers of the coupler. The sol-gel silica fiber on the right side has been treated with the HF solution and the sol-gel silica fiber on the left has not. A blue light is observable on the surface of the sol-gel silica fiber on the left while almost no light is

observable on the surface of the sol-gel silica fiber on the right. This is because the sol-gel silica fiber without the HF solution treatment scatters light while the sol-gel silica fiber treated with the HF solution does not scatter light. This conclusion is also supported by observing the end of the sol-gel silica fibers. The fiber had HF solution treatment has a brighter blue light image than the fiber without HF treatment, because more light was guided through the treated fiber. In addition to remove rough structure on the surface of a sol-gel silica fiber, the HF solution treatment procedure could also provide a technique for controlling the diameter of a sol-gel silica fiber. In further work, HF treatment procedures will be optimized in order to make high quality sol-gel silica fiber with expected diameter.

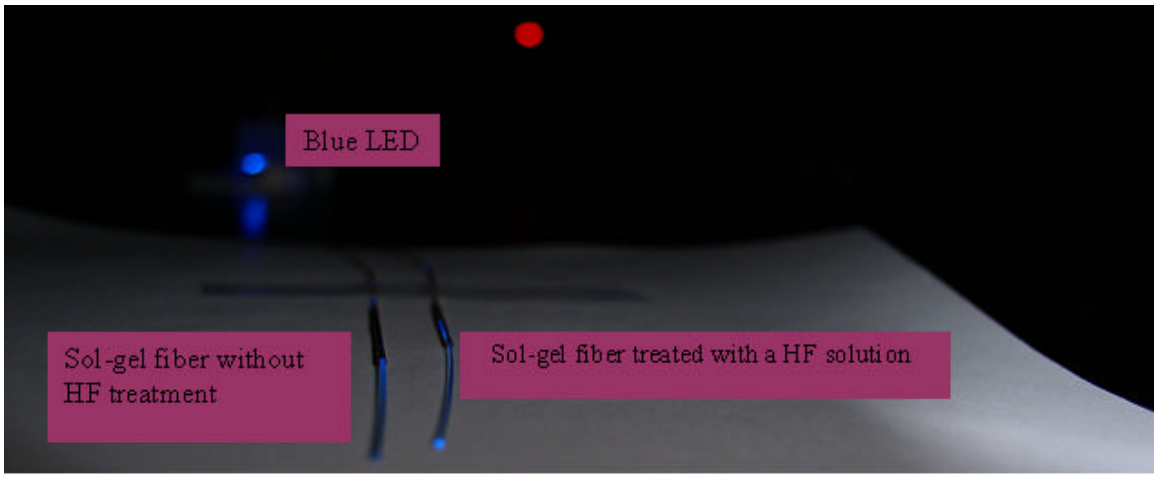

Fig. 3.2.3. Efficiency of light guiding and light scattering by sol-gel silica fibers with (right) and without (left) treatment by a 5% HF solution. The sol-gel silica fiber without the HF solution treatment scatters more light out of the fiber and guides a very small part of light through the fiber. The sol-gel silica fiber treated with the HF solution guides most of the light to the distal end. Almost no scattered light is observable on the surface of this treated fiber.

A general guideline for making porous silica fibers which can be used as transducers of fiber optic sensors has been established based on this work. This guideline will be followed in our further work to prepare porous silica fibers.

1. TMOS and TEOS have been chosen as precursors.
2. The volume ratio of a precursor to water is less than 2.
3. HCl and NH_3 solutions have been chosen as catalysts.
4. A silica sol solution is gelatinized at room temperature in a closed Tygon tube. The Tygon tube is kept perpendicular and straight during the gelatinizing process.
5. A silica gel fiber is dried in air or in a controlled gas environment inside a straight Tygon tube. If the silica gel fiber is dried in open air, the fiber has to be continuously rolled in order to make a straight fiber.
6. A dried fiber is treated with a HF solution of appropriate concentration to remove the rough structure on the surface of a new sol-gel silica fiber and to control the diameter of the fiber.

3.3. Preparing nanometer particles of noble metals and immobilization of nanometer particles into porous silica materials

Nanoparticles of noble metals were synthesized via ion reduction in the micelle/reverse systems [12-15]. Reverse micelles are nanodroplets of water sustained in an organic phase by a surfactant that can hold and dissolve inorganic salts. The inorganic salts are then converted to an insoluble inorganic nanoparticle after chemical reaction and removal of water. Metal cations in the aqueous phase of the reverse micelles may be reduced to metallic nanoparticles by adding a reducing agent such as hydrazine or sodium borohydride. Micelles are nanometer droplet of organic solvent distributed in water via a surfactant. A metal complex which is soluable in the organic solvent can be distributed into the micelles. When a reducing agent is added to the micelle solution, the metal complex is reduced in the micelles and the resulted metal atoms inside individual micelle aggregate to form metal particles.

The molar ratio of H_2O to surfactant (ω_0) is a very important factor in reverse micelle, since it determines the quality of reverse micelle and the size of the water pools. And finally the particle size is determined by the size of the water pools inside the reverse micelle.

$$\omega_0 = [H_2O]/[\text{Surfactant}] \qquad (3.3.1)$$

In a micelle system, the concentration of a surfactant in the solution is critical to decide the formation of micelles, the size, number and shape of the organic solvent droplets in the micelle system. Critical micelle concentration (CMC) for a specific surfactant is the concentration at which the surfactant starts to form micelles in water. With the increase of surfactant concentration in a micelle solution, the number of micelles increased and the size of the micelles reduced.

The advantage of micelle/reversed micelle techniques for nanometer particles preparation is their ability to afford great control over the particle size with a narrow size distribution as well as shape by controlling the physical and chemical properties of the micelle/reverse micelle systems.

Both micelle and reversed micelle techniques were employed in this work for preparing nanometer particles of noble metals. The surfactants used for forming micelle solution and reversed micelle solution include Igepal CO 520, Triton X-100 and SDS. Igepal CO-520 is a nonionic surfactant, Triton X-100 is a cationic surfactant and SDS is an anionic surfactant. Another technique employed in this project for preparing nanometer noble metal particles is using a stabilizer, which is a mercapto-silane. In this work, 3-mercaptopropyltrimethoxysilane was used. When a noble metal complex in a micelle was reduced in the existence of this reagent, the formed particles were surrounded by the mercapto-silnae and stabilized in the micelle solution. This mercapto-silane is then hydrolyzed together with another silica precursor and the noble metal particles were immobilized inside the obtained silica gel after the gelatinization of the obtained silica sol solution.

The relationship of the experimental conditions and the particles morphology will be discussed in the section of microstructure of the prepared materials.

3.4. Visual appearance of sol-gel derived materials

The sol-gel derived materials prepared in this project have been visually examined. A pure sol-gel silica material is transparent and colorless within certain drying time. When the material was stored in air for a long time (several months drying time), the material turns out to be pink colored. It was believed that when a porous silica gel was formed from a solution, the pores inside the material were filled with liquid solvents, such as water and alcohols. The material looks transparent because the refractive index of the solvent and the silica in the gel is very close. When a newly formed silica gel was kept in air, the liquid solvents inside the pores gradually vaporized and some voids formed inside the material. The refractive index of air filled in the voids is much lower than that of solid silica. When a light beam travels from the solid silica into a void, the direction of the light beam changes and part of the light scattered out of the material. In a Rayleigh scattering model, a material with scattering center in a size smaller than light's wavelength scatters light of short wavelength more than light of longer wavelength. Therefore, when a dried sol-gel material is illuminated with a white light, it appears in a pink color. This observation indicates that a porous silica fiber can be a good waveguide for a visible or a near infrared light, but is not a good waveguide for a UV light.

A doped porou silica mateial is usually transparent as long as the concentration of the compound doped inside the porous silica is within certain range. Depending on the optical properties of the doped compound, a hybrid porous silica matrial can show an intensive color. Fig. 3.4.1 to Fig. 3.4.9 are pictures of several examples of doped porus silica materials. These include porous silica doped with metal salt, metal oxide and nanometer partilces of noble metals. A metal ion doped porous silica material usually has a color of the metal ion in water because the metal ions in the porous silica exist as hydrated ions (Fig. 3.4.1 to Fig. 3.4.3). A metal oxide doped porous silica mateiral usually display a color of the doped oxide (Figs. 3.4.4 and 3.4.5). The color of porous silica material doped with nanometer particles of noble metal depends on the type of metal and the method for preparing the nanometer particles (Fig. 3.4.6 to Fig. 3.4.9).

Fig. 3.4.1. A picture of Co^{2+} ions doped sol-gel silica fibers. The fibers were formed by injecting a Co^{2+} containing silica sol solution into a small tygon tube. The silica sol solution was gelatinized and dried inside the tube. The three sol-gel silica monoliths were formed by gelatinization of the Co^{2+} doped silica sol solution in small pipette tips.

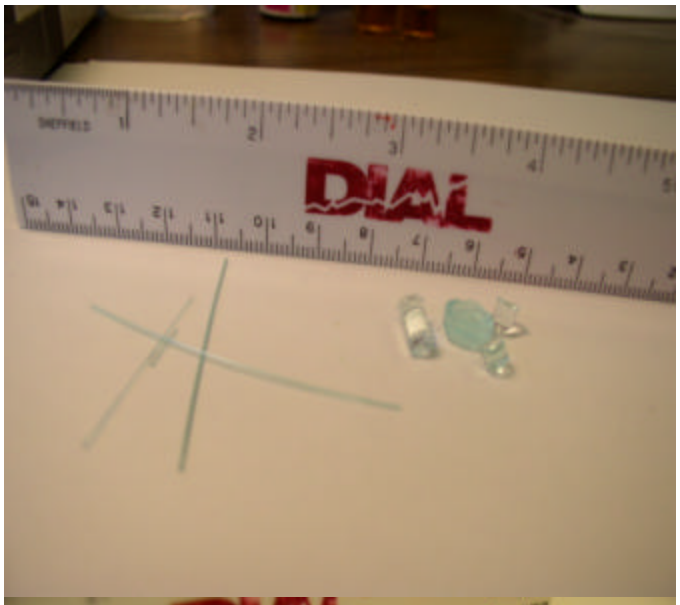

Fig. 3.4.2. A picture of Cu^{2+} ions doped sol-gel silica fibers. The fibers were formed by injecting a Cu^{2+} containing silica sol solution into a small tygon tube. The silica sol solution was gelatinized and dried inside the tube. The sol-gel silica monoliths were formed by gelatinization of the Cu^{2+} doped silica sol solution in small glass vials.

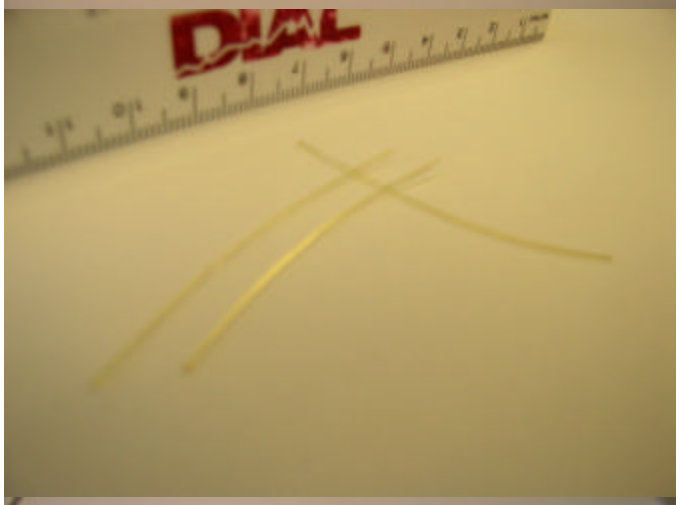

Fig. 3.4.3. A picture of Eu^{3+} ions doped sol-gel silica fibers. The fibers were formed by injecting a Eu^{3+} containing silica sol solution into a small tygon tube. The silica sol solution was gelatinized and dried inside the tube.

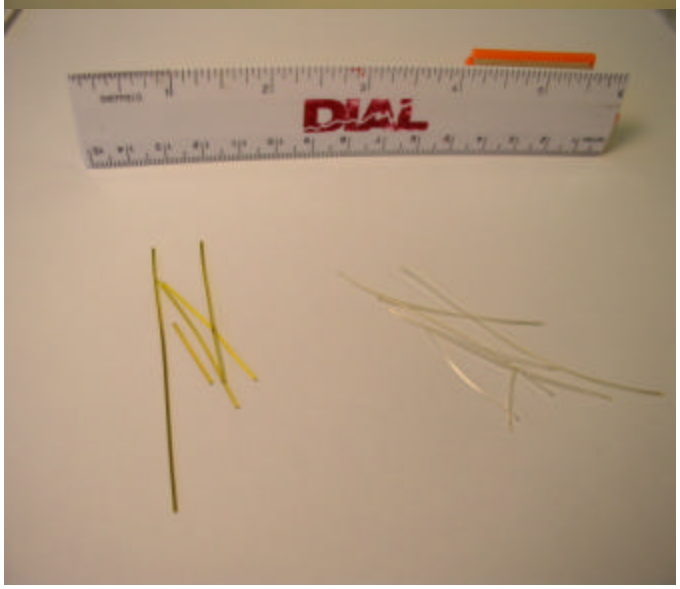

Fig. 3.4.4. A picture of vanadium oxide doped sol-gel silica fibers. The procedure for making the vanadium oxide doped porous silica fibers was described in the text of this report. The fibers on the left have been heat treated by heating the fibers to 600 ^{o}C in a furnace with air flowing through the furnace during the heating process. The fibers in the right are not heat treated.

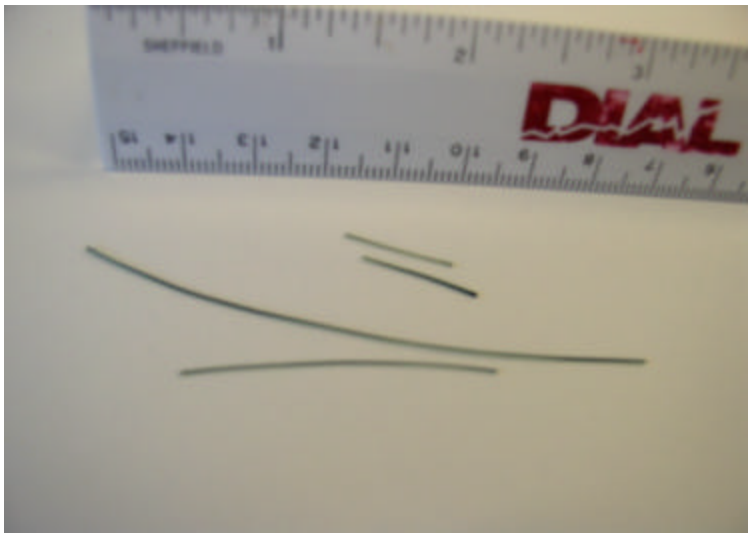

Fig. 3.4.5. A picture of molybdenum oxide doped sol-gel silica fibers. The molybdenum oxide doped fibers have a blue color, although in this picture the color is not clear. The procedure for making the vanadium oxide doped porous silica fibers was described in the text of this report.

Fig. 3.4.6. A picture of a palladium nanometer particles doped sol-gel silicca material. This material is transparent and shows a purplish-brown color.

Fig. 3.4.7. A picture of nanometer metal particles immobilized sol-gel silica materials prepared with methods described in the text. Samples in the front row are materials prepared with stabilizer 3-mercapto-propyltrimethoxysilane (from left to right: Ag, Au, Pd, Pt, Ag). Samples in the back row are materials prepared with micelle/reversed micelle methods using Igepal CO-500 (the first tow samples from left), Triton X-100 (the third and fourth from left) and SDS (the fifth to seventh from left) as surfactant.

Fig. 3.4.8. A picture of silver colloid solution in reversed micelles and silver nanometer particles doped sol-gel silica materials. The silver colloid solution (inside the first vial from left) is a brown colored solution. The color of the silver nanometer particles doped sol-gel silica materials are from yellow (#3, #4 and the first small piece from right) to brown (#2) to purple (the second small piece from right). These silver nanometer particles doped porous silica materials are transparent, except the first small piece (yellow) from right.

Fig. 3.4.9. A picture of a gold colloid solution in reversed micelles and nanometer gold particles doped sol-gel silica materials. The gold colloid solution (inside the glass vial on the left) is a pink colored solution. The color of the gold nanometer particles doped sol-gel silica materials is from pink (the one on the right) to blue (the one in the middle). These gold nanometer particles impregnated porous silica materials are not transparent.

3.5. Microstructure and morphology of sol-gel derived materials

3.5.1. Microstructure of sol-gel derived porous silica material

The sol-gel derived porous silica materials have been investigated with SEM. The obtained images of some sol-gel derived materials are showing in Figs. 3.5.1 to 3.5.4. Fig. 3.5.1 shows the side surface microstructure of a pure sol-gel silica fiber made from the hydrolysis of tetramethylorthosilicate (TMOS). The "bumps and hollows" surface structure of the sol-gel silica fiber is believed to be originated from the surface structure of the Tygon tube used to form the fiber. The microstructure inside the fiber was also studied with the SEM. The fiber was cut with a blade, and the fresh surface was observed with the SEM. The SEM image shown in Fig. 3.5.2 indicates that the resolution

of the SEM is not high enough to observe the microstructure inside the sol-gel fiber. Sol-gel materials prepared with different precusors and different catalysts were also studied with the SEM. The microstruture of these materials is similar to that of the pure sol-gel silica fiber described above.

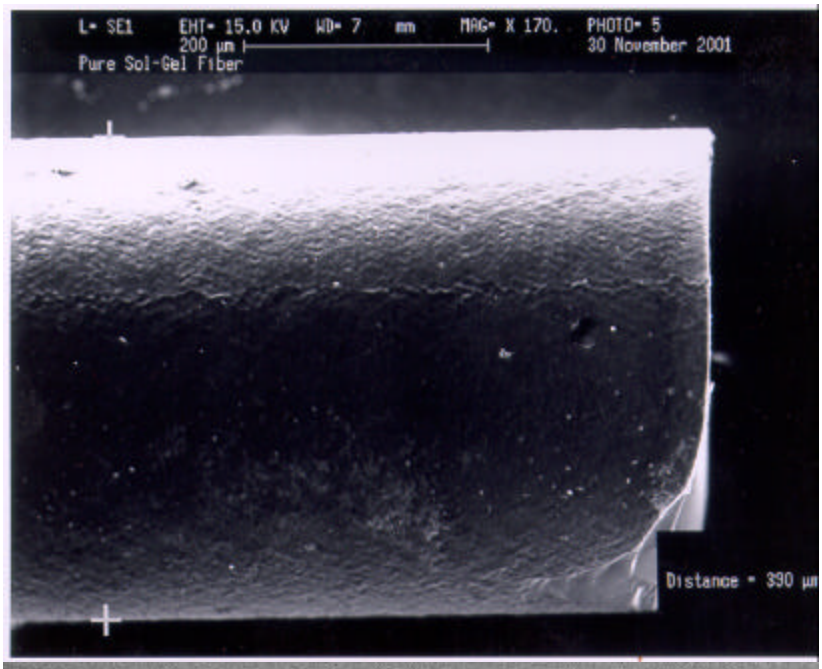

Fig. 3.5.1. A SEM image of the side surface of a pure sol-gel silicate fiber.

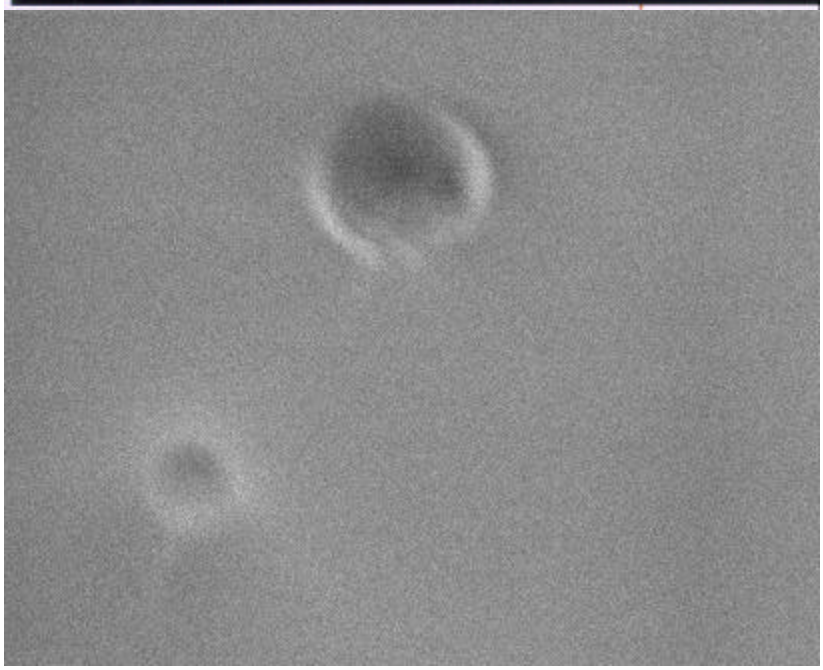

Fig. 3.5.2. SEM of fresh cutted pure sol-gel silicate fiber end surface.

Figure 3.5.3 shows the image of microstructure of a silver nanometer particles doped sol-gel silica material. The size and morphology of the nanocomposites are controlled by micelle and gel formation conditions. The SEM image clearly shows the porous structure inside the silicate material. Compare the images of different silver

nanocomposites, if using TMOS as silicate source, due to TMOS hydrolysis rate is greater than that of tetraethylorthosilicate (TEOS), the aggregation of paticles aggregated was observed. This phenomena was not observed in the silver/TEOS sample. Figure 3.5.4A shows the SEM image for the composite of gold nanoparticles doped in SiO_2, which was synthesized with micelle/sol-gel technique. From the image, spherical particles around 100 nm were seen to be homogenously distributed in the sol-gel silicate matrices or on the surface of the silicate.

The SEM images of palladium and platinium naoparticles doped porous silica materials sysnthesized with micelle/sol-gel technique are shown in Fig. 3.5.4. Platinium nanocomposites prefer to form wire-like and lamellar structure, as shown in Fig. 3.5.4B. By controlling the Pd precursor and organic solvent, we successfully got Pd nanocomposites with different morphologies, such as speherical or leaf-like structures, shown in Fig. 3.5.4C and Fig. 3.5.4D.

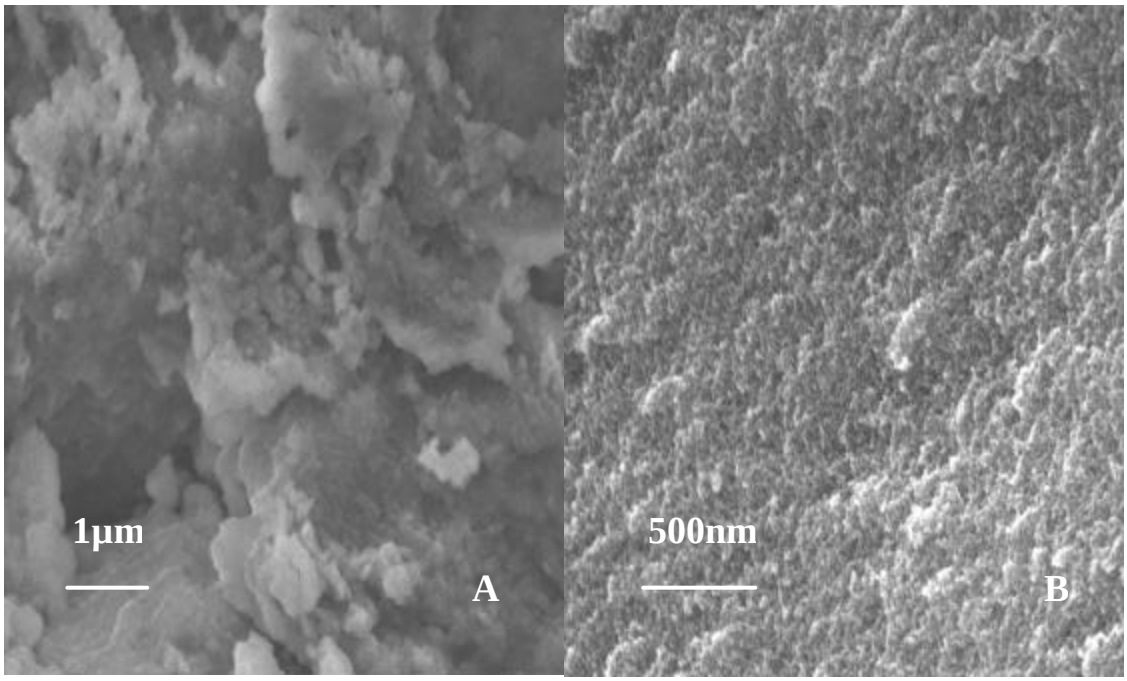

Fig. 3.5.3. SEM iamges of silver particles doped sol-gel silicate materials, using (A) TMOS as silica source; (B) TEOS as silica source.

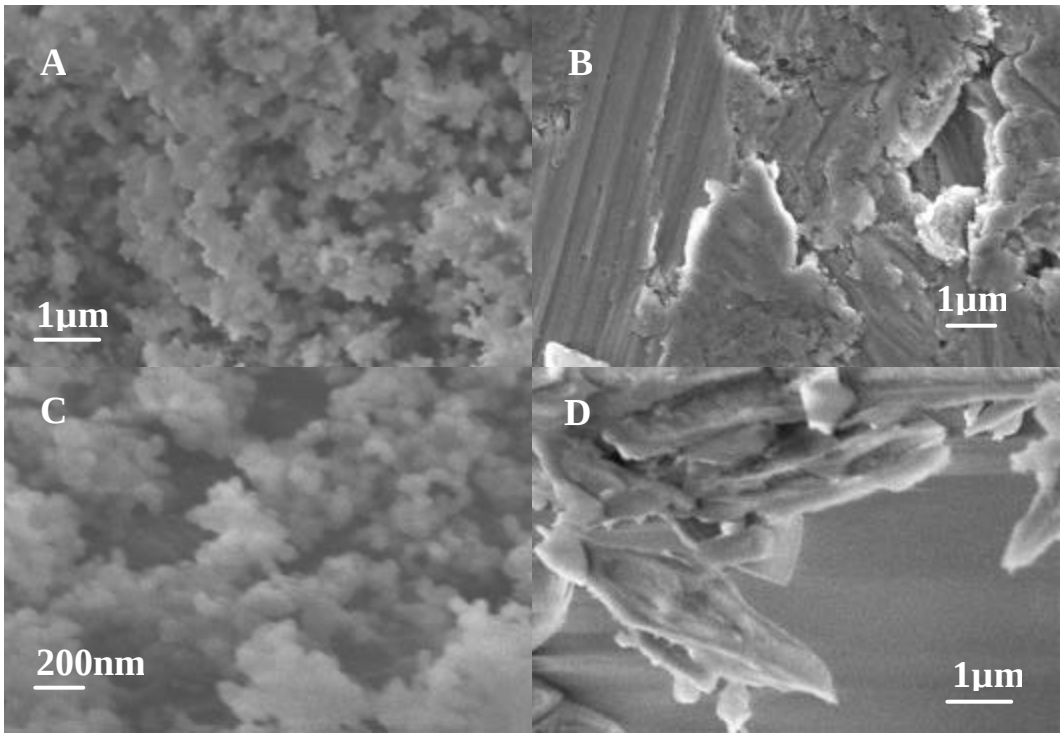

Fig. 3.5.4. SEM images of (A) Au nanoparticles doped sol-gel silicate materials; (B) Pt nanoparticles doped sol-gel silicate materials; (C) Pd nanoparticles doped sol-gel silicate materials; (D) Pd nanoparticles doped sol-gel silicate materials.

3.5.2. Microstructure of nanometer noble metal particles immobilized in porous silica materials

The structure of nanometer metal particles immobilized porous silica materials have been studied with transmission electron microscope (TEM). In order to observe the structure of metal particles immobilized in a sol-gel silica material with a TEM, a freshly made silica sol solution was dropped onto a carbon film coated copper grid and dried at air. The sol-gel silica membrane formed on the copper grid was then observed with a TEM (JEOL JEM-100CX II) operated at 80KV.

The methods used to prepare the metal nanometer particles were evaluated through comparing the TEM images of the prepared samples. It was found that the methods have the best control of the size of the metal particles are the reverse micelle methods. No matter the surfactant is non-ionic surfactant Triton X-100 (Fig. 3.5.5) or Igepal CO-520 (Fig. 3.5.6) or negative charge surfactant SDS (Fig. 3.5.7), the particle size is homogenously distributed and is controlled by the water pool diameter, which is determined by the water and surfactant ratio w_0. If surfactant Triton X-100 was used to form reverse micelles, due to the large amount of the surfactant needed, the samples are very difficult to dry. The particles size is around 25-50nm. If SDS was used to form reverse micelles, the samples are much easier to dry. But due to the fact that SDS is negative charge surfactant, it should be very careful to control the amount of the acid, which is used to catalyze the hydrolysis reaction, so that the reverse micelle won't be destroyed by too much H^+. By using this method, the gold nanoparticle size is around 10 nm. For samples prepared with Igepal CO-520 as the reversed micelle formation

surfactant, the silica gel samples are easier to dry compared to the samples prepared with Triton X-100 as the surfactant, but harder to dry than samples prepared with SDS. The particles size is around 15-20 nm.

When a micelle technique was used to prepare noble metal nanometer particles, the particle size is also controlled and also homogenously distributed. For instance, the particle size of palladium particles is all around 37.5nm (Fig. 3.5.8). By using this method, due to fact that water is around the micelle spherical structure, it is much easier to hydrolyze a silica precursor and form gels. Transparent gels are formed and dried quickly.

Using MPTS as a stabilizer is a good method to form transparent gel and the gel can dry quickly. The color of the Ag, Pd sol with MPTS is yellow, while that of the Au, Pt sol with MPTS is transparent. With this method, the obtained metal particles have a much bigger size compared with the particles obtained with micelle/reversed miclle methods. The TEM images are shown in Fig. 3.5.9. For example, Au nanoparticle is about 100nm.

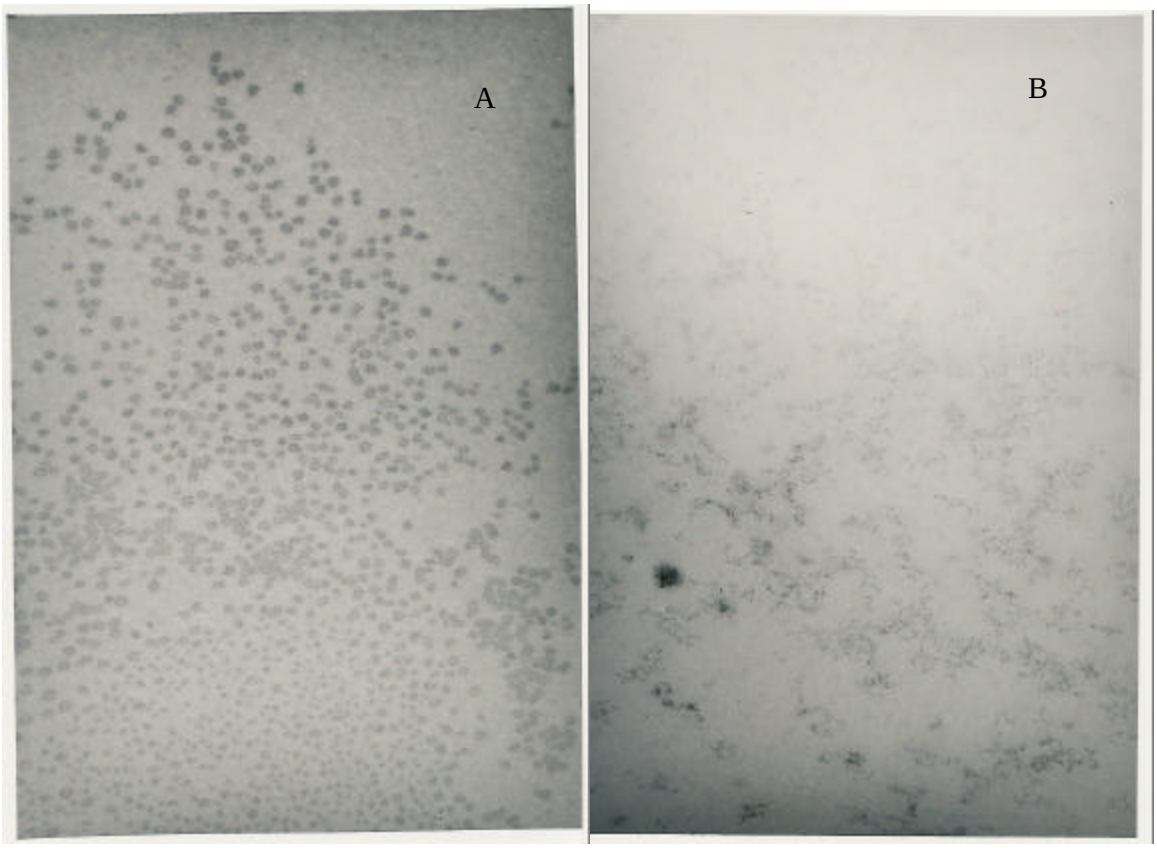

Fig. 3.5.5. TEM images of nanometer metal particles prepared with Triton X-100 reverse micelle method: (A) Pd particles immobilized in a sol-gel silicate material, (B) Ag particles immobilized in a sol-gel silicate material.

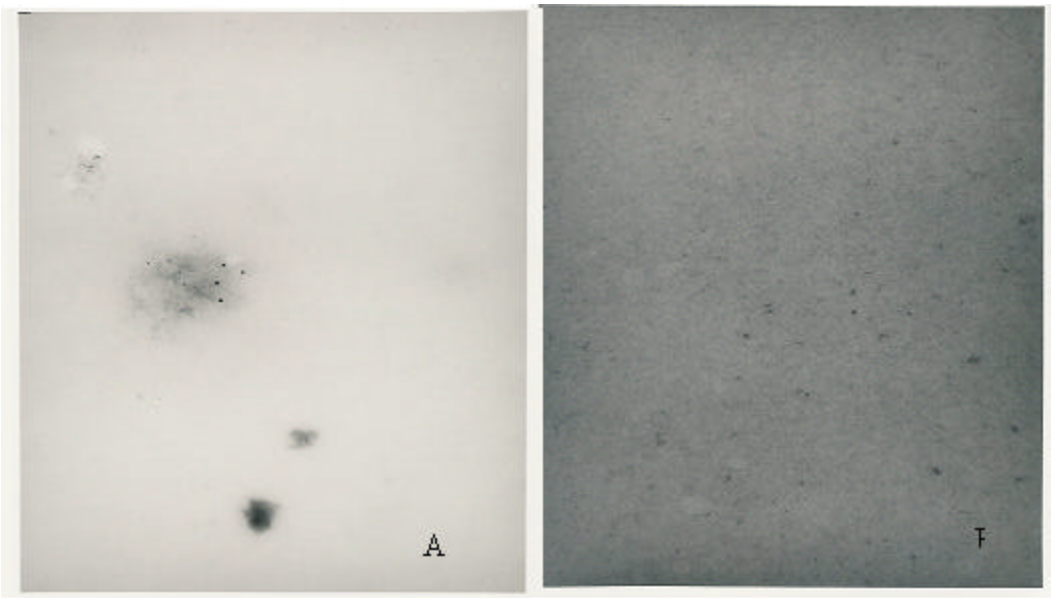

Fig. 3.5.6. TEM images of nanometer metal particles prepared with Igepal CO-520 reverse micelle method: (A) Pd particles immobilized in a sol-gel silicate material; (B) Ag particles immobilized in a sol-gel silicate material.

Fig. 3.5.7. A TEM image of nanometer gold particles immobilized in a sol-gel silicate material.

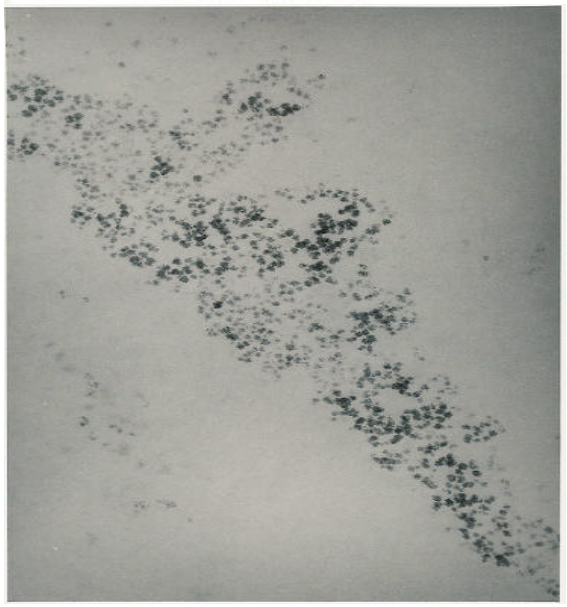

Fig. 3.5.8. A TEM image of a nanometer palladium particles doped silica material prepared with Triton X-100 micelle method.

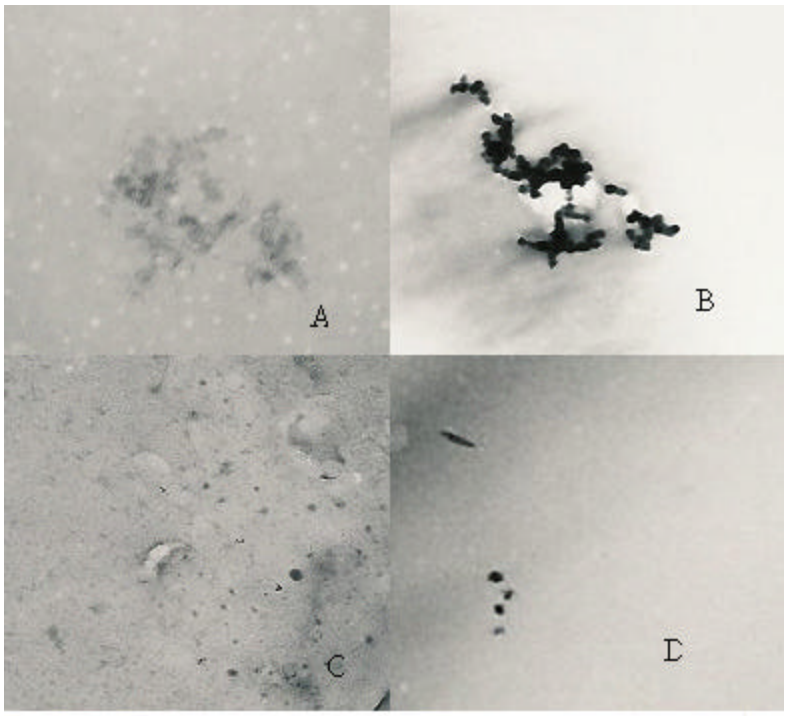

Fig. 3.5.9. TEM images of nanometer metal particles prepared with the stabilizer (3-mercaptopropyltrimetho xysilane) method. (A) Ag-SH/SiO_2**;** (B) Au-SH/SiO_2; (C) Pd-SH/ SiO_2; and (D) Pt-SH/ SiO_2.

3.5.3. Microstructure of semiconductor metal oxide coatings on the surface of silica optical fibers

The surface morphology of the SnO_2 coating on the bent optical fiber probe and the thickness of the coating were analyzed with SEM. Figure 1a shows a SEM image of the SnO_2 thin film coated on an optical fiber surface. The SnO_2 thin film in Figure 1 is homogeneously dispersed and porous network version over the optical fiber surface. It can be seen clearly that the crystalline SnO_2 crystal clusters in the SEM image. The thickness of the coating is around 1 μm (Fig. 3.5.10). Detailed SEM analysis was conducted for the SnO_2 film (Fig.3.5.11) to determine the nature of the crystalline aggregates that were observed. The particle diameter evaluated from Fig. 3.4.19c was found to be 20-80 nm.

During investigating the optical properties of SnO_2 membranes exposed to reducing gases at high temperatures, it was found that a thick SnO_2 membrane coated on an optical fiber core can work at temperature as high as 800 ^oC for a long time. However, when the thin SnO_2 membrane coated on an optical fiber core exposed to an H_2 containing gas sample above 800 ^oC, the spectroscopic response of the membrane to H_2 gas disappears after around 40 minutes exposure. In order to figure out what is responsible to the change, the SnO_2 membranes were examined with SEM after the high temperature gas sensing applications. It was found that in the case of thin SnO_2 membrane, part of the SnO_2 coating on the surface of the optical fiber core disappears after exposed to reducing gas at 800 ^oC (Fig. 3.5.12). However, the thick SnO_2 coating still covers almost all the bent optical fiber core after the exposure to the reducing gas at a temperature as high as 900 ^oC (Fig. 3.5.13). These SEM observations indicate that the

thin SnO_2 membrane on the optical fiber core was blown away or melted and shrank together on the optical fiber core during the high temperature applications.

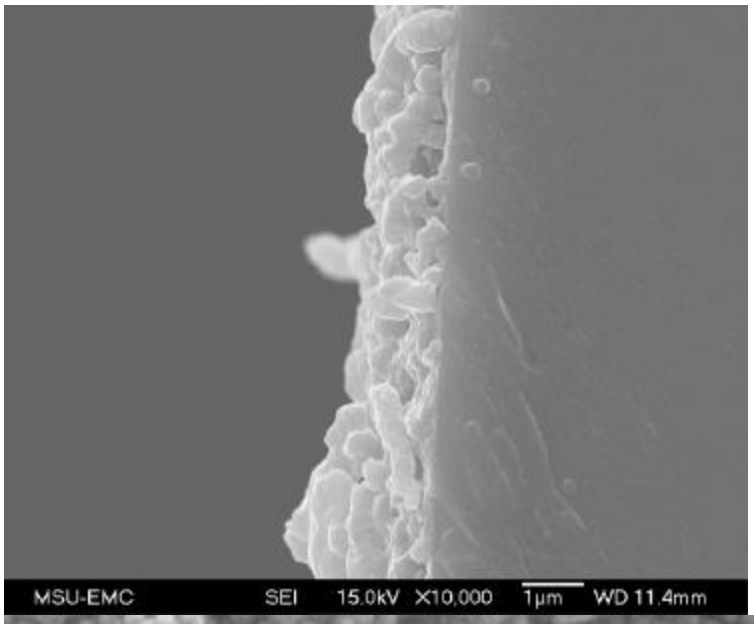

Fig. 3.5.10. A SEM image of a porous SnO_2 material, which is coated on the surface of a bent optical fiber probe. This image shows the thickness of the coating, which is less than 1 μm.

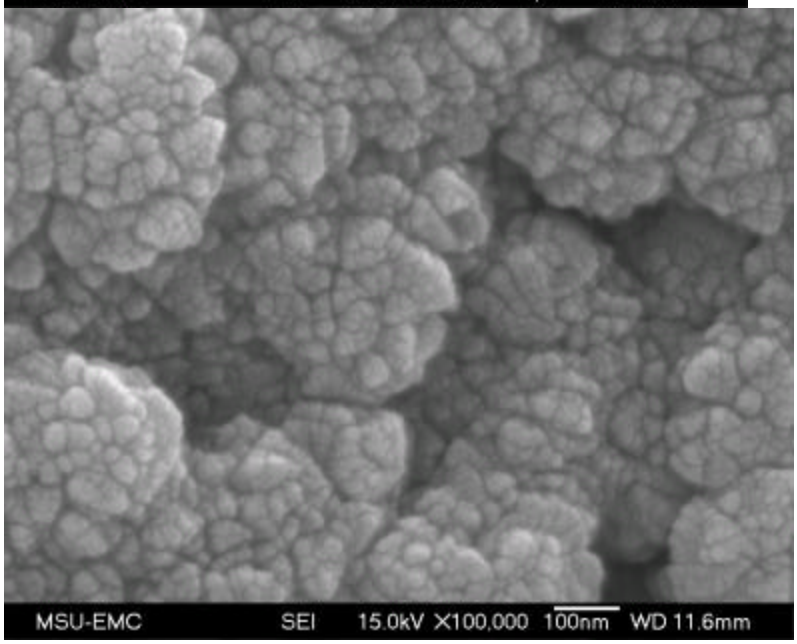

Fig. 3.5.11. A high resolution SEM image of the sol-gel derived SnO_2 coating on the surface of a bent optical fiber probe. This image shows the particles size of the SnO_2 crystals are from 20 nm to 80 nm.

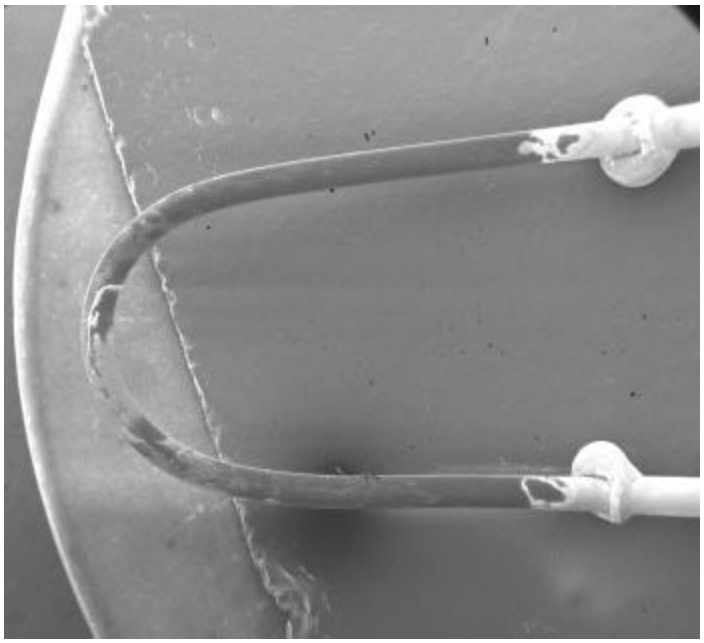

Fig. 3.5.12. A SEM image of a SnO_2 membrane (thin) coated on a bent optical fiber core after high temperature gas sensing applications. It was observed that some of the SnO_2 membrane coated on the fiber's surface was lost after the high temperature gas sensing applications.

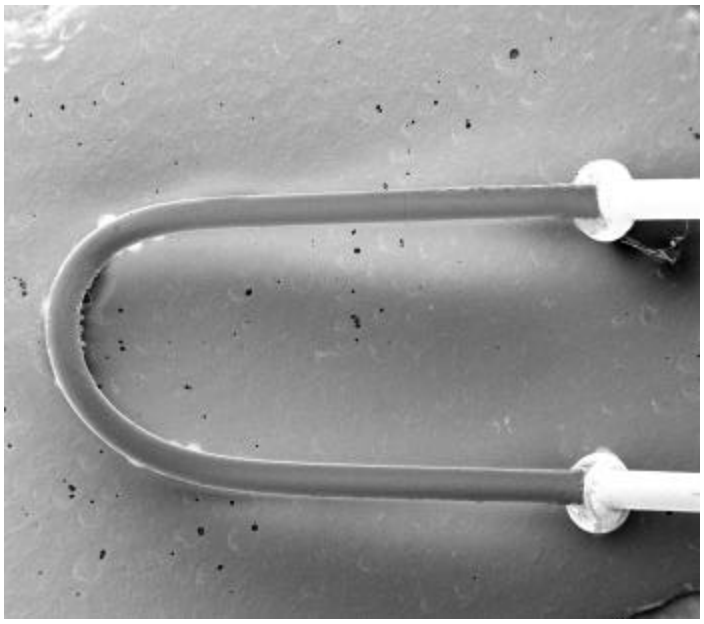

Fig. 3.5.13. A SEM image of a SnO_2 membrane (thick) coated on the surface of a bent optical fiber core. It was observed that the SnO_2 membrane stayed on the fiber's surface after the high temperature gas sensing applications.

3.6. Optical absorption spectrum of sol-gel derived materials at ambient temperature and high temperatures

3.6.1. Optical absorption spectrum of pure porous silica materials at ambient temperature and high temperature

A pure porous silica optical fiber has been examined for its light guiding capability in UV/Vis and NIR region. In this test, a small piece of pure porous silica optical fiber was connected with two gold jacketed silica optical fiber as described in the Experimental section. A conventional silica optical fiber was used as a reference fiber. The connection of the porous silica optical fiber with gold-jacketed silica optical fibers causes insertion loss because mismatching problem. Therefore, the obtained result is a rough indication of light guiding capability of the fiber compared with the conventional silica optical fiber.

The obtained transmission spectrum at room temperature is shown in Fig. 3.6.1. This spectrum indicates that this porous silica optical fiber can guide light in broad wavelength region from 350 nm to 850 nm. In deep UV region, most of the light injected into the porous silica optical fiber was scattered and the transmission is low. Also observed in the transmittance spectrum is the band structure of high transmittance at around 600 nm. This is the result of fluorescence emission in the sol-gel material excited by UV light from the deuterium lamp. The fluorescence emission of porous silica optical fiber will be discussed in another section of this report.

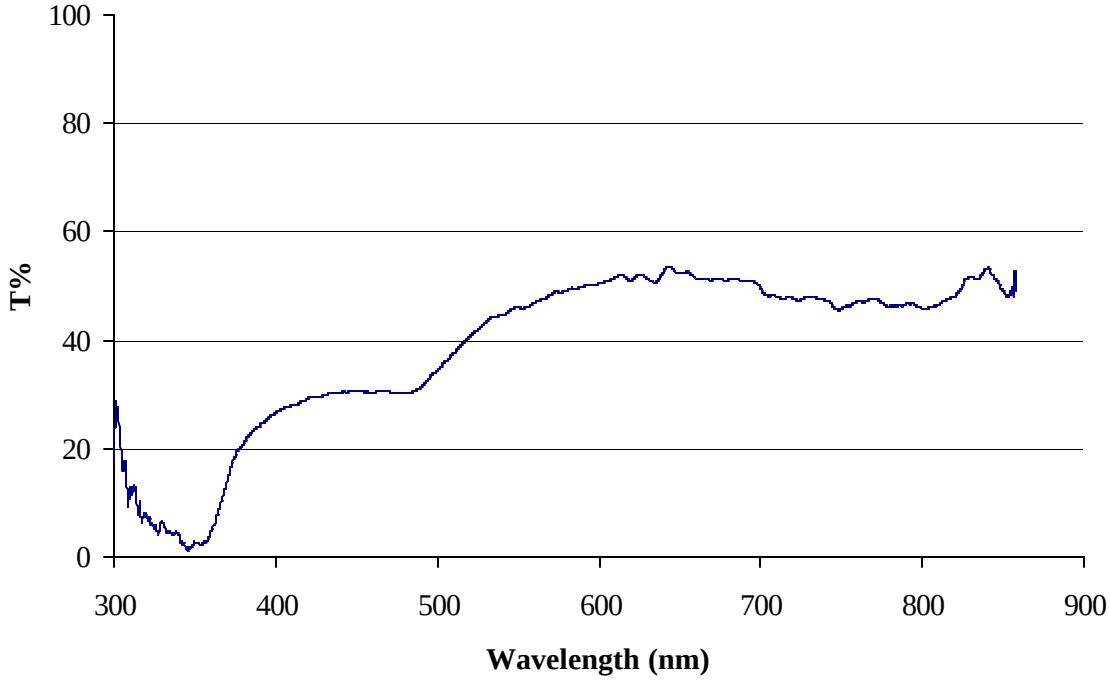

Fig. 3.6.1. An optical transmission spectrum of a porous pure silica optical fiber prepared with a sol-gel technique. This spectrum was obtained at room temperature. With the increase of temperature, the transmittance of the fiber decreased in the recorded wavelength region.

During heating the fiber to a high temperature (450 ^{o}C), the capability of the fiber for guiding UV/Vis light decreased. It was believed that the vaporization of water molecules from the pores inside the sol-gel silica fiber during the heating process

generated more light scattering voids inside the porous silica fiber, and therefore, more light were acattered out of the fiber at higher temperatures.

In the NIR region, the pure porous silica optical fiber shows strong absorption at 940 nm, 1240 nm, 1400 nm and 1900 nm (Fig. 3.6.2). These absorption spectra are originated from vibration of Si-OH, H-OH in the fiber. With the increase of temperature, water was vaporized out of the fiber and the transmittance at 850-1300nm and 1450-1900 nm regions increased. This fiber is a very good light guiding media in 1450-1900 nm region at high temperature.

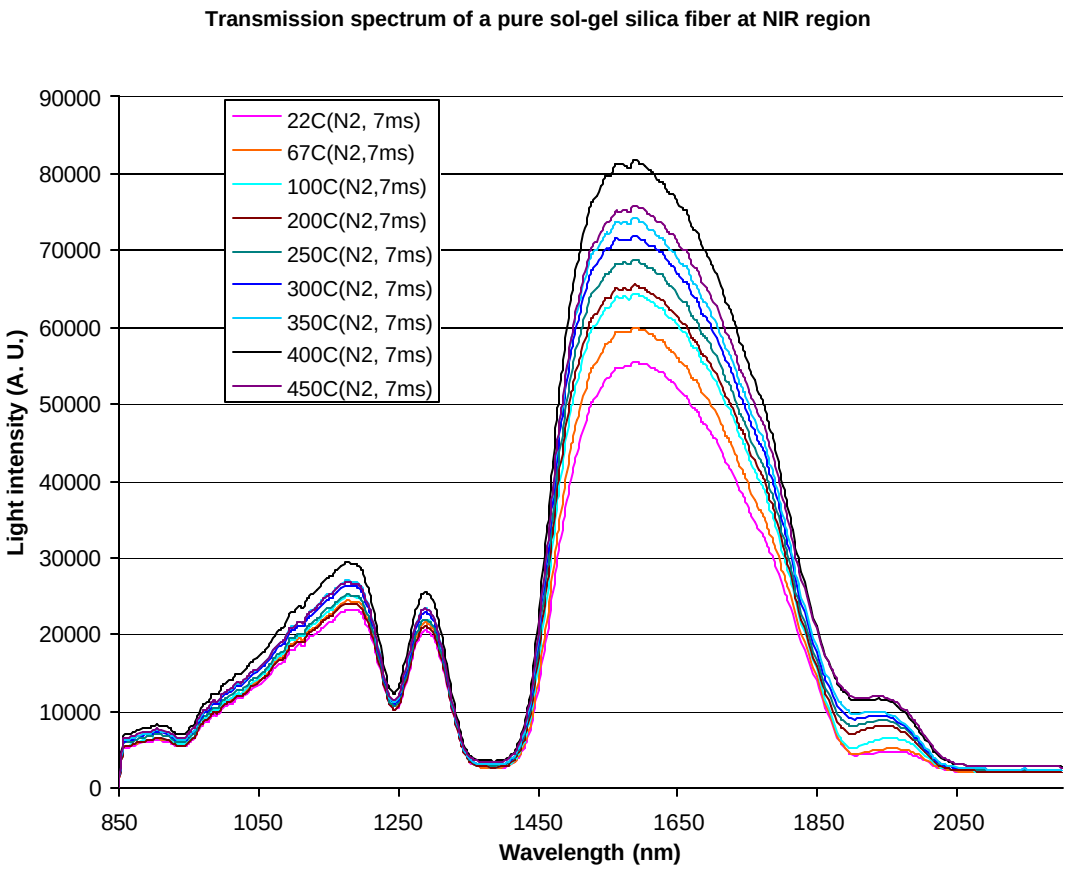

Fig. 3.6.2. NIR transmission spectra of a pure sol-gel silica fiber recorded at different temperatures. With the increase of temperature, the efficiency of the fiber for guiding NIR light increased first, and then decreased. The low transmission peaks at around 940 nm, 1350 nm and 1900 nm were believed cuased by water molecules trapped inside the fiber. The species responsible for the low transmission at around 1250 nm has not identified yet. In the wavelength region lower than 1900, the increase of temperature from 400 ^{o}C to 450 ^{o}C caused less light be transmitted through the fiber. However, at around 1900 nm, light intensity continuously increased with the increase of temperature. It was believed that the increase of temperature drives more water out of the fiber, and the light absorption at around 1900 nm decreased at higher temperature.

3.6.2. Optical absorption spectrum of porous silica materials doped with metal ions and metal oxide and nanometer noble metal particles

The optical absorption properties of the porous silica materials doped with metal ions and metal oxide in UV/Vis and NIR wavelength region were investigated with the active core fiber optic absorption spectrometric method. Two examples of the obtained spectra are shown in Figs. 3.6.3 and 3.6.4.

As shown in these figures, in the UV/Vis region, colored metal ions (Co^{2+}, Cu^{2+}, Fe^{3+}, Ni^{2+}) doped poorus silica materials absorbed light at room temperature and the absorption signal increased with the increase of temperature. The fibers doped with metal ions which show no color have similar transmission spectrum in the UV/Vis wavelength region as that of a pure porous silica optical fiber as shown Fig. 3.6.1. Semiconductor metal oxide (SnO_2, TiO_2, ZrO_2, W_2O_5, Mo_2O_5, VO_2) doped porous silica materials shows intensive color as indicated in graphes 3.4.4 and 3.4.5. These materials strongly absorbs light in UV/Vis region. Figs. 3.4.5 is examples of absorption spectra for porous silica fiber doped with Mo_2O_5, TiO_2, VO_2, W_2O_5 and ZrO_2.

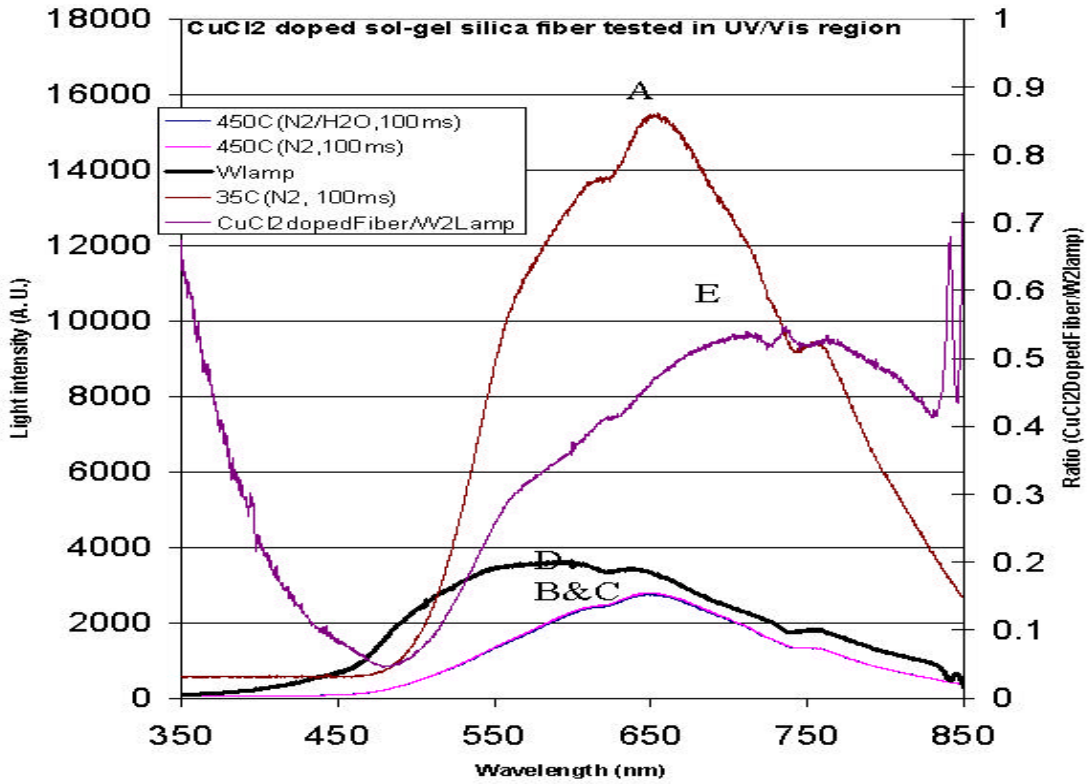

Fig. 3.6.3. UV/Vis transmission spectra of a $CuCl_2$ doped sol-gel silica fiber. Experimental conditions for obtaining individual spectrum: A). 35 ^oC, N_2 gas; B). 450 ^oC, N_2 gas; C). 450 ^oC, moisturized N_2 gas; D). Spectrum of light from the tungsten lamp (directly injected into the UV/Vis spectrmeter); E). light intensity ratio of spectrum A/Spectrum D, which shows the attenuation of light by the $CuCl_2$ doped sol-gel silica against wavelength. This fiber absorbs blue light with peak absorption wavelength at around 470 nm.

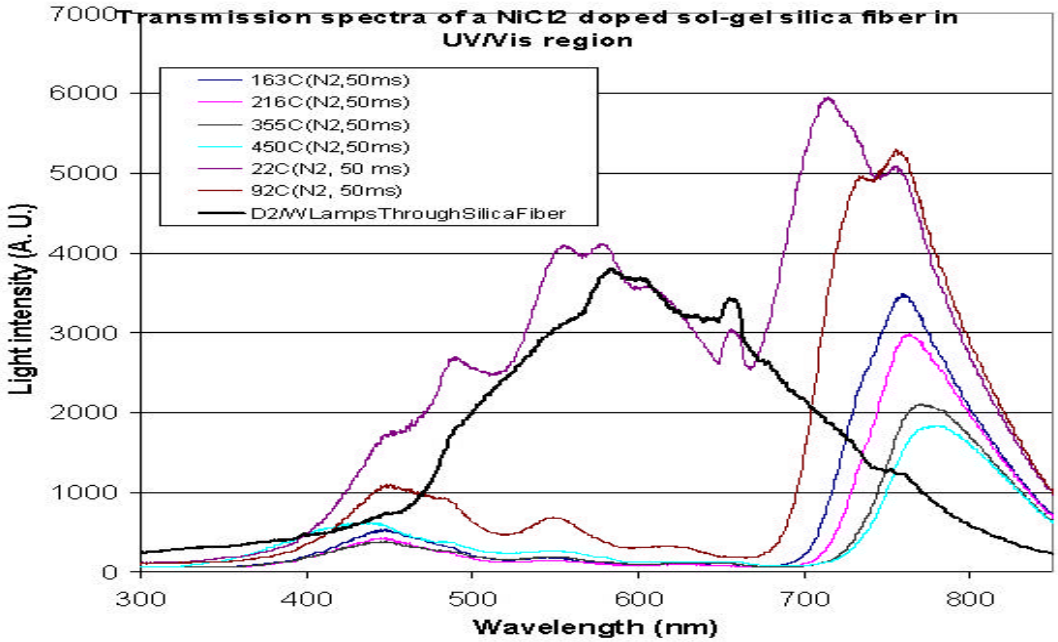

Fig. 3.6.4. UV/Vis transmission spectra of a $NiCl_2$ doped sol-gel silica fiber recorded at different temperatures. With the increase of temperature, light intensity from 500 nm to 700 nm was strongly attenuated. The spectrum in black line is the light intensity distribution without the $NiCl_2$ doped sol-gel silica. Two absorption peaks caused by $NiCl_2$ doped in the sol-gel silica fiber were identified through comparing the black line spectrum and transmissin spectra of the $NiCl_2$ doped sol-gel silica fiber.

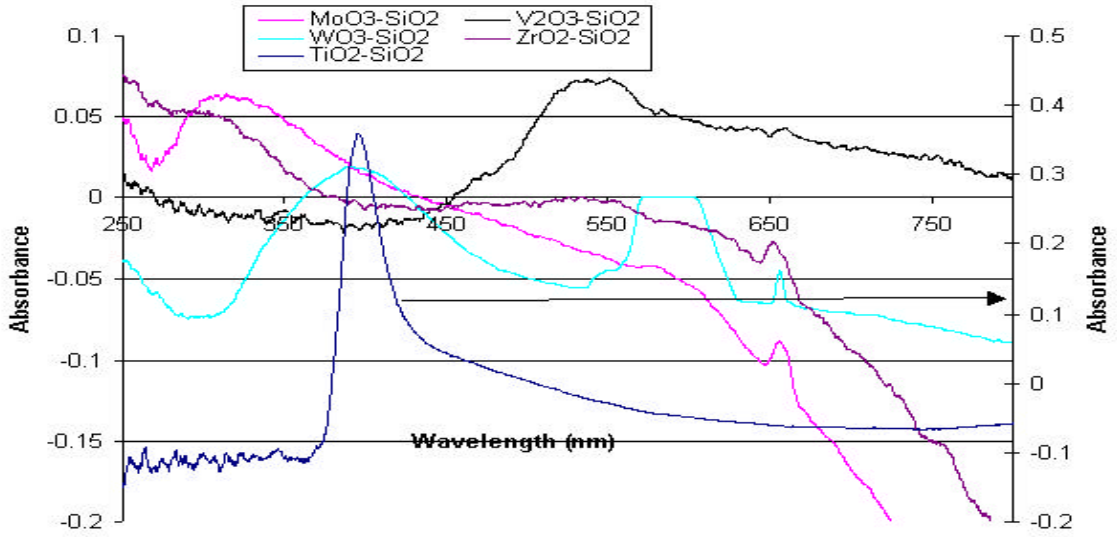

Fig. 3.6.5. UV/Vis absorption spectra of semiconductor metal oxide doped porous silica materials obtained with a fiber optic EW absorption spectrometric method. These colored semiconductor metal oxides give strong absorption signal in UV/Vis region.

Nanometer noble metal particles doped porous silica materials show different colors depending on the element and the method for preparing the nanometer metal particles. These materials usually absorb light in UV/Vis region. The absorption signal can be assigned to the plasmon absorption of the nanometer metal particles inside the composite materials [16]. Fig. 3.6.6 is an example fiber optic EW absorption spectrum of an Ag-SH-SiO_2 nanocomposite material coated on the surface of an optical fiber. This nanocomposite material has a yellow color and shows strong absorption at aroun4 400 nm.

In NIR region, the light transmission behavior of these porous silica optical fibers is similar to that of a pure porous silica optical fiber. The NIR transmission spectra of several doped porous silica optical fibers are shown in Figs. 3.6.7 and 3.6.8

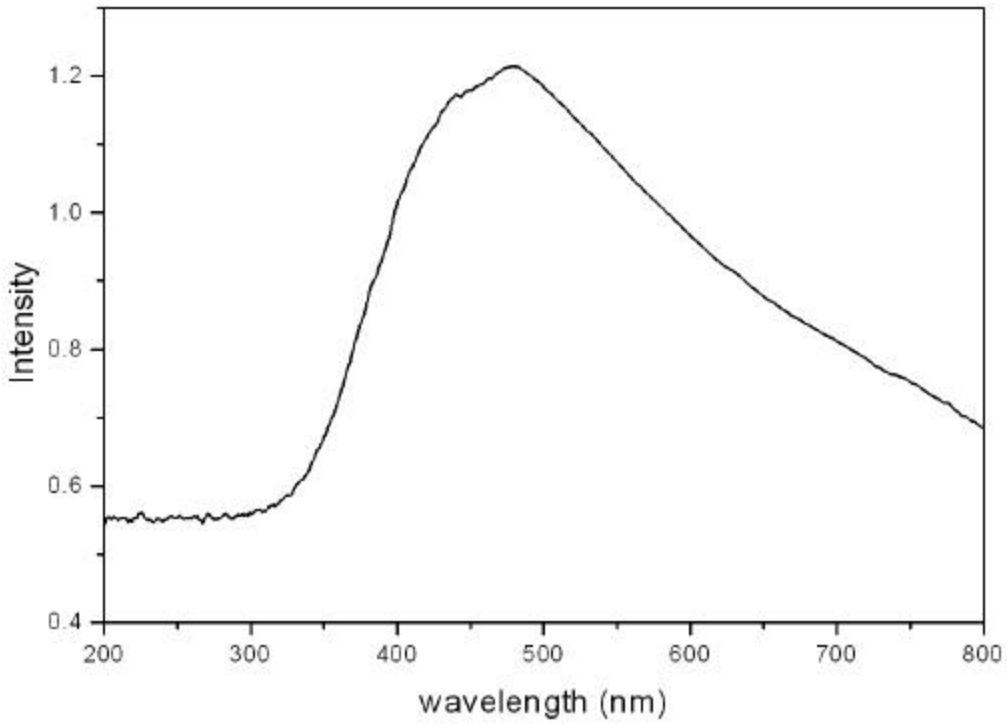

Fig. 3.6.6 An optical fiber EW absorption spectrum of a nanocomposite Ag-SH-SiO_2 material coated on the surface of a silica optical fiber. This material shows a yellow color and strongly absorb light with peak absorption wavelength at around 450 nm. The absorption spectrum with peak wavelength at 477 nm can be assigned to the plasmon absorption of the silver nanoparticles inside the composite coating on the surface of the optical fiber core.

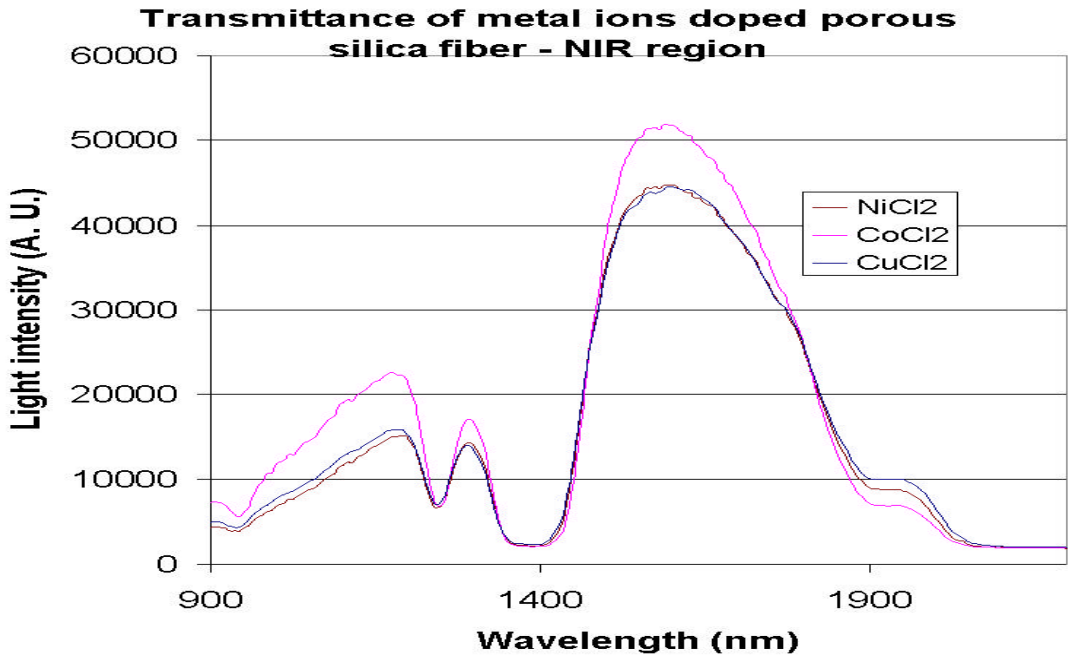

Fig. 3.6.7. Transmission spectra of metal ions doped porous silica optical fibers. The transmission spectrum of such a metal ion doped porous silica optical fiber is similar to that of a pure porous silica optical fiber. This means that the metal ions doped inside the porous silica fiber do not absorb light in the NIR region.

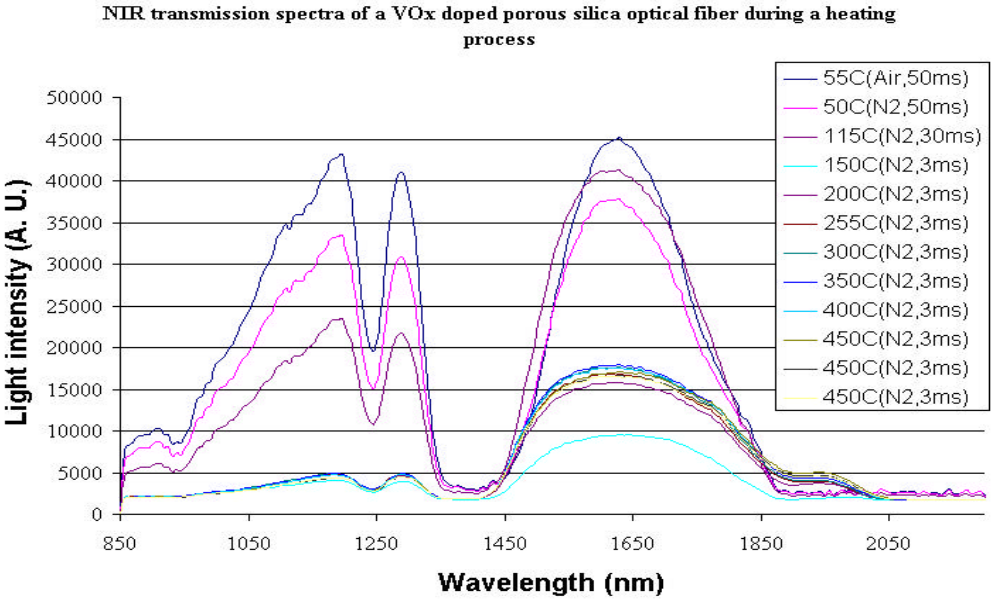

Fig. 3.6.8. Transmission spectra of a VO_2 doped porous silica optical fiber during a heating process. The change of transmission spectrum of such this VO_2 doped porous silica optical fiber is similar to that of a pure porous silica optical fiber in a heating process. This means that the metal oxide doped inside the porous silica fiber do not absorb light in the NIR region.

3.6.3. Optical absorption spectrum of porous silica optical fibers doped with metal ions and metal oxide materials exposed to high temperature gases

Light guiding property of the heat treated porous silica optical fibers exposed to nitrogen gas samples containing trace H_2, CO and moisture have been examined at UV/Vis and NIR regions by using fiber optic spectrometric methods by using the method described in Section 2.6 of this report. During a test, a porous silica optical fiber connected with the gold-jacked fibers housed inside the gas flow cell was heated from room temperature with a 1 hour ramp to 450 ^oC. Nitrogen gas was flowed through the gas cell during the heating process. The temperature of the gas cell was then kept at 450 ^oC, and the composition of gas sample was changed in order to investigate the response of the fiber to different gas component. The composition of tested gas samples is listed in Table 1.

Table 1. The composition of gas samples used in the investigation of the optical properties of sol-gel derived silica fibers

Sample	Gas composition
Sample 1	N_2 (moisture < 1ppm)
Sample 2	N_2 plus 0.1% H_2
Sample 3	N_2 plus 0.5% CO
Sample 4	N_2 plus 0.1% H_2 and moisture (0.x%*, but exact concentration has not measured)
Sample 5	N_2 plus 0.5% CO and moisture (0.x%*, but exact concentration has not measured)

- Moisture was added to the gas sample through bubbling the dry gas through a bottle filled with water. The concentration of water vapor in the obtained gas sample has not measured, but was estimated to be in 0.x% level based on our previous experience.

The efficiency of a pure sol-gel silica fiber for guiding NIR light was not significantly affected when H_2, moisture and CO was added to the N_2 gas stream flowing through the gas cell (Figs. 3.6.9 and 3.6.10). It was expected that moisture added to the gas sample could be absorbed by the porous silica fiber and cuases NIR absorption signal at around 940 nm, 1450 nm and 1900 nm. However, it was found that the absorption of moisture to the porous silica material is not significant at the temperature of 450 ^oC. Both H_2 and CO are optically inert at the tested NIR wavelength region and thus, the existence of these molecules in the gas sample does not affect the light guiding capability of the fiber.

The addition of moisture, H_2 and CO to the nitrogen gas flowing through the gas flow cell does not significantly affect the efficiency of metal ions doped sol-gel silica fibers and metal oxide doped porous silica optical fibers for guiding NIR light. The test results for the $CuCl_2$ doped sol-gel silica fiber and VOx doped sol-gel silica fiber are showing in Figs. 3.6.11 and 3.6.12. It was believed that CO is a reactive gas. The CO added to the high temperature gas sample could reduce Cu(II) to Cu(I) and eventaully to cupper metal. The vanadium oxide in the fiber could also be reduced by CO gas in the high temperature environment. However, test results indicate that these reduction has not

happened. After the test, the fibers were visually examined. It was found that the $CuCl_2$ doped fiber still shows a green color, and the VO_2 doped fiber shows a yellow color while the original VO_2 doped fiber shows a brownish yellow color after heat treatment. A $NiCl_2$ doped sol-gel silica fiber was also tested for the exposure to CO added gas sample. It was found that the color of the fiber changed from green to blue after exposed to the CO containing gas sample at a high temperature.

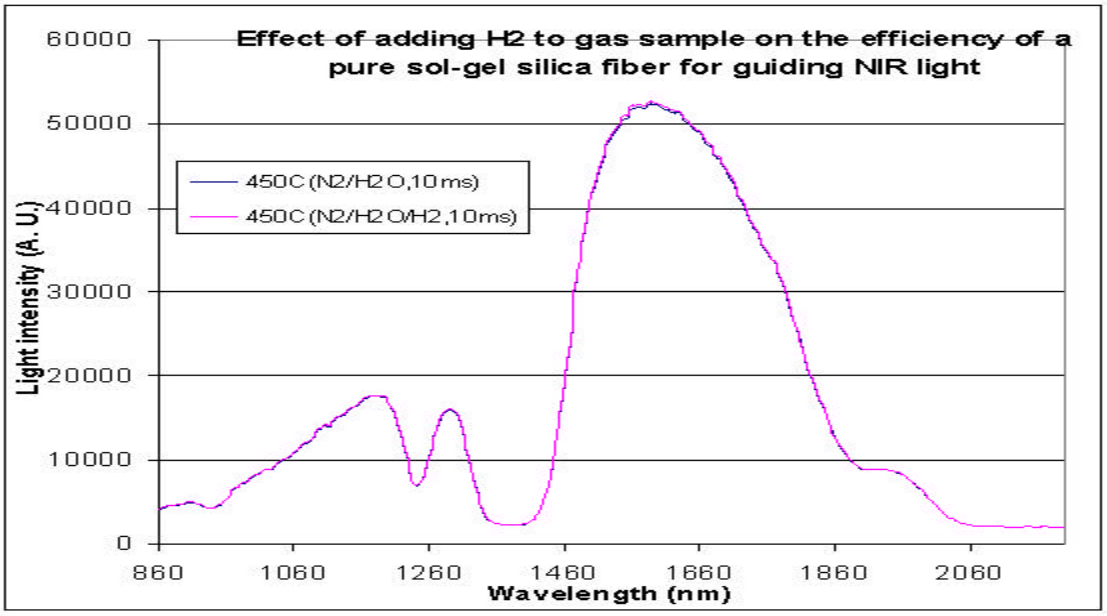

Fig. 3.6.9. NIR transmission spectra of a pure sol-gel silica fiber recorded at 450 ^{o}C. The addition of H_2 gas to the moisture containing N_2 gas sample did not significantly effected the fiber's capability for guiding NIR light in the tested wavelength region.

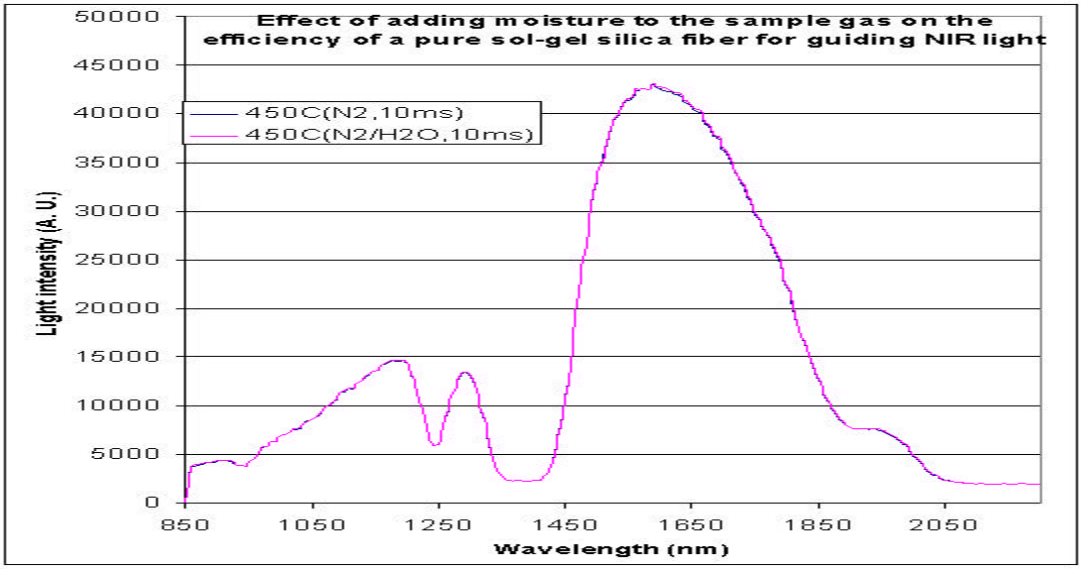

Fig. 3.6.10. NIR transmission spectra of a pure sol-gel silica fiber recorded at 450 ^{o}C. The addition of moisture to a dry N_2 gas sample did not significantly effected the fiber's capability for guiding NIR light in the tested wavelength region.

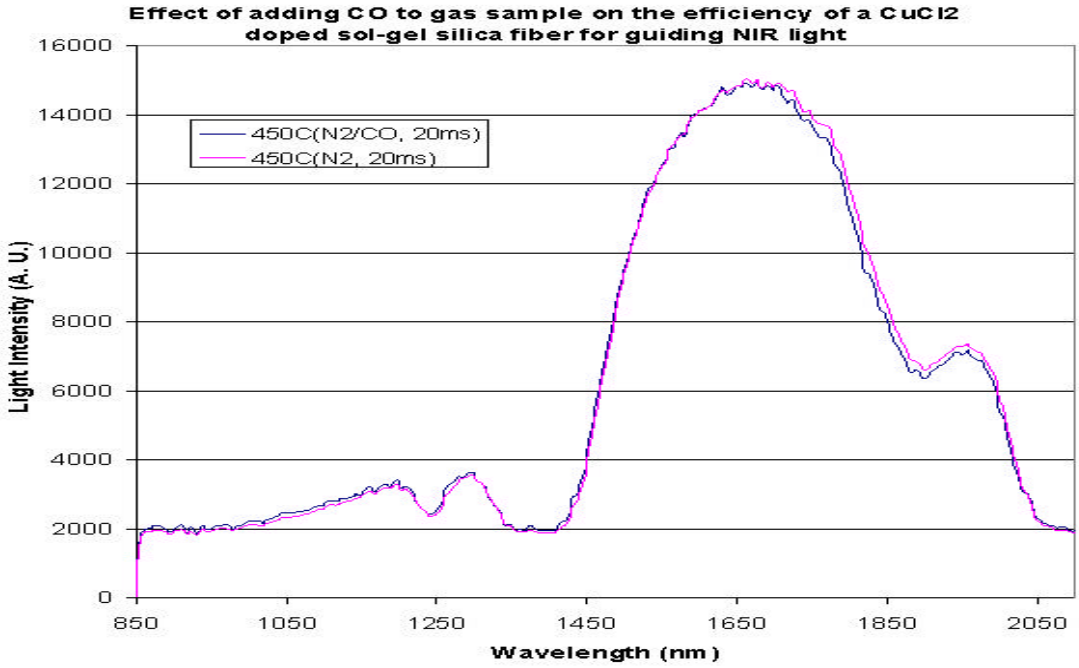

Fig. 3.6.11. NIR transmission spectra of a $CuCl_2$ doped sol-gel silica fiber recorded at 450 ^oC. The exposure of the sol-gel silica fiber to 0.5% CO in a dry N_2 gas sample effected the fiber's capability for guiding NIR light, but not significant.

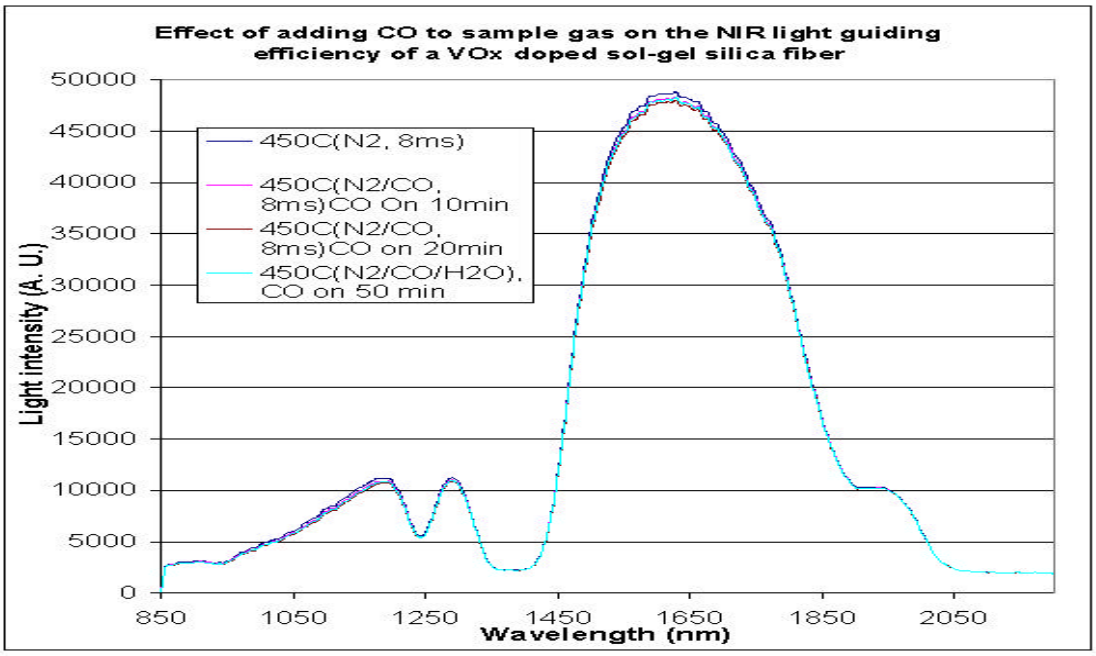

Fig. 3.6.12. NIR transmission spectra of a VO_2 doped sol-gel silica fiber recorded at 450 ^oC. The addition of 0.5% CO to a dry N_2 gas sample flowing through the gas cell slightly decreased the fiber's capability for guiding NIR light in the whole tested wavelength region. The addition of moisture to N_2/CO gas sample did not significantly effect the fiber's capability for guiding NIR light.

The addition of water vapor to the N_2 gas stream flowing through the gas cell slightly increased the efficiency of the pure sol-gel silica fiber for guiding UV/Vis light. The addition of H_2, CO to the N_2 gas stream did not significantly change the behaviour of the fiber for guiding UV/Vis light.

A increase of light guiding efficiency of the $CuCl_2$ doped sol-gel silica fiber at 450 ^oC was observed in UV/Vis region when H_2 gas was added to the gas stream flowing through the gas cell (Fig. 3.6.13). The reason for this change has not understood yet. The effect of adding moisture, CO to the gas stream on the fiber's capability of light guiding in UV/Vis region is not significant. The change of light guiding capability of other metal ions (Co^{2+}, Ni^{2+}, Eu^{3+}) doped porous silica optical fibers exposed to nitrogen gas samples containing moisture, 1% H_2 and 0.5% CO is similar to the $CuCl_2$ doped porous silica optical fiber. The addition of moisture and CO into the N_2 gas sample does not significantly affect the capability of the fibers for guiding light in UV/Vis region. However, the existence of 1%H_2 in the N_2 gas sample causes an increase of lgith guiding capability of these fibers in the UV/Vis region.

A strong optical absorption signal was observed when a Fe^{3+} doped porous silica optical fiber was exposed to a N_2 gas sample contaning trace H_2 at 450 ^oC (Fig. 3.6.14). The behavior of this porous silica optical fiber is much defferent from other metal ions doped porous silica optical fiber.

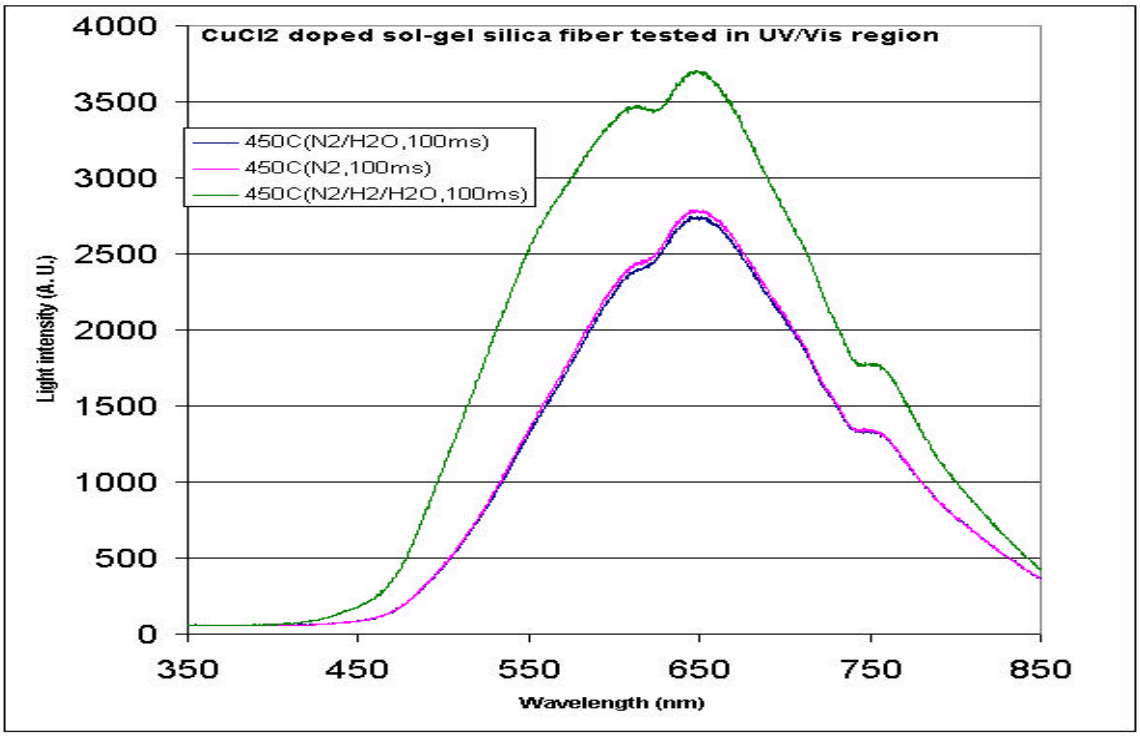

Fig. 3.6.13. An optical transmission spectra of a $CuCl_2$ doped porous silica optical fiber exposed to N_2 gas samples containing moisture and H_2.

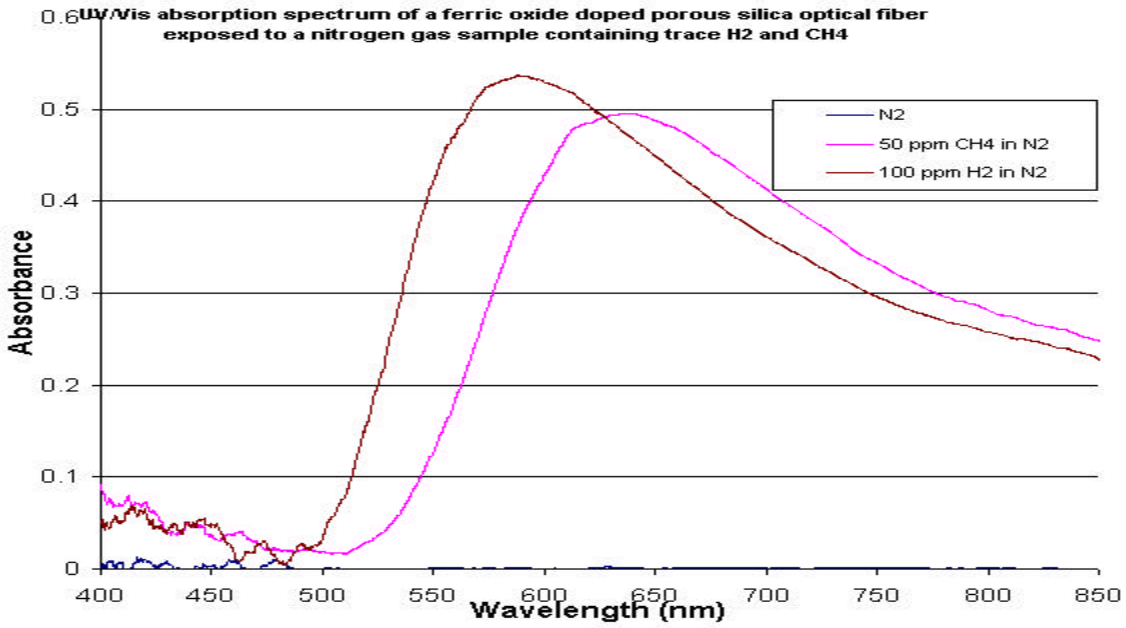

Fig. 3.6.14. UV/Vis optical absorption spectra of a ferric oxide doped porous silica optical fiber exposed to a nitrogen gas sample containing trace H_2 or CH_4. The temperature of the gas sample is 450 ^oC. The absorption peak wavelength for H_2 containing gas and CH_4 containing gas is different, which indicates that this fiber can be used for selective sensing a gas sample in the existence of another gas component in the gas sample.

3.6.4. Optical absorption spectrum of noble metal nanoparticles doped porous silica optical fibers at ambient temperature

The optical properties of silver and palladium particles immobilized sol-gel silica materials on the exposure to hydrogen gas have also been investigated during this report period. It was found that the silver particles immobilized sol-gel silica materials do not respond to hydrogen gas. However, the palladium particles immobilized sol-gel silica materials responded to hydrogen gas. A palladium particles immobilized porous silica material prepared with a Triton X-100 reversed micelle method was made in the form of a fiber. This fiber shows a yellow color when a light beam from a tungsten lamp was guided through the fiber. The fiber's transmittance spectra in the visible and NIR region were recorded as the fiber was exposed to gas samples of nitrogen and 1% hydrogen in nitrogen at room temperature. It was found that in the UV/visible region, the change of gas sample from pure nitrogen to 1% hydrogen in nitrogen does not change the spectrum of the fiber. However, a change of gas sample from pure N_2 to 1% H_2 in N_2 reduced the fiber's capability for guiding NIR light (Fig. 3.6.15). A palladium particles immobilized sol-gel silica material prepared by using the MPTS stabilizer method was coated on the surface of a bent optical fiber core. This coated bent probe was also tested for sensing hydrogen gas at room temperature. It was found that when the gas sample was switched from N_2 to 1% H_2 in N_2, the light intensity guided through the coated bent optical fiber probe was also reduced in the NIR region.

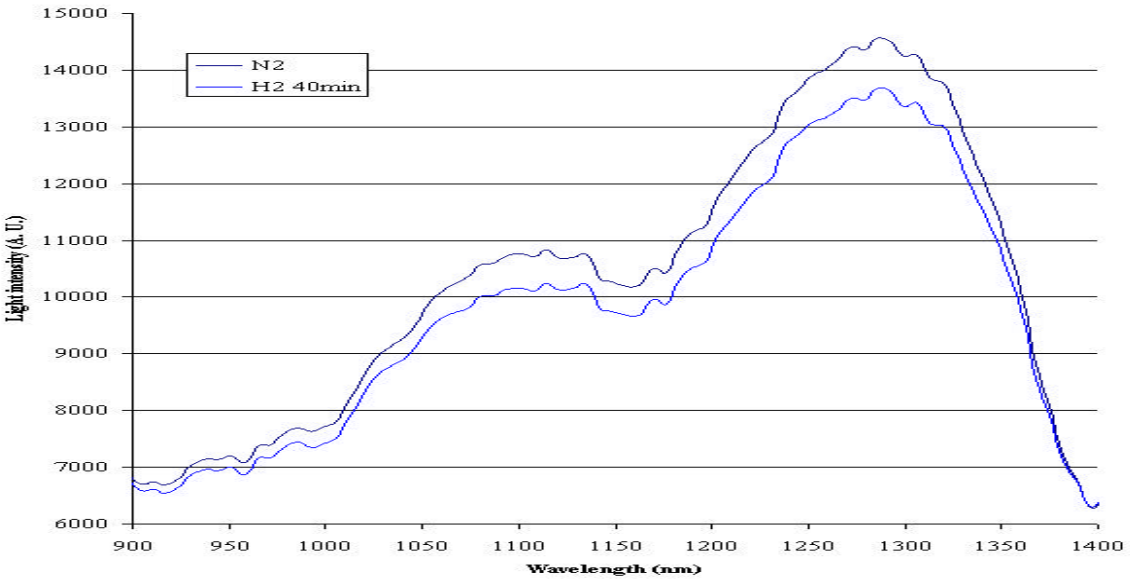

Fix. 3.6.15. Optical response of a nanometer palladium particles doped porous silica fiber to N_2 gas sample containing 1% H_2. The exposure of the Pd partcles doped fiber to trace H2 in the N2 gas causes the attenuation of light intensity guided through the optical fiber.

3.6.5. Optical absorption spectrum of semiconductor metal oxide coatings on the surface of silica optical fibers at high temperatures

At a high temperature, when the gas sample flowing through the flow cell is changed from pure nitrogen to a reducing gas component containing gas sample, it was found that the SnO_2 membranes coated on optical fiber cores has spectroscopic response to this change. Fig. 3.6.16 shows the absorption spectrum of a SnO_2 membrane (thick) coated on a bent optical fiber probe exposed to a 10% H_2 containing nitrogen gas sample. The absorption spectrum was obtained with light intensity guided through the bent optical fiber probe exposed to pure nitrogen gas as a reference. Obviously, the absorption signal is caused by H_2 in the gas sample. The optical spectroscopic response of this SnO_2 membrane to the H_2 containing gas sample at other temperatures has also been investigated. It was found that the membrane start to response to H_2 from <400 ^oC. In the tested temperature range, the probe responded to H_2 up to 900 ^oC. There is a shift of peak absorption wavelength when the temperature increased from 400 ^oC to 900 ^oC. At lower temperature, the peak absorption wavelength is in the UV region. With the increase of temperature, the peak absorption wavelength gradually moved to visible region.

The spectroscopic response of the two SnO_2 membranes to CH_4 (5% in N_2) and CO (10% in N_2) in UV/Vis region was also investigated. It was found that both of the membranes do not response to these two gases in UV/Vis region at the tested temperature region (Fig. 3.6.16). These preliminary results illustrate the possibility of developing a H_2 selective fiber optic sensor for monitoring H_2 at high temperature gas. This sensor could be very useful for monitoring of hydrogen in coal gasification and syngas reforming processes.

The spectroscopic response of the SnO_2 membranes coated on the optical fiber cores to H_2, CH_4 and CO at high temperatures in NIR region has also been investigated.

It was found that all the three reducing gases cause a negative absorption signal in the NIR region (Fig. 3.6.17). The peak absorption wavelength for CO and H_2 is at around 1900 nm. However, the peak absorption wavelength caused by CH_4 is at around 1600 nm. Therefore, the NIR absorption signal at 1900 nm can be used to detect the total amount of H_2 and CO, and the NIR absorption signal at 1600 nm can be used to sense CH_4.

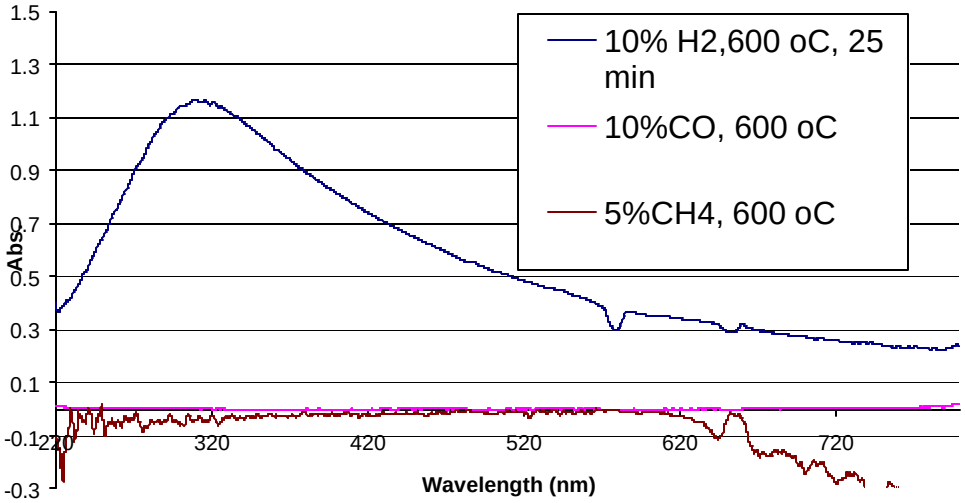

Fig. 3.6.16. Spectroscopic responses of a SnO_2 membrane coated on a bent optical fiber core exposed to gas samples containing different reducing gases at 600 ^oC. The spectra indicate that this membrane responses to H_2 in the UV/Vis region, but is insensitive to CH_4 and CO in this wavelength region.

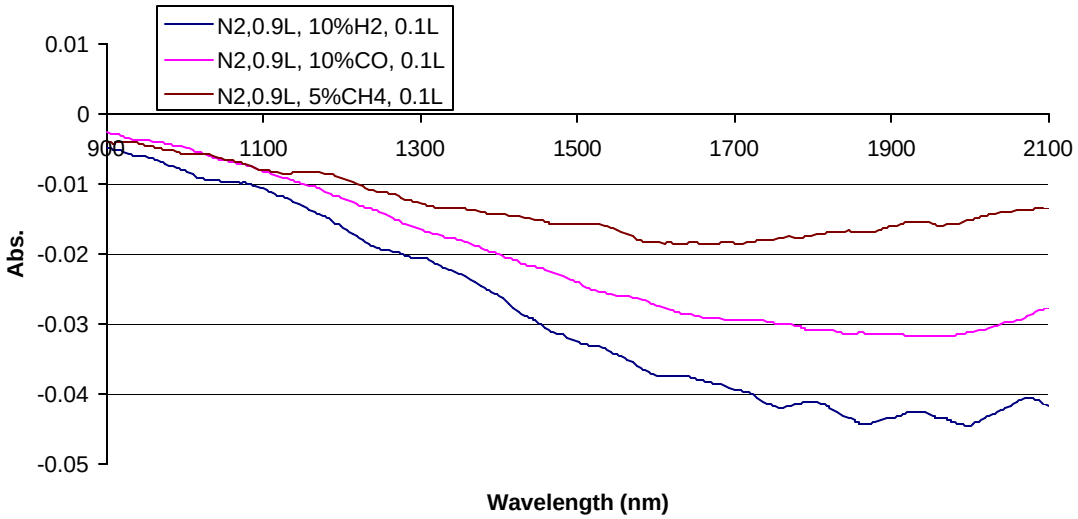

Fig. 3.6.17. NIR absorption spectra of a SnO_2 membrane (thick) coated on a bent optical fiber core exposed to gas samples containing different reducing gas (H_2, CH_4, CO) at 600 ^oC.

3.7. Fluorescence emission property of sol-gel derived materials at room temperature and high temperatures

3.7.1. Fluorescence emission spectrum of pure porous silica materials at ambient temperature and high temperatures

Porous silica materials have been reported emits fluorescence when excited with UV light sources [17-19]. The fluorescence spectrum of a porous silica material varies depending on the microstructure of the material, the inner surface composition of the pores inside the porous silica. In this project, the fluorescence property of porous silica materials has been investigated with UV LEDs as excitation light source. At ambient temperature, most of the heat-treated pure porous silica materials emit blue or green colored fluorescence. However, fluorescence emission has not observed for most of the porous silica which has not treated at high temperature. It was believed that the heat-treatment process changed the surface oxygen content of the porous material, which generate fluorophore centers in the materials.

The fluorescence property of a porous silica optical fiber at 450 ^{o}C was investigated by using the 370 nm UV LED as an excitation source. The recorded fluorescence spectrum shown in Fig. 3.7.1 was believed the result of several fluorescence spectra added together. The peak wavelengths of the three fluorescence spectra are 500 nm, 545 nm, 557 nm, 575 nm, 589 nm, 614nm and 644 nm, respectively. These fluorescence spectra from porous silica materials have also been separately observed by other research groups [17-19].

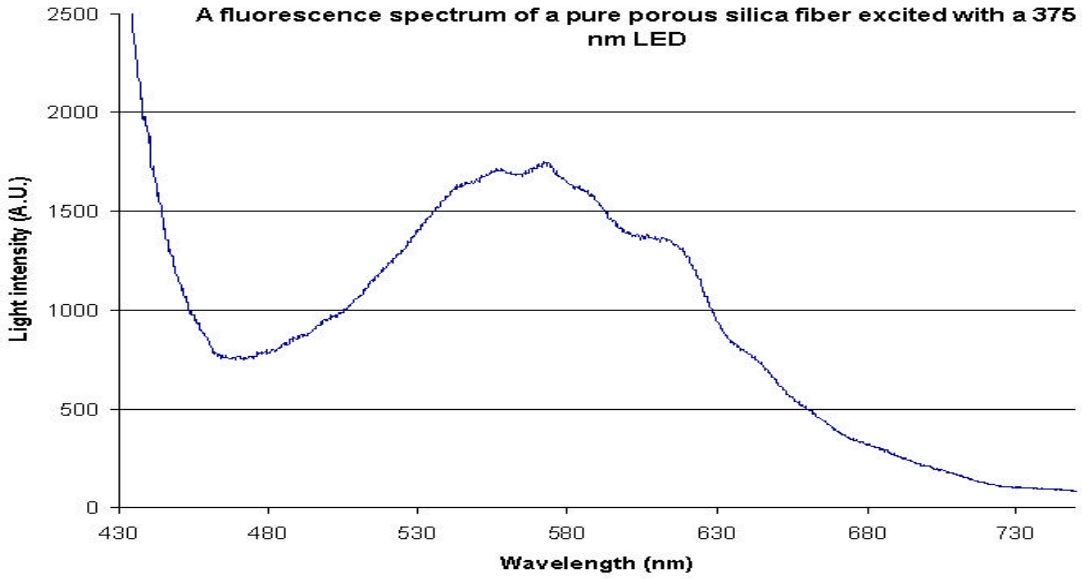

Fig. 3.7.1. An optical transmittance spectrum of a pure sol-gel silica optical fiber obtained at 450 ^{o}C. Light from the 370 nm LED was fed into one end of the optical fiber and light emerged from the opposite end of the fiber was detected with the optical fiber compatible UV/Vis spectrometer. A second spectrum with peak intensity at around 580 nm is observed in additional to the original LED light (peak intensity at around 370 nm). This second spectrum is the fluorescence signal emitted from the porous silica optical fiber. This fluorescence spectrum is the result of several spectra (500 nm, 545 nm, 557 nm, 575 nm, 589 nm, 614nm and 644 nm, respectively) added together.

3.7.2. Fluorescence emission spectrum of porous silica optical fibers doped with metal ions and metal oxide materials exposed to high temperature gases

The impurity doped into a porous silica material as metal ions, metal oxides or nanometer metal particles could affect the fluorescence emission property of porous silica materials. In our experiments, it was found that the doping of transitional metal ions into a porous silica material could quench some of the fluorescence spectrum observable in pure porous silica optical fiber. Fig. 3.7.2 is an example. This spectrum was obtained by exciting the fluorescence of a cadmium ions doped porous silica optical fiber with a 375 nm LED. Compared with the fluorescence spectrum of pure porous silica fiber, the spectrum of this metal ions doped fiber is simpler. Some of the fluorescence spectrum observed in the pure porous silica fiber disappeared in this fiber.

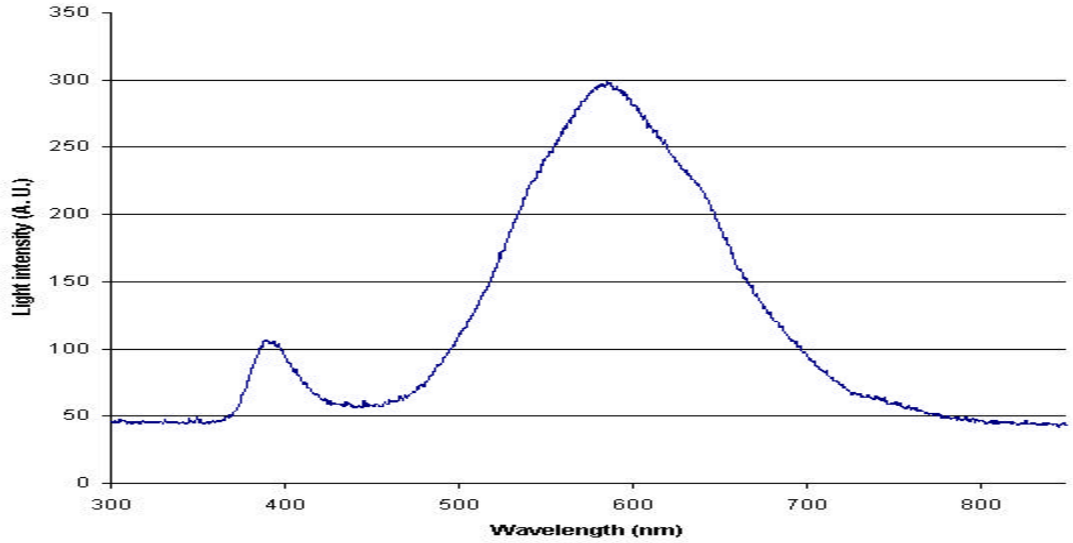

Fig. 3.7.2. An optical transmittance spectrum of a cadmium ions doped sol-gel silica optical fiber obtained at 450 ^{o}C. Light from the 370 nm LED was fed into one end of the optical fiber and light emerged from the opposite end of the fiber was detected with the optical fiber compatible UV/Vis spectrometer. Compared with the fluorescence spectrum of pure porous silica fiber, the spectrum of this metal ions doped fiber is simpler. Some of the fluorescence spectrum observed in the pure porous silica fiber disappeared in this fiber.

If a doped metal ion itself emits fluorescence, then, the fluorescence property of the doped silica material is dominated by the doped metal ions. One example of such material is the rare-earth metal ions doped porous silica materials. The rare-earth metal ions are well known fluorophores both in solution and in solid phases when excited with a UV light source.

In this work, Er^{3+} and Eu^{3+} ions doped porous silica fibers were prepared by using TEOS as a silica precursor with the sol-gel process described in the experimental section as an example. The formed doped porous silica optical fibers were tested for recording their fluorescence spectrum by using a 375 nm LED as an excitation source. The obtained FL spectra are shown in Fig. 3.7.3. The Eu^{3+} doped silica fiber emits fluorescence with peak emission wavelength at 615 nm, which can be assigned as the f-f electronic transition $5D^0$-$7F^2$ [20]. In this spectrum, the FL signal from poorus silica

fiber itself is still observable as a broad spectrum. The Er^{3+} doped porous silica fiber gives very strong FL signal with peak emission wavelengths at 507 nm, 580 nm, 606 nm 691 nm and 746 nm, respectively.

The fluorescence property of such a silica material is very useful for sensing temperature of corrosive gas samples at high temperature. First, the material can work at high temperature. Second, the mateial is resistant to corrosive gases. Third, the fluorescence intensity or life-time is affected by temperature. A temperature sensing technique with this Eu^{3+} doped porosu silica fiber as a transducer will be described in next section of this report.

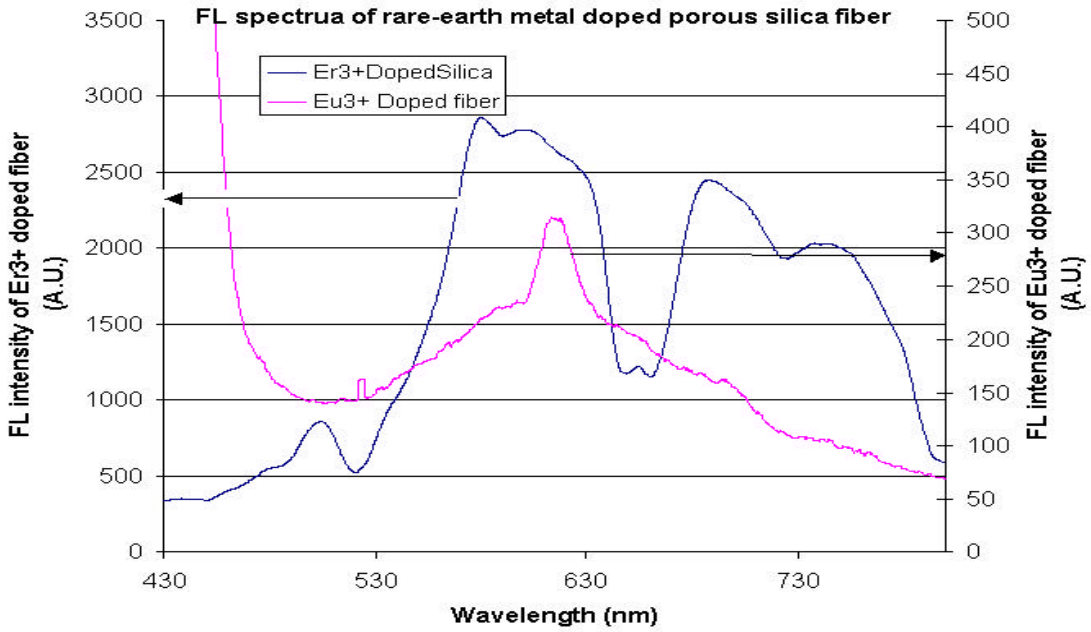

Fig. 3.7.3. Fluorescence emission spectra of Er^{3+} and Eu^{3+} doped porous silica optical fibers excited with a 375 nm LED. These rare-earth metal ions doped inside the porous silica optical fibers give intensive fluorescence signal. These rich fluorescence signals are useful for sensing temperatures at corrosive gas environment.

3.8. Fiber optic temperature sensing techniques with sol-gel derived refractive materials as transducers for applications in IGCC process control

Coal gasification and syngas reforming/cleaning in IGCC processes involves a series of high temperature/high pressure gas reactions [21,22]. In situ, real time information of the reaction system, such as gas composition, temperature, pressure, is critical for controlling the reactions to processes at optimized reaction conditions in order to achieve highest efficiency and lowest environmental pollution.

Because temperature affects the physical/chemical properties of almost every material, many techniques have been proposed/developed to sense/monitor temperature for different applications. For example, the linear expansion of silica optical fibers has been used in designing Bragg grating based optical fiber temperature sensors and Fabry-Pérot interference based temperature sensors [23-25]. The electric resistance of metals and semiconductors is temperature dependent, and temperature sensors have been designed based on measuring the resistance or conductivity of metal and semiconductor materials. Thermocouples are another class of temperature sensors based on the measurement of electrical properties. A thermocouple is based on the measurement of a voltage drop across dissimilar metals, which is temperature dependent. Temperature also affects the resonant frequency of piezoelectric crystal, and temperature sensors based on this phenomenon have also been reported [26].

Optical techniques are very useful for high temperature measurement/monitoring. Plank's model of blackbody emission forms the base of temperature measurement through monitoring infrared emission from a target sample. This technique has been widely used for monitoring high temperature furnaces used in industrial processes, such as glass-making, steel-making. Optical emissions or absorption by free radicals, atoms or ions in high temperature gas or plasma have been used to remote monitor temperature of high temperature gases related to combustion system, discharge and rocket tail plume [27-29].

Fluorescence spectrometry is another optical technology used to sense temperature [30-33]. An excited fluorophore molecule can drop back to its ground state through radiation emission (fluorescence) or through collision with another molecule. The fluorescence emission and collision processes are in equilibrium for a system at certain temperature. The change of temperature will change the frequency of collision, and therefore shifts the equilibrium of the two processes. This shift results in a change of fluorescence intensity and the fluorescence lifetime. Temperature sensors based on the monitoring of fluorescence intensity and the detection of fluorescence lifetime have been developed. These techniques can be used for high temperature sensing if appropriate fluorophore is used.

It is very difficult to use conventional temperature sensing techniques described above in coal gasification, syngas reforming/cleaning process due to the nature of the reaction environment. A coal gasification system is usually operated at a temperature as high as 1000 ^{o}C. The gas component, such as H_2O, O_2, CO, NH_3, H_2S, are very reactive at high temperature. Many widely used temperature-sensing devices, such as thermocouple, can not be used because the gas components are corrosive to the metal alloy at this high temperature environment. The optical techniques, such as blackbody emission, optical absorption/emission spectrometry of radicals, atoms, ions and molecules, are applicable for high temperature sensing. However, the dusty nature of the

gasification system makes the application of traditional optical techniques in this system extremely difficult. The particles in the gasifier will not only interfere with light transmission, but also corrode optical windows, which are needed in traditional optical methods for sending light into such a system or collecting optical signal from such a system.

In this work, two temperature-sensing techniques by using sol-gel derived refractive materials as transducers have been investigated. These materials are corrosive-resistant, can work in the corrosive gas environment of coal gasification and syngas cleaning processes. Preliminary test results illustrated the potential of application of these sensing techniques for monitoring high temperatures in IGCC processes.

3.8.1. Thermochromic properties of sol-gel derived refractive semiconductor metal oxide materials and temperature sensing at high temperatures

This first technique is based on the thermochromic property of sol-gel derived refractive metal oxides (TiO_2, ZrO_2, V_2O_3, MoO_3, WO_3). These metal oxides were immobilized into silica material with the sol-gel techniques described in the experimental section. The formed composite materials were coated on the surface of gold-jacketed silica optical fibers to form testing optical fiber probes. The temperature responses of these thermochromic nanocomposite membranes coated on the bent optical fiber probes were investigated by using fiber optic EW absorption spectrometry. In such a test, a coated bent optical fiber probe was inserted into a ceramic tube, which was set inside a temperature controllable split furnace as shown in Fig. 2.7. The two ends of the optical fiber probe were connected to an optical fiber compatible light source and an optical fiber compatible UV/Vis spectrometer, respectively. One end of the ceramic tube was open during the test, and therefore, the tube was air-filled. The temperature of the furnace was controlled to increase step-by-step from room temperature to 1000 ^oC. The EW absorption spectrum of the probe was recorded at each temperature step during the heating process with light intensity guided through the bent optical fiber probe at room temperature as a reference. The recorded responses are described below:

A: The response of TiO_2-SiO_2 membrane to temperature

The recorded EW absorption spectra of the TiO_2-SiO_2 membrane during a heating process are shown in Fig. 3.8.1. The TiO_2-SiO_2 coating gives an EW absorption spectrum with peak wavelength at around 390 nm. The peak absorption wavelength of the absorption spectrum is red-shifted during the heating process. It was found that when the absorbance signal at 396 nm was monitored, the relationship of the EW absorbance signal with temperature from 22 ^oC to 340 ^oC can can be described by an equation: $Abs = 3*10^{-06}T^{2.12}$ (Fig. 3.8.2). If monitored at 433 nm, as shown in Fig. 3.8.3, the absorbance signal linearly increases with temperature from 244 ^oC to 368^oC. The best application range of this probe for monitor temperature is from 22 ^oC to 340 ^oC.

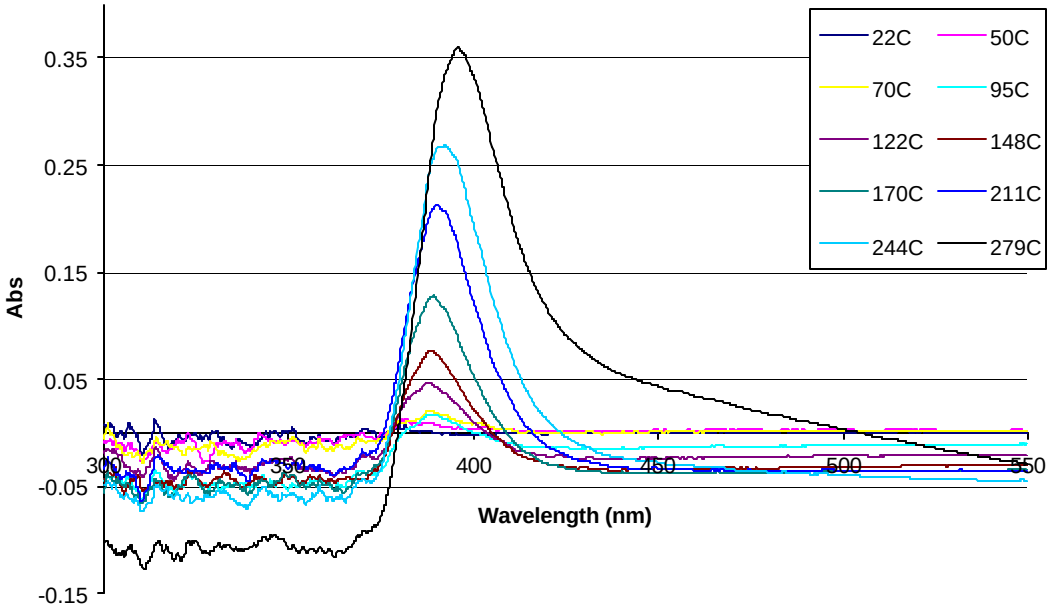

Fig. 3.8.1. EW absorption spectra of a TiO_2-SiO_2 nanocomposite membrane coated on a bent optical fiber probe exposed to different temperatures.

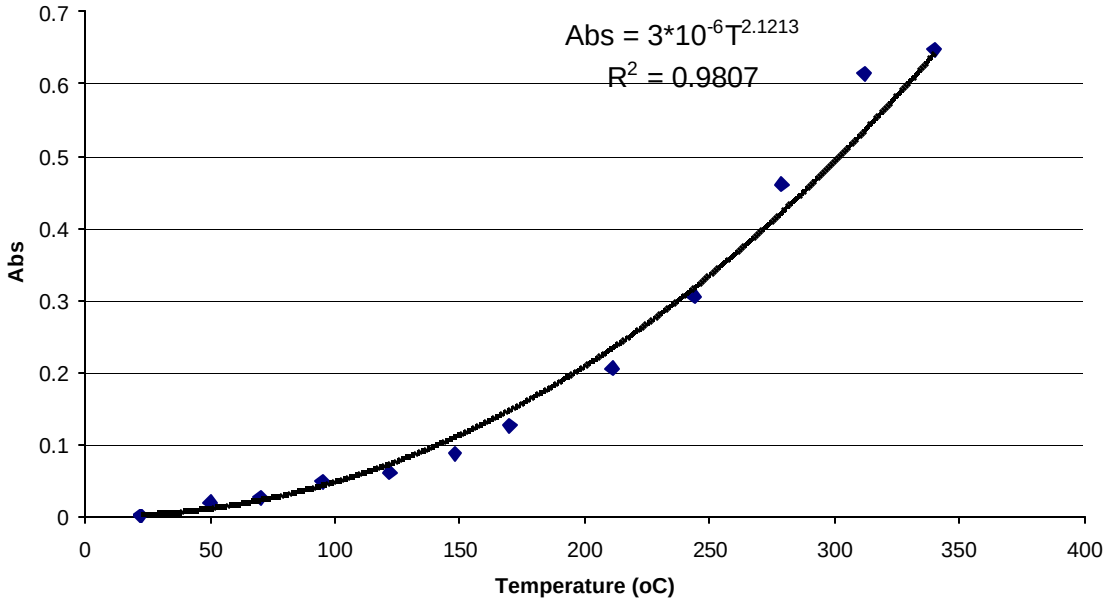

Fig. 3.8.2. The relationship of EW absorbance signal (detected at 396 nm) of a TiO_2-SiO_2 nanocomposite membrane coated on a bent optical fiber probe with temperature from 22 ^oC to 340 ^oC.

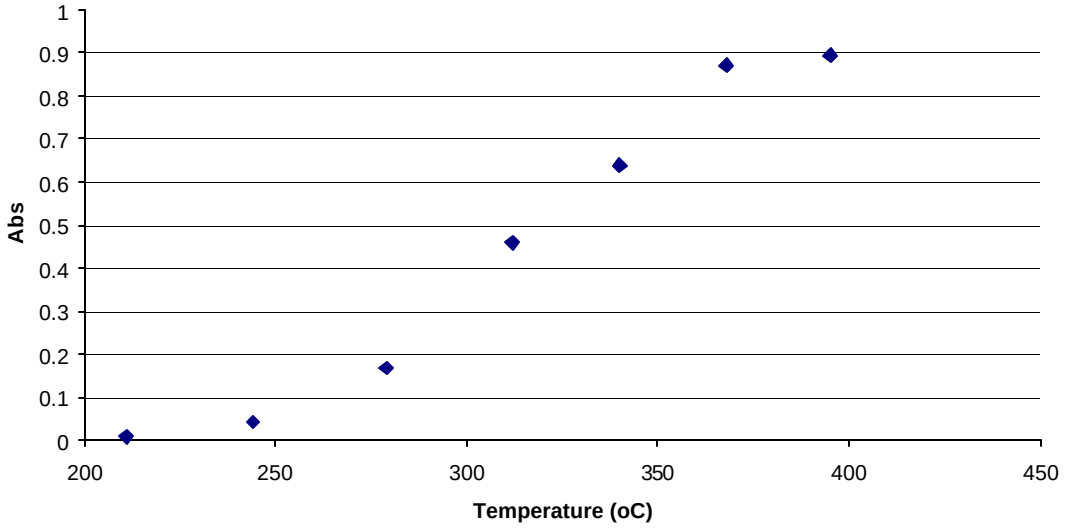

Fig. 3.8.3. The relationship of EW absorbance signal (detected at 428 nm) of a TiO_2-SiO_2 nanocomposite membrane coated on a bent optical fiber probe with temperature from 210 ^oC to 400 ^oC.

B: The response of ZrO_2-SiO_2 membrane to temperature

The recorded EW absorption spectra of ZrO_2-SiO_2 nano composite membrane coated on the surface of a bent optical fiber probe during a heating process are shown in Fig. 3.8.4. The ZrO_2-SiO_2 composite membrane shows a broad absorption spectrum in UV region with peak absorption wavelength at around 306 nm. With the increase of temperature, the EW absorbance signal in UV region increased. The absorbance signal detected at 306 nm has a linear relationship with temperature from 400 ^oC to 900 ^oC (Fig. 3.8.5).

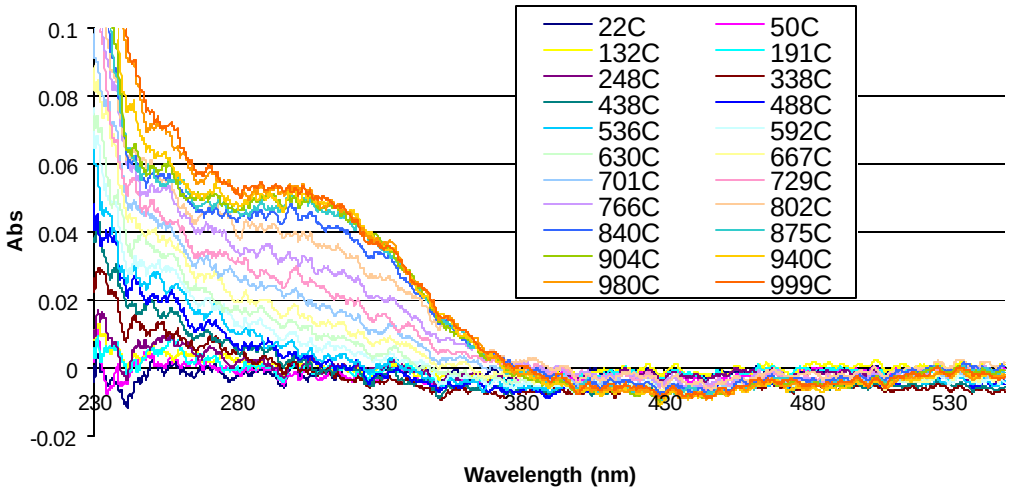

Fig. 3.8.4. EW absorption spectra of a ZrO_2-SiO_2 nanocomposite membrane coated on a bent optical fiber probe exposed to different temperatures.

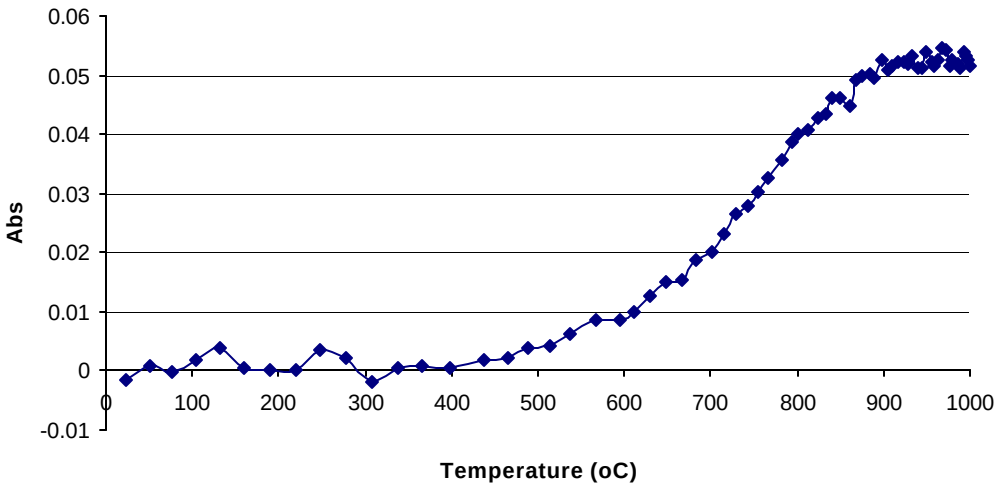

Fig. 3.8.5. The relationship of EW absorbance signal (detected at 306 nm) of a ZrO_2-SiO_2 nanocomposite membrane coated on a bent optical fiber probe with temperature from room temperature to 1000 ^oC.

C: The response of V_2O_3-SiO_2 membrane to temperature

The recorded EW absorption spectra of V_2O_3-SiO_2 membrane coated on the surface of a bent optical fiber probe during a heating process are shown in Fig. 3.8.6. The V_2O_3-SiO_2 composite membrane shows an absorption spectrum in visible region with peak absorption wavelength at around 550 nm. With the increase of temperature, the absorbance signal in increased. The absorbance signal detected at 550 nm has a linear relationship with temperature in the range from 179 ^oC to 623 ^oC (Fig. 3.8.7).

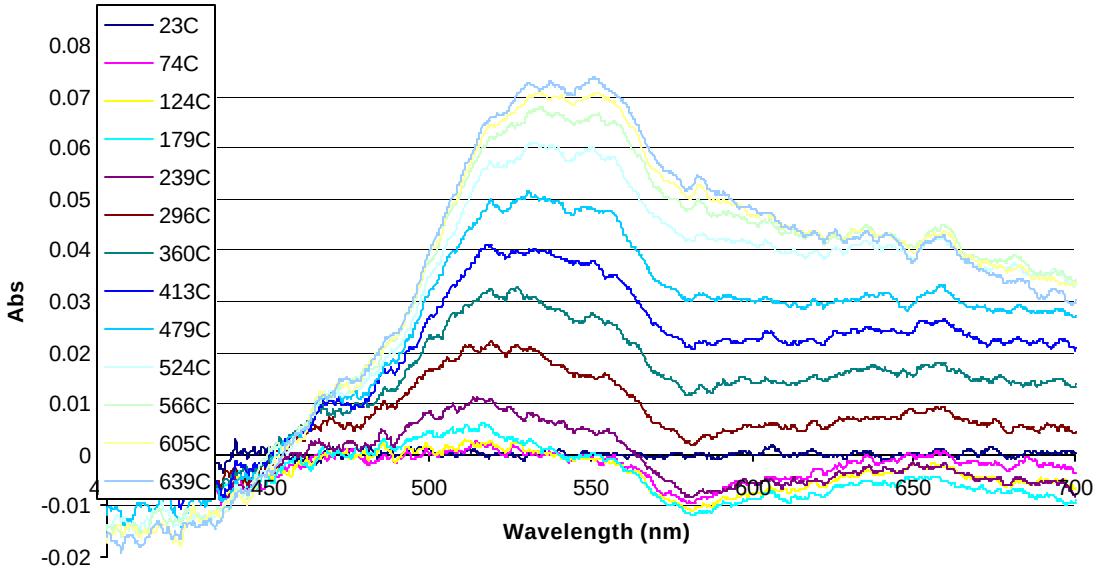

Fig. 3.8.6. EW absorption spectra of a V_2O_3-SiO_2 nanocomposite membrane coated on a bent optical fiber probe exposed to different temperatures.

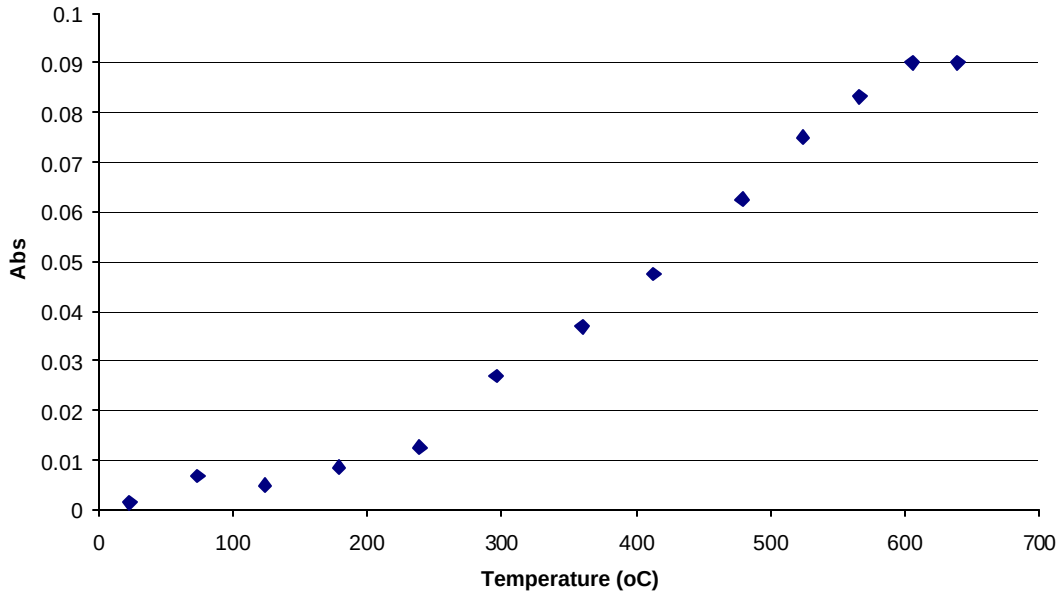

Fig. 3.8.7. The relationship of EW absorbance signal (detected at 550 nm) of a V_2O_3-SiO_2 nanocomposite membrane coated on a bent optical fiber probe with temperature from room temperature to 600 ^oC.

D: The response of W_2O_5-SiO_2 membrane to temperature

During the heating process, the W_2O_5-SiO_2 composite membrane showed an absorption spectrum in UV region with peak absorption wavelength at around 398 nm. With the increase of temperature, the absorbance signal in increased. The absorbance signal at 398 nm has a linear relationship with temperature in the range from 200 ^oC to 1000 ^oC, (Fig. 3.8.8).

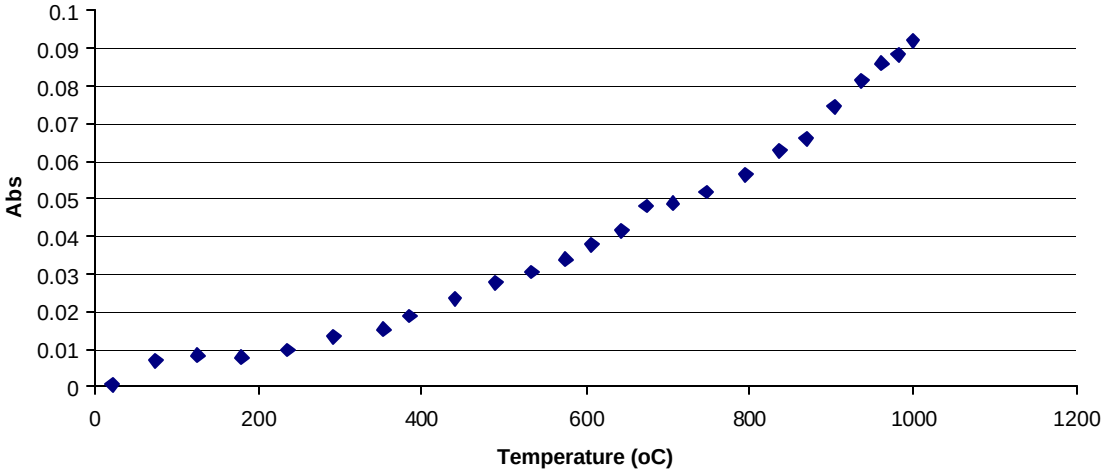

Fig. 3.8.8. The relationship of EW absorbance signal (detected at 398 nm) of a W_2O_5-SiO_2 nanocomposite membrane coated on a bent optical fiber probe with temperature from room temperature to 1000 ^oC.

E: The response of Mo_2O_5-SiO_2 membrane to temperature

During the heating process, the Mo_2O_5-SiO_2 composite membrane showed an absorption spectrum in UV region with peak absorption wavelength at around 315 nm. With the increase of temperature, the absorbance signal in increased. The absorbance signal at 315 nm has a linear relationship with temperature in the range from 50 ^oC to 350 ^oC, (Fig. 3.8.9).

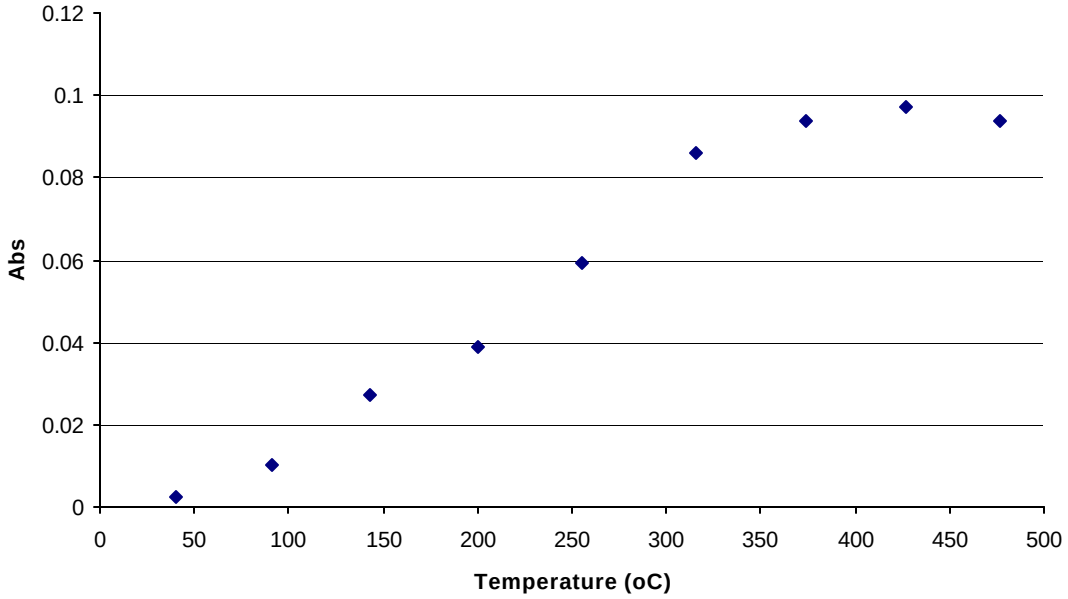

Fig. 3.8.9. The relationship of EW absorbance signal (detected at 315 nm) of a Mo_2O_5-SiO_2 nanocomposite membrane coated on a bent optical fiber probe with temperature from room temperature to 500 ^oC.

3.8.2. Conclusion of composite refractive thermochromic material for temperature sensing

The thermochromic property of TiO_2-SiO_2, ZrO_2-SiO_2, V_2O_3-SiO_2, Mo_2O_5-SiO_2 and W_2O_5-SiO_2 nanocomposite materials has been investigated for sensing temperature in high temperature region. The nanocomposite TiO_2-SiO_2 can be used to monitor temperature from room temperature to 340 oC. The ZrO_2-SiO_2 nanocomposite membrane can be used to monitor temperature from 400 ^oC to 900 ^oC. The nanocomposite V_2O_3-SiO_2 can be used to monitor temperature from 200 ^oC to 600 ^oC. The W_2O_5-SiO_2 nanocomposite membrane can be used to monitor temperature from 200 ^oC to 1000 ^oC. The Mo_2O_5-SiO_2 nanocomposite membrane can be used to monitor temperature from 50 ^oC to 350 ^oC. The applicable temperature region of these refractive thermochromic materials is coincident with the operation temperature region of coal gasification, syngas reforming/cleaning operation. The high temperature applicable sensing technique is also expected to be useful in monitoring solid oxide fuel cell, which is usually operated in the temperature region from 700 ^oC to 1000 ^oC.

3.8.3. Fluorescence properties of rare-earth metal ions doped porous silica optical fibers and temperature sensing at high temperatures

Fluorescence spectrometry is another optical technology used to sense temperature [30-33]. An excited fluorophore molecule can drop back to its ground state through radiation emission (fluorescence) or through collision with another molecule. The fluorescence emission and collision processes are in equilibrium for a system at certain temperature. The change of temperature will change the frequency of collision, and therefore shifts the equilibrium of the two processes. This shift results in a change of fluorescence intensity and the fluorescence lifetime. Temperature sensors based on the monitoring of fluorescence intensity and the detection of fluorescence lifetime have been developed. These techniques can be used for high temperature sensing if appropriate fluorophore is used.

In one work of this project, an Eu^{3+} doped silica fiber was prepared by using the sol-gel process described in the experimental section of this report. The fluorescence intensity of the Eu3+ ions doped in the porous silica optical fiber was used as an indicator of temperature. The Eu^{3+} doped silica fiber was connected with two gold-jacketed silica optical fiber with a ceramic fiber holder developed in this project. The fiber holder with the silica fibers was deployed into a ceramic tube, which is inserted into a split tube furnace as described above. Light from a 375 nm LED was focused into the free end of one of the gold-jacketed silica optical fiber by using a quartz lens. The light signal emerged from the free end of the second gold-jacketed silica optical fiber was monitored with an optical fiber compatible UV/Vis spectrometer. During testing the response of the Eu^{3+} doped silica fiber to temperature, the split furnace was heated from room temperature to 500 ^{o}C step-by-step, and the optical intensity injected into the spectrometer was monitored.

The obtained fluorescence spectra of the Eu^{3+} doped silica fiber during the heating process are shown in Fig. 3.8.10. With temperature increasing, the fluorescence intensity signal decreased. The relationship of fluorescence intensity at 615 nm with temperature in the tested region from 80 ^{o}C to 500 ^{o}C is shown in Fig.3.8.11.

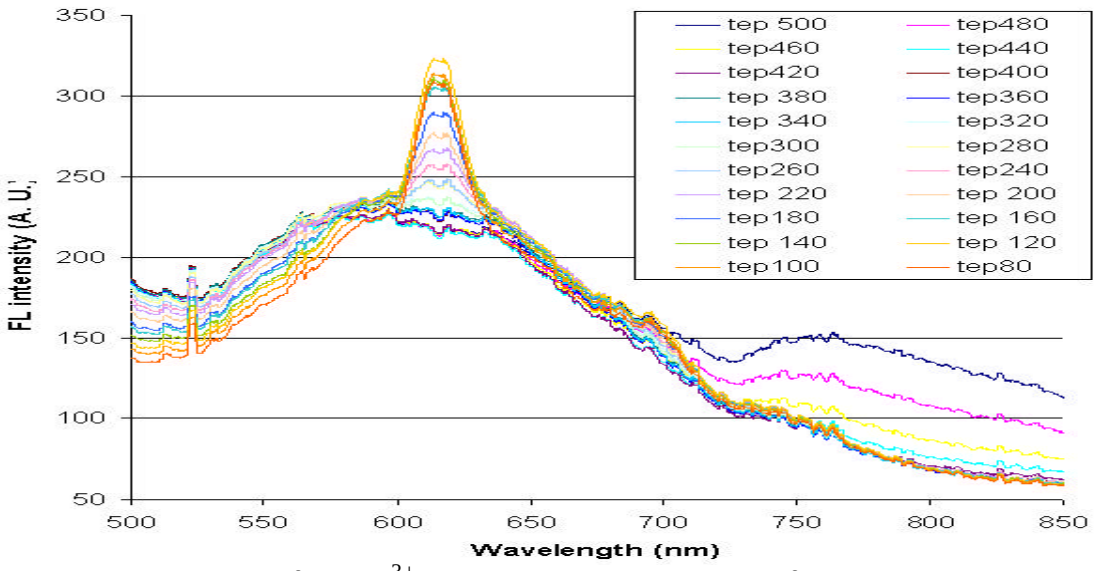

Fig. 3.8.10. FL spectra of an Eu^{3+} doped porous silica optical fiber exposed to a N_2 gas sample of different temperatures. A 375 nm LED was used as an excitation source in obtaining these spectra.

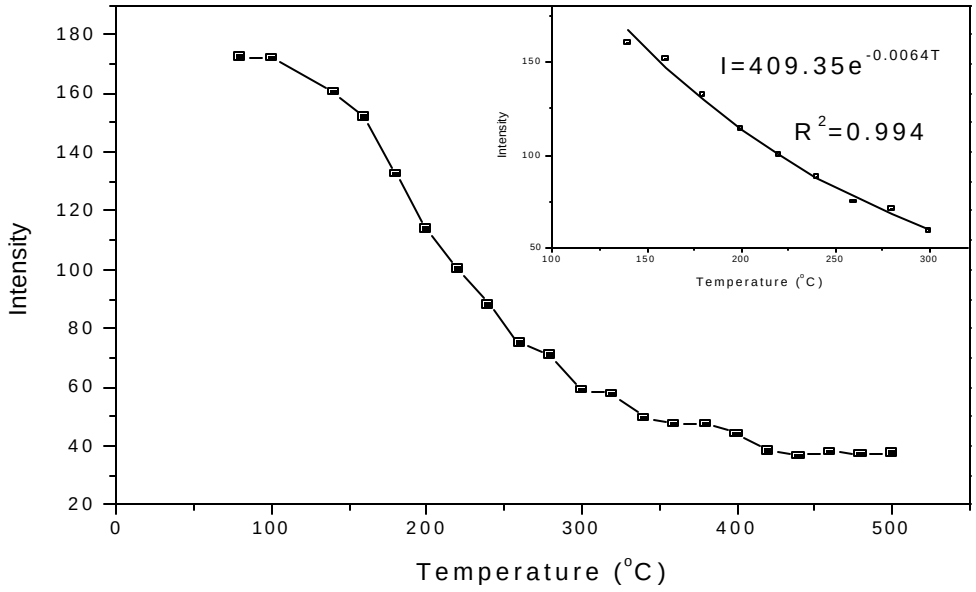

Fig. 3.8.11. The relationship of the fluorescence intensity emitted from an Eu^{3+} doped silica fiber with temperature.

It can be found out that in the temperature range from 140 ^{o}C to 300 ^{o}C, the relationship of fluorescence intensity and temperature follows the equation (3.8.1):

$$I=409.35e^{-0.0064T} \qquad (3.8.1)$$

A linear calibration curve for this temperature range can be obtained by using the attenuation of the fluorescence signal in dB as a sensing signal [11]. dB is defined as equation (3.8.2)

$$dB = 10*\lg I_{140^{o}C}/I \qquad (3.8.2)$$

From equation (3.8.1) and (3.8.2), we can get the linear relationship of dB and temperature in the temperature range from 140 ^{o}C to 300 ^{o}C as,

$$dB=0.0278T-3.890 \qquad (3.8.3)$$

With the increase of temperature, the fluorescence signal decreased. The relationship of fluorescence intensity at 615 nm with temperature in the tested region from 100 ^{o}C to 500 ^{o}C is shown in Fig. 3.8.11.

In summary, a temperature sensor applicable for monitoring temperature from 100 oC to 500 oC can be developed by using a Eu3+ doped porous silica optical fiber as a temperature indicator. A simple LED was used as an excitation light source and a photodiode with a band pass filter can be used as a detector to monitor the fluorescence intensity signal. Compared to fluorescence lifetime based temperature detection techniques, this sensor is much simpler in structure and low-cost.

3.9. Optical fiber ammonia sensors using sol-gel derived porous silica materials for sensing trace ammonia at ambient temperature and high temperature gas samples

In IGCC processes, nitrogen-containing compounds in coal are converted to ammonia in the gasification. The concentration of ammonia in coal-derived syngas can be as high as 3000 ppm [34]. Ammonia is an air pollutant. In addition, it is also a reactive gas component, can cause damage to the power generation infrastructure which using the coal-derived syngas as a fuel [34]. Therefore, ammonia has to be eliminated before sending the syngas to a power generation unit, and thus, a technique for monitoring the concentration of ammonia in the syngas during syngas purification process is needed.

Present state-of-the-art techniques for detecting ammonia in gas samples include ion mobility spectroscopy [35], gas chromatography [36,37], ultraviolet (UV) absorption spectrometry [38,39], near infrared (NIR) absorption spectrometry [40,41] and chemiluminescence techniques [42,43]. The chemiluminescence techniques are simple in instrument structure and low cost in operation. However, this is an indirect method. It needs an NH_3-to-NO conversion technique to convert NH_3 to NO [42]. The produced NO is then detected with an ozone chemiluminescence (CL) technique [43]. This technique is sensitive, can be used to detect ammonia in a gas sample to ppb level. However, several factors, such as the matrix of the gas present with ammonia, the length of the time of the converter in use, the temperature of the converter, etc. affect the NH_3 to NO conversion process. Periodic calibration is required with zero gas and NH_3-calibration gases applied at the point of sample extraction to correct the conversion efficiency. In addition, the major components of coal-derived syngas, such as CO_2, H_2O, CO, also affect the CL detection.[10] It is difficult to use this technique for detecting ammonia in coal-derived syngas, because the gas sample from this source is too "dirty".

Gas chromatographic separation coupled with mass spectrometric detection is sensitive for detecting trace gas component in complex gas samples [36,37]. However, this method requires sophisticated instruments. In addition, this technique also has limitation in analyzing "dirty" samples due to the limitation of GC separation capacity and possible adsorption of compounds on the surface of GC column, transmitting tube and vacuum system of mass spectrometer. Ion mobility spectroscopy can be used to detect/monitor trace ammonia in complex gas samples [35]. However, problems similar to that in GC-MS also exist in this technique.

UV and NIR absorption spectrometric techniques have been reported for monitoring ammonia in gas stream [38-41]. But both the spectrometric techniques have problems in practical applications. Ammonia molecules in gas phase absorb light with wavelength around 200 nm. This absorption phenomenon can be used to detect ammonia in gas phase. However, in coal-derived syngas there are a lot of other compounds, such as carbon dioxide, carbon monoxide, moisture, volatile and semi-volatile organic molecules, which also have strong absorption at around 200 nm. These compounds in stack gas strongly interfere with ammonia detection by UV absorption method. Ammonia in gas phase can also be detected with near IR (around 1.5 μm) absorption technique. This technique also suffers the interference from co-existent species in coal-derived syngas. In addition, expensive, sophisticated instruments are required for both of the absorption techniques.

We have reported two optical fiber sensors for continuous monitoring ammonia in gas streams [44,45]. Organic reagents (pH indicators) and silver nanoparticles immobilized in porous silica were used in the reported sensors. In this work, tow ammonia sensing techniques were developed. The first technique uses a $CuCl_2$ doped porous silica optical fiber as a transducer for sensing trace ammonia at high temperatures. The second sensor uses a silver nanometer particles immobilized porous silica optical fiber as a transducer for sensing trace ammonia for application in ambient temperature.

3.9.1. An optical fiber ammonia sensor using a $CuCl_2$ doped porous silica optical fiber as a transducer for monitoring trace ammonia in high temperature gas samples

A: Sensing mechanism

Ammonia can react with cupper ions (Cu^{2+}) to form a blue colored complex, $[Cu(NH_3)_4]Cl_2$ which absorbs light with peak absorption wavelength at t around 560 nm. This reaction has been used for a long time in traditional analytical chemistry for detecting trace Cu2+ ions in aqueous solutions. In aqueous solution, the reaction

$$Cu^{2+} + 4NH_3 == Cu(NH_3)_4{}^{2+} \qquad (3.9.1)$$

yields an equilibrium constant (K)

$$K = [Cu(NH_3)_4{}^{2+}]/[Cu^{2+}][NH_3]^4 \qquad (3.9.2)$$

equal to $3.9x10^{12}$ [46].

The resulting complex has a peak absorption around 560 nm and this complexation reaction has been used in traditional UV/Vis absorption spectrometry for the determination of copper ions in water through the addition of excess ammonia into the sample solution [47].

In the sensor of this work, this reaction was employed for detecting trace ammonia in a gas sample. The complex formation reaction was carried out in a porous silica optical fiber instead in an aqueous solution. $CuCl_2$ was doped into the porous silica optical fiber with the sol-gel techniques described in the experimental section of this report. Ammonia molecules in a gas sample diffuse into the porous silica optical fiber and react with the doped Cu^{2+} ions to form the $[Cu(NH_3)_4]Cl_2$ inside the porous silica optical fiber. Through monitoring the optical absorption signal of the porous silica optical fiber, the concentration of the complex formed inside the fiber can be detected. The concentration of ammonia in a gas sample is in dynamic equilibrium with the concentration the ammonia-cupper complex inside the fiber. Therefore, the concentration of ammonia concentration in a gas sample can be detected through detecting the absorption signal of the Cu^{2+}doped porous silica optical fiber.

B: Sensor structure

The optical fiber ammonia sensor of this work consists of a short piece of the $CuCl_2$-doped porous silica optical fiber, which is connected with two gold-jacketed silica optical fibers, a light source and an optical fiber spectrometer. The sol-gel silica optical fiber was connected with the golden-jacketed optical fibers by using a laboratory made ceramic holder with method described in the experimental section of this report. In

assembling the fiber optic sensor, two 400/440/510 μm (core/cladding/jacket diameter) gold jacketed silica optical fibers (Fiberguide Industries, Stirling, NJ) were first prepared by etching the gold jacket from the fiber ends via aqua-regia (3:1 HCl:HNO_3). Next, one side of each gold jacked fiber was inserted into a 1 cm piece of 700 μm ID/850 μm OD fused silica capillary (Polymicro Technologies, Phoenix, AZ). A short piece (3.5 cm) of the treated $CuCl_2$-doped sol-gel silica fiber was then placed inside both pieces of fused capillary, forming a continuous fiber path. The resulting fiber assembly was placed in the groove of the laboratory made optical fiber holder and stabilized using the holding plates and screws (Fig. 3.9.1). This setup allowed light to travel from a light source through the sensor and to a detecting element without the use of any glue, which could break down under the high temperatures of use for this sensor.

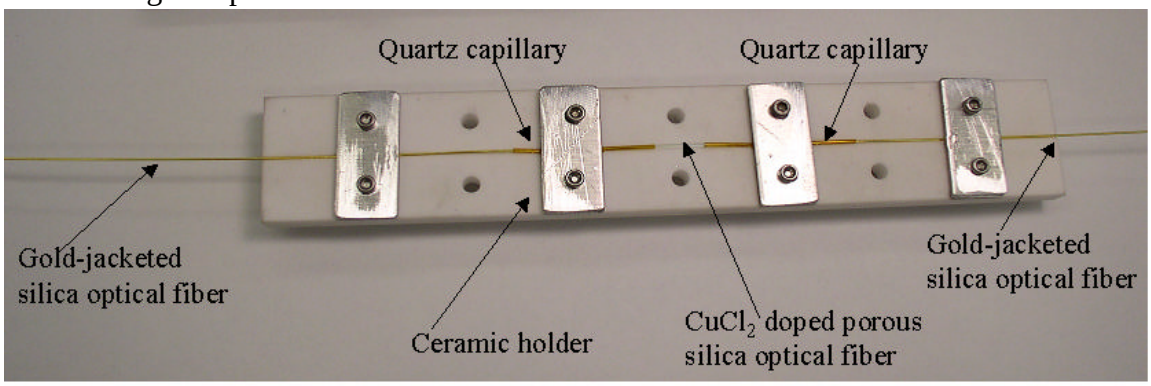

Fig. 3.9.1. A picture of a fiber optic sensor head of this work fixed in a ceramic sensor holder. The $CuCl_2$ doped sol-gel silica optical fiber is connected with two gold-jacketed silica optical fibers. The connected fibers were fixed on the sensor head holder with plates and screws.

C: Testing the sensor

In testing the sensor, the split tube furnace was initially heated to the appropriate testing temperature at an average rate of 100 °C/hour with compressed air flowing through the flow cell. Once the desired temperature was reached, air gas samples of various concentrations of NH_3 were introduced into the chamber, and UV/Vis absorption spectrum of the $CuCl_2$-doped optical fiber was monitored with the fiber optic spectrometer. Temperature fluctuations of ±20 °C were observed when the furnace was held at a specific temperature and these changes resulted in a slight increase or decrease in the optical response of the sensor. Therefore, each measurement was taken at the peak of the optical signal to ensure consistency and reproducibility of test results. The sensor was allowed to equilibrate with the surrounding gas environment for 20 min before each measurement was taken.

D: UV/Vis absorption spectrum of a $CuCl_2$ doped porous silica optical fiber exposed to an air sample containing trace NH_3

The absorption spectrum of the $Cu[NH_3]_4^{2+}$ complex formed in a porous sol-gel silica optical fiber was investigated with experimental set-up as described in the Experimental section. In this experiment, the optical fiber compatible deuterium/tungsten combo lamp was used as a light source and the optical fiber compatible UV/Vis spectrometer was used for recording the absorption spectra. The split tube furnace was used to control the temperature of the reaction environment. An air gas sample

containing trace ammonia (37.5 ppm) was flown through the quartz flow cell and the absorption spectrum of the $CuCl_2$-doped porous sol-gel silica optical fiber was recorded with pure air as a reference sample. The recorded absorption spectra were shown in Fig. 3.9.2. The spectra were recorded after 20 minutes exposure of the $CuCl_2$-doped sol-gel silica optical fiber to the sample gas. As indicated in these spectra, the peak absorption wavelength of the formed complex in the sol-gel silica optical fiber is around 540 nm. The observed difference in the peak absorption wavelength of the complex in a sol-gel silica optical fiber with the reported peak absorption wavelength [47] of the complex in an aqueous solution is caused by the error of instrument wavelength calibration. The UV/Vis absorption spectrum of the complex in an aqueous solution recorded with our optical fiber compatible spectrometer is shown in Fig. 6. The peak absorption wavelength of this complex is actually the same either the complex exists in an aqueous solution or in a sol-gel silica optical fiber.

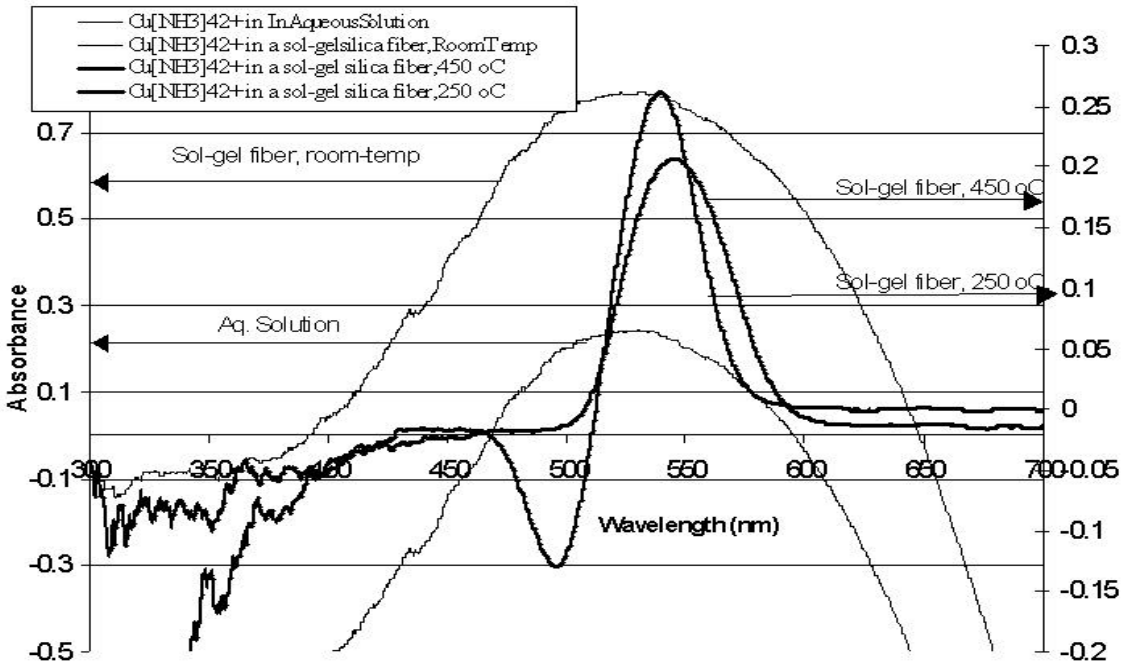

Fig. 3.9.2. UV/Vis absorption spectra of $Cu(NH_3)_4^{2+}$ complex in water and porous sol-gel silica optical fiber of different temperatures.

E: Thermal equilibration of $Cu(NH_3)_4Cl_2$ formation and reversibility of the fiber optic sensor for ammonia sensing at high temperature

Although the formation of the copper-ammonia complex is reversible, the dynamic equilibrium is very slow at room temperature and too long for sensor applications. However, metal coordinating compounds are usually unstable at high temperature if an extra ligand does not co-exist with the complex. Therefore, $Cu(NH_3)_4^{2+}$ can be decomposed to release ammonia molecules at elevated temperatures (300 °C) [48]. This decomposition process is rapid. Therefore, if the copper ion doped sensor is heated to a temperature above 300 °C, the NH_3 in the complex will be released and the absorption signal will return to the baseline.

It is commonly accepted that metal coordinating compounds are unstable at high temperatures and thermogravimetric data indicate that most metal coordinating compounds will be decomposed if heated to a temperature higher than 300 °C [48]. However, in thermogravimetric studies, the coordinating compound is usually heated with air or pure nitrogen in the gas phase of equilibrium with the complex. Therefore, the concentration of the ligand in the gas phase is almost zero. Under such conditions, the equilibrium of the complex formation moves to the direction of decomposition. The metal coordinating compound can actually be stable if there is ligand existing in gas phase in equilibrium with the complex. S. Tao and T. Kumamaru studied the stability of 8-hydroxyquinoline complexes of some transitional metals, and found that the 8-hydroxyquinolinates of B(III), Cr(III), Nb(III), V(III), Zr(IV) are stable at a temperature as high as 900 °C [49-51]. These coordinating compounds can be vaporized together with the ligand using a high temperature furnace without decomposition.

The significant of the equilibrium of metal complex with its ligand in a high temperature gas to the present work of ammonia sensor development is that ammonia in a high temperature gas stream can react with copper ions doped in a porous silica fiber to form a complex. The reaction is reversible depending upon the concentration of ammonia in the gas phase. Therefore, a reversible sensor can be constructed to continuously monitor ammonia in a high temperature gas stream.

Figure 3.9.3 shows the time response of the absorbance signal of a $CuCl_2$-doped sol-gel silica fiber sensor detected at 545 nm with 7.5 ppm ammonia added into the gas stream at the starting point of the recording. The absorbance signal increased with time and reached a maximum after 20 minutes. At 90 min, the ammonia gas was turned off resulting in the decomposition of the complex and the absorbance signal returning to the baseline, clearly indicating the reversible nature of the complex at elevated temperatures.

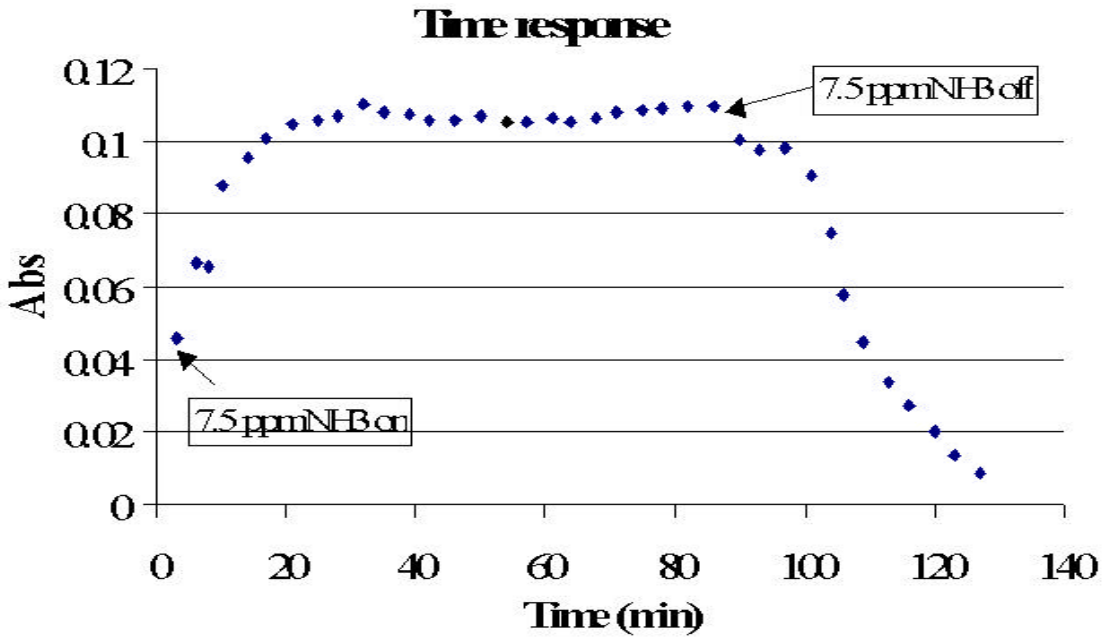

Fig. 3.9.3. Time response of $CuCl_2$ doped porous silica optical fiber ammonia sensor exposed to an air gas sample containing 7.5 ppm NH_3.

F: Quantitatively monitoring ammonia concentration in a high temperature air stream with $CuCl_2$-doped sol-gel silica fiber sensor

Quantitative detection of ammonia in a high temperature air stream with a $CuCl_2$-doped sol-gel silica fiber sensor of this work is based on the following. First, the concentration of the copper-ammonia complex inside the fiber can be determined using fiber optic UV/Vis detection (Beer's law). Second, the concentration of the copper-ammonia complex in the sol-gel silica fiber is in equilibrium with the concentration of ammonia in the gas phase, as described above in Equation 3.9.1.

Figure 3.9.4 shows the absorption spectra of the sol-gel fiber sensor with different concentrations of ammonia in an air stream at a temperature of ~450 °C. The absorbance at 545 nm has a linear relationship with the logarithm of ammonia concentration in the gas phase as seen in Fig. 3.9.5. This calibration curve is believed to deviate from the normal Beer's law because the copper ions in the sol-gel silica fiber are distributed on the inner surface of the pores inside the silica fiber. The reaction of ammonia with copper ions inside the fiber therefore follows a Langmuir single layer absorption isotherm, which indicates that the concentration of the copper-ammonia complex inside the porous material has a logarithmic relationship with that of gaseous ammonia in contact with the porous material.[28] The detection limit of the sensor was determined to be 0.3 ppm based on the three times the standard deviation of the baseline.

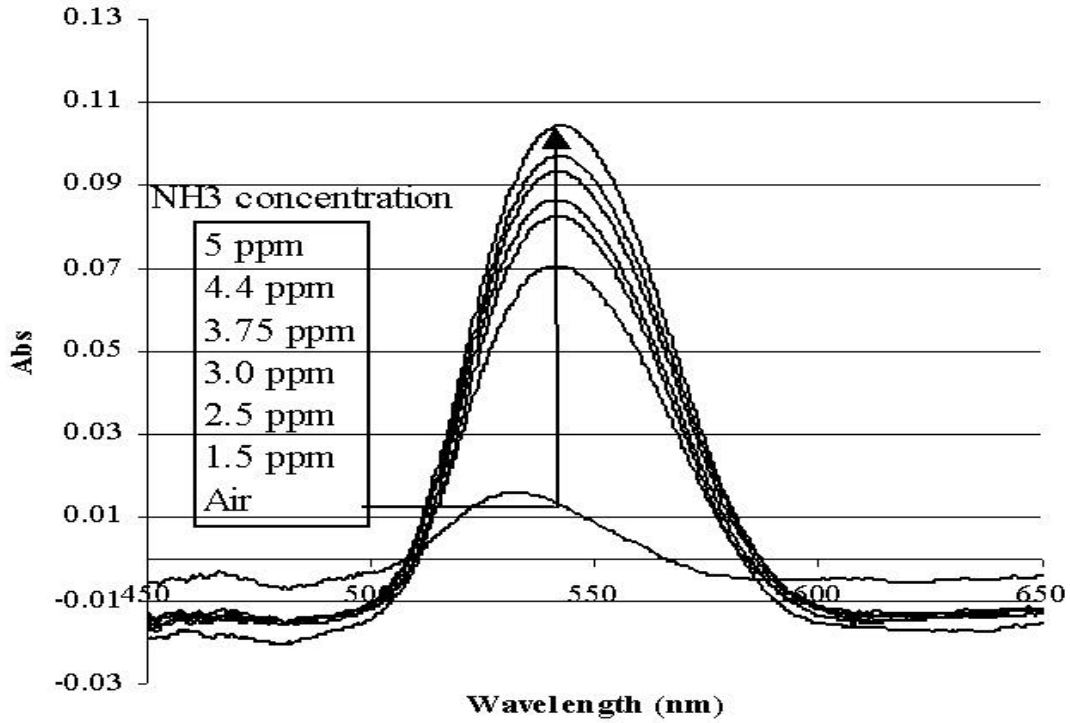

Fig. 3.9.4. Response of the Cu^{2+} doped porous silica optical fiber to gas sample containing NH_3 of different concentration.

G: Effect of gas temperature on calibration

The formation of $Cu[NH_3]_4^{2+}$ in the porous silica optical fiber is also affected by temperature. The complex formation is an exothermic reaction. With the increase of reaction temperature, the equilibrium shifts toward the decomposition of the complex.

Therefore, it is expected that the sensitivity of the fiber optic sensor of this work for sensing ammonia depends on the temperature of the gas sample. Calibration curves of the sensor at different gas temperatures were determined and the test results are shown in Fig. 3.9.5. A decrease in sensitivity was observed with an increase in temperature.

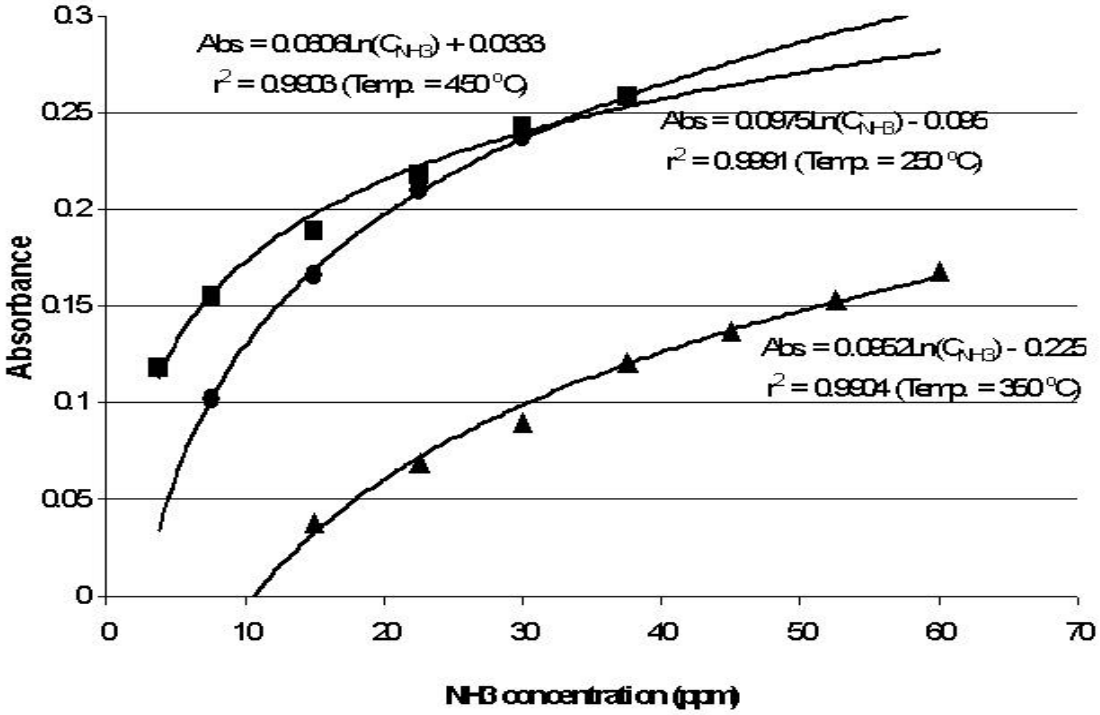

Fix. 3.9.5. Effect of temperature on the calibration of the Cu^{2+} doped porous silica optical fiber for sensing trace NH_3 in gas samples.

H: Effect of other gases on the sensor for sensing ammonia

The effect of several gases, such as moisture, CO_2, H_2S, SO_2, NO_2, on the sensor for detecting ammonia has also been investigated. In the tested range, it was found that the existence of moisture up to 4% and CO_2 up to 10% in the gas sample does not interfere with the sensor for sensing ammonia. However, the existence of H_2S, SO_2, NO_2, was found interfering with the fiber optic sensor for sensing ammonia. The existence of SO_2 and H_2S in ppm level also causes optical absorption signal at around 550 nm. The existence of NO_2 causes negative interference. It was believed that the interference is originated from the oxidation of ammonia by NO_2 in the gas sample. The oxidation in fact reduced ammonia concentration in the gas sample.

I: Conclusion

A copper chloride doped in a porous sol-gel silica fiber can react with gaseous ammonia (upon diffusion into the fiber) to form a coordinating complex and the concentration of that complex can be determined using a fiber optic spectrometric technique. In addition, the copper-ammonia complex formation is reversible at elevated temperatures and as a result, the sensor can be used for continuously monitoring ammonia in high temperature gas streams. Sub-ppm levels of ammonia were quantitatively determined using a 3.5 cm $CuCl_2$-doped sol-gel silica fiber as a transducer

of the sensor. Future work will focus on developing techniques to eliminate interferences from matrix gases of coal-derived syngas or exhaust gas from combustion sources.

3.9.2. An optical fiber ammonia sensor using a coating of silver nanometer particles immobilized porous silica as a transducer for monitoring trace ammonia at ambient temperature

A: Sensing mechanism

Silver nanometer particles are ammonia-philic. These particles can absorb ammonia molecules from a gas sample. The silver particles swell after absorbing ammonia molecules. When the silver particles was immobilized in a porous silica material, this swelling significantly affecting the optical properties of the composite material.

The optical fiber ammonia sensor described in this work uses a coating of nanometer silver particles immobilized porous silica material on a bent optical fiber probe as a transducer. The absorption of ammonia molecules onto silver particles immobilized inside the porous silica coating significantly attenuates the capability of the bent optical fiber probe for guiding light. Ammonia concentration in the gas sample is detected through monitoring the capability of the coated probe for guiding light. This is a reversible sensing technique because the absorption of ammonia molecules by silver nanometer particles is a reversible process.

B: Transducer formation by coating Ag-doped silica nanocomposite on a bent optical fiber probe

A bent optical fiber probe was prepared with a procedure described in a previous report [44, 52]. In brief, about 1 cm of the center part of a 300 μm FT-300-UMT-0.39-NA Tecs Hard Clad Multimode fiber (Thorlabs Inc. Newton, NJ) was burned away the outside polymer jacket and cladding. The bare fiber core was further bent in the flame. The bent optical fiber tip was cleaned by inserting the tip into a piranha solution (mixture solution of H_2SO_4 and H_2O_2, volume ratio 7:3) for 1 hour [42,52]. The cleaned fiber tip was rinsed with DI water before coating. For coating the Ag-SH-SiO_2 on the surface of the bent optical fiber tip, the tip was dipped into the prepared Ag-SH-SiO_2 solution for one day followed by 2 weeks air-drying.

C: Testing the coated bent optical fiber probe for sensing ammonia

In order to test the response of the coated bent optical fiber probe to trace ammonia in a gas sample, the two ends of the fiber probe were connected to an optical fiber compatible tungsten lamp (Model DT 1000CE, Analytical instrument Systems, Inc. Flemington, NJ) and an optical fiber compatible UV/Vis spoectrometer (SD 2000, Ocean Optics Inc. Dunedin, FL), respectively. The coated bent tip of the probe was housed inside a gas flow cell. The response of the bent fiber probe coated with silver nanoparticles doped porous silica to trace ammonia in a gas sample was tested by monitoring the light intensity transmitted through the bent optical fiber probe while a gas sample flowing through the flow cell.

D: Response of the bent fiber probe coated with silver nanoparticles doped porous silica to trace ammonia in a gas sample

During the test, pure nitrogen gas was used as sample matrix. The recorded transmittance spectrum of the coated bent optical fiber probe exposed to pure nitrogen and a gas sample of 1% NH_3 in nitrogen is shown in Fig.3.9.6. When the gas sample flowing through the flow cell was changed from pure nitrogen to the 1% NH_3 in nitrogen,

the transmitted light intensity quickly decreased in the recorded visible wavelength region. This change is reversible. When the gas sample flowing through the flow cell was switched back to N_2, the guided light intensity increased back again (Figure 3.9.7).

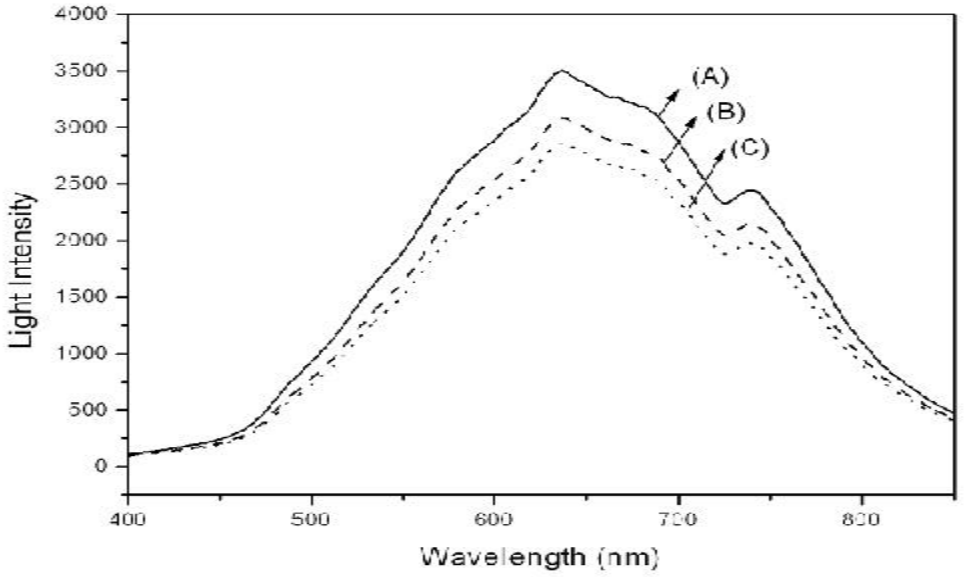

Fig. 3.9.6. The change of light intensity guided through the Ag-SH-SiO_2 coated fiber probe (A) stabilized in N_2 gas, (B) when flowing gas is just switched to 1% NH_3 mixed with N_2 at flow rate 2 L/minute, (C) in 1%NH_3 balanced with N_2 for 10 min at flow rate 2 L/minute.

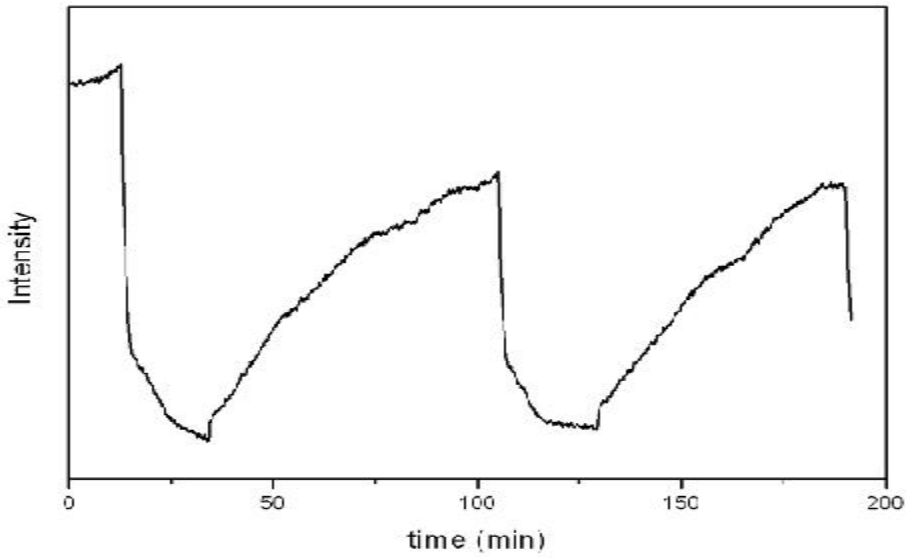

Fig. 3.9.7. The time response of Ag-SH-SiO_2 coated bent optical fiber probe to the change of sample gas composition monitored at 640 nm.

The response of the Ag-doped porous silica coating to ammonia containing gas sample was compared with that of a pure porous silica coating prepared with exactly the same sol-gel process. It was found that a pure porous silica coating prepared with a sol-gel process also responded to ammonia. When a bent optical fiber probe having such a porous silica coating was exposed to ammonia containing gas sample, the intensity of light guided through the probe is decreased. However, the attenuation of light intensity caused by pure porous silica coated is much less than that caused by Ag-SH-SiO_2 coated bent optical probe (Figs. 3.9.8 and 3.9.9). Another difference between the two coatings is that the response of the Ag-doped porous silica coating to ammonia is reversible, while the response of the pure porous silica coating to ammonia gas is irreversible.

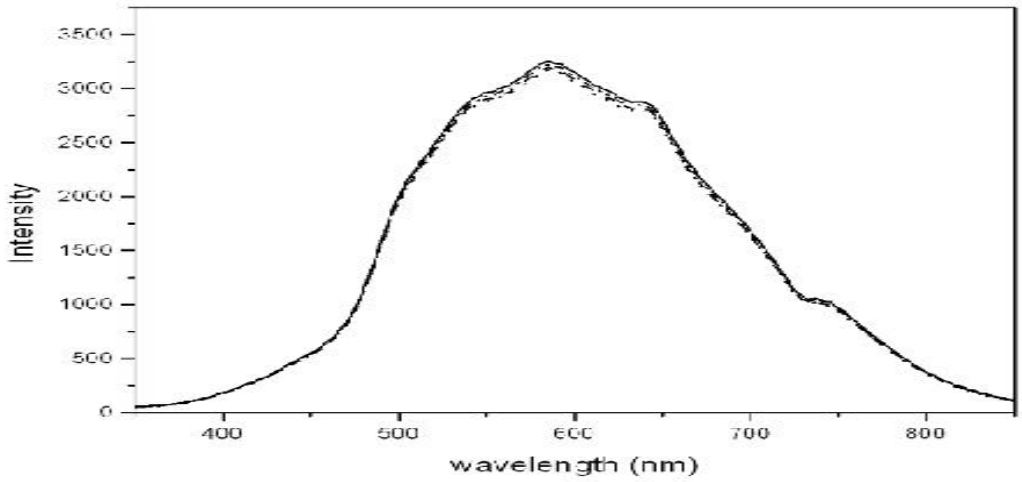

Fig. 3.9.8. The change of light intensity guided through a porous silica coated bent optical fiber probe exposed to gas samples. (A) pure N_2 gas (solid), (B) 1 ppm NH_3 in N_2 gas (dash dot dot), (C) 5 ppm NH_3 in N_2 gas (dash), (D) 10 ppm NH_3 in N_2 gas (dot).

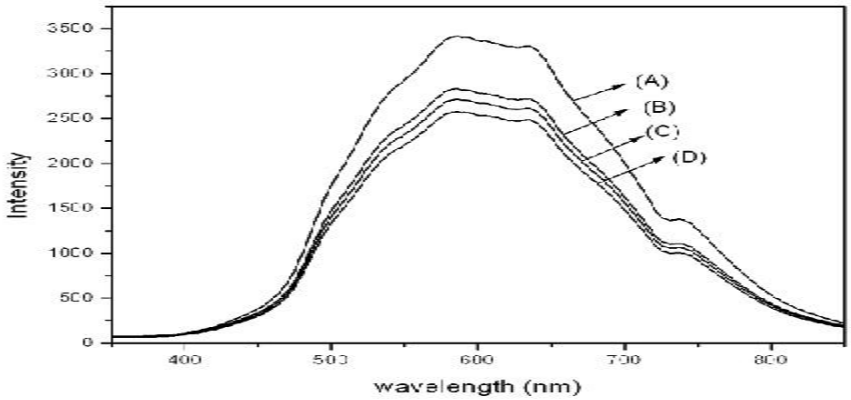

Fig. 3.9.9. The change of light intensity guided through an Ag-SH-SiO_2 coated bent optical fiber probe exposed to gas samples. (A) pure N_2 gas, (B) 1 ppm NH_3 in N_2 gas, (C) 5 ppm NH_3 in N_2 gas, (D) 10 ppm NH_3 in N_2 gas.

As we know, silver nanoparticles have strong interaction with $-NH_2$ functional group [53]. The affinity between silver nanoparticles and the ammonia gas will cause ammonia to be bonded with silver nanoparticles first rather than being absorbed onto the silica surface. Therefore, the interaction of silica in the Ag-doped porous silica coating with ammonia actually does not affect the reaction of Ag nanoparticles with ammonia, and does not interfere with the applications of the particles for ammonia sensing.

In broad concentration range, sensing signal in dB (= $10*\log(I_{N2}/I_{sample})$ has a logarithm relationship with the concentration of ammonia in a gas sample. In low concentration range, a linear calibration can be obtained as shown in Fig. 3.9.10. The detection limit (3 σ) of the prepared probe for sensing ammonia is estimated to be 61 ppb.

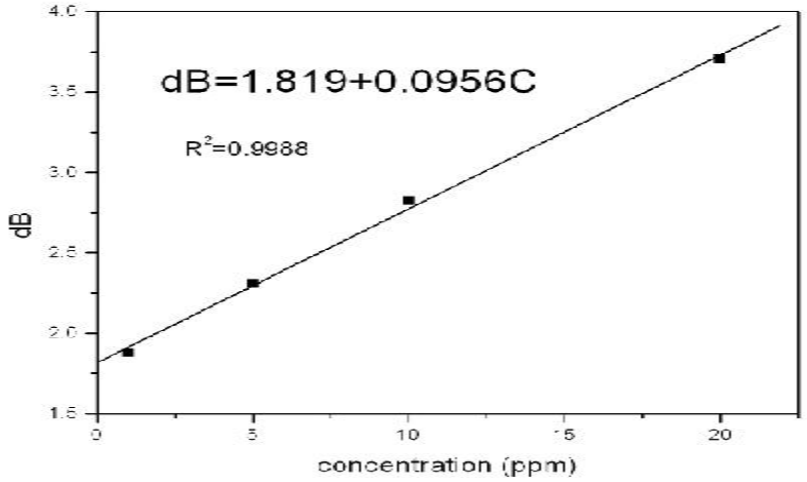

Fig. 3.9.10. A calibration curve of the Ag-SH-SiO_2 coated bent optical fiber probe for sensing ammonia in low concentration range. The sensing signal is defined as dB = $10*\log(I_{N2}/I_{sample})$. Where, I_{N2} and I_{sample} are the light intensity guided through the probe when the probe was exposed to a pure N_2 gas sample and NH_3 containing N_2 gas sample, respectively.

E: Conclusion

An optical fiber probe for sensing trace ammonia in gas samples was successfully developed by coating a thin layer of Ag–SH-SiO_2 on a bent optical fiber probe. The coating on the bent optical fiber probe was characterized by UV-Vis spectrum and SEM. Determined by the SEM, the coating is uniform over the entire surface of the tip and is around 33 nm thick. The response of the coated bent optical fiber probe to trace ammonia in a gas sample was detected by detecting the light intensity that transmitted through the fiber probe. The response of the fiber probe to NH_3 is sensitive and reversible. The characteristic of the coated bent fiber probe for ammonia sensing, such as sensitivity, reversibility, reduced size, and low cost in both fabrication and operation make it applicable for monitoring trace ammonia in industry process line as well as in environment protection.

3.10. An optical fiber hydrogen sulfide sensor using a cadmium oxide doped porous silica optical fiber as a transducer

A: Need of new H_2S sensor technology for monitoring IGCC processes

In IGCC process, sulfur-containing compounds in raw material coal are converted to ammonia in the gasification. The concentration of hydrogen sulfide in coal-derived syngas can be as high as several thousand ppm depending on the quality of raw material coal [54,55]. Hydrogen sulfide is a well-know poisoning compound to many noble metal based catalysts, which are widely used in fuel gas processing and in fuel cell for power generation. For example, platinum is presently used as a catalyst in proton exchange membrane (PEM) fuel cell for converting hydrogen molecules to proton. The catalyzing function of platinum can be deactivated by trace hydrogen sulfide in the fuel gas at concentration as low as 0.0x ppm level. Therefore, hydrogen sulfide must be eliminated before sending a coal-derived syngas to a power generation unit, and thus, a technique for monitoring trace hydrogen sulfide during coal-derived syngas purification process is needed.

Present state-of-the-art techniques for detecting hydrogen sulfide in gas samples include ion mobility spectroscopy [35], gas chromatography [36,37], ultraviolet (UV) absorption spectrometry [56,57], near infrared (NIR) absorption spectrometry [40,41] and chemiluminescence techniques [58,59]. Gas chromatography and ion mobility spectrometry are very sensitive for hydrogen sulfide detection, and can be used to detect hydrogen sulfide in a gas sample down to ppb level. However, these are basically laboratory methods. It is difficult to use them for direct determination of hydrogen sulfide in high temperature gas streams from coal gasification processes, because these gas streams contain volatile, semi-volatile compounds, tars and dust.

Hydrogen sulfide absorbs UV light in deep UV region (<200 nm) [56]. Although direct UV absorption spectrometry has been reported for detecting hydrogen sulfide, it is difficult to use this method for monitoring H_2S in complex gas samples. A UV assisted IR absorption spectrometric method has been proposed for detecting H_2S [57]. This is an indirect method, in which H_2S is first converted to SO_2 through irradiation of the gas sample with a UV light. The generated SO_2 is detected with an IR absorption spectrometric method. Obviously, there are many factors, including UV light intensity, matrix gas composition, affecting the quantitative result of this method.

Flame chemiluminescence spectrometry is a sensitive method for detecting sulfur compounds [58,59]. In this method, a gas sample is introduced into a hydrogen/air flame. The reaction of sulfur compounds with oxygen in the flame environment generates excited sulfur dioxide, which emit near infrared light in the process of relaxing back to its ground state level. This method is very sensitive and has been used as a detecting technique for gas chromatographic separation techniques. This method could be developed for continuous monitoring sulfur compound, such as H_2S, CH_3SH, in coal-derived syngas.

In recent development, sensor techniques using semiconductor materials as transducers have been intensively investigated for monitoring H_2S in air gas from fermentation process as well as in natural gas [60-62]. These sensors are based on detecting the resistance change of a semiconductor membrane exposed to a H_2S containing gas sample. The working temperature of these sensors has been reported from room-temperature to as high as 300 ^oC [61]. The semiconductor membrane based sensors

can detect H_2S down to ppb level. The problems with semiconductor membrane based sensors include lack of selectivity and temperature-sensitivity of the sensing signal. For example, the sensing signal of most semiconductor membrane based sensors is sensitive to moisture level, which is an important matrix component in almost all the gas samples. Most semiconductor based sensors are also sensitive to other reducing gases, such as CH_4, NH_3. Therefore, the application of traditional semiconductor membrane based sensors in coal-derived syngas monitoring is problematic.

B: Mechanism of the proposed sensor technique

The H_2S sensor of this work is based on the formation of CdS in a porous silica optical fiber through the reaction of H2S molecules diffused into the porous silica optical fiber with Cd^{2+} doped inside the fiber. The formed CdS in side the fiber absorbs UV light with peak absorption at 375 nm. The concentration of H_2S in a gas sample is in dynamic equilibrium with the concentration of H2S in the gas sample. Therefore, the concentration of trace H_2S in a gas sample can be detected through detecting the optical absorption signal of the Cd^{2+} doped porous silica optical fiber.

C: Fabrication of a cadmium oxide doped porous silica optical fiber

A Cd^{2+} doped porous silica optical fiber was prepared with the sol-gel techniques described in the Experimental section of this report.

D: Fiber optic spectrometric investigation of the optical properties of the doped porous silica optical fiber exposed to gas samples at high temperatures

The structure of the optical fiber H_2S sensor is similar to that of the ammonia gas sensor described in Section 3.9, which uses a Cu^{2+} doped porous silica optical fiber as a transducer.

E: The optical properties of cadmium oxide doped porous silica optical fiber

The optical properties of the cadmium oxide doped porous silica fiber at high temperatures were investigated. In studying the optical absorption property of the cadmium oxide doped fiber, a pure porous silica optical fiber without any doping prepared with the sol-gel process described above was used as a reference fiber. The optical properties of the pure sol-gel silica optical fibers prepared with the sol-gel process used in this work have been investigated in our previous work [4,5]. The pure porous silica optical fibers were found not absorb light in the UV/Vis region. However, these fibers scatter UV light, especially in the deep UV region. The optical absorption spectrum of the cadmium oxide doped porous silica optical fiber was obtained by comparing the light intensity guided through the doped fiber with the light intensity guided through a pure porous silica optical fiber. Therefore, the obtained absorption spectrum shown in Fig. 3.10.1 is an indicator of light guiding capability of the doped silica optical fiber compared to that of the pure sol-gel silica optical fiber. This absorption spectrum was obtained at a temperature of 450 ^oC and pure nitrogen gas flowed through the quartz flow cell during the test. The recorded spectrum indicates that the cadmium oxide doped fiber slightly absorbs near infrared light with peak absorption wavelength at around 725 nm. In the short wavelength region, the doped porous silica fiber can guide more light than the pure sol-gel silica optical fiber.

The fluorescence property of the cadmium oxide doped porous silica optical fiber at 450 ^oC was investigated by using the 370 nm UV LED as an excitation source. The recorded fluorescence spectrum shown in Fig. 3.10.2 was believed the result of three fluorescence spectra added together. The peak wavelengths of the three fluorescence

spectra are 510 nm, 580 nm and 640 nm, respectively. These fluorescence spectra from porous silica materials have also been separately observed by other research groups [17-19]. Therefore, it was believed that these fluorescence spectra are originated from porous silica material. In our previous experiments, pure porous silica fibers excited with a 370 nm LED were found emit fluorescence with peak wavelength at around 510 nm and 580 nm. However, we have not observed the fluorescence spectrum with peak wavelength at 640 nm in our previous work with pure porous silica optical fiber. It is possible that this fluorescence signal is too low to be detected in our previous work

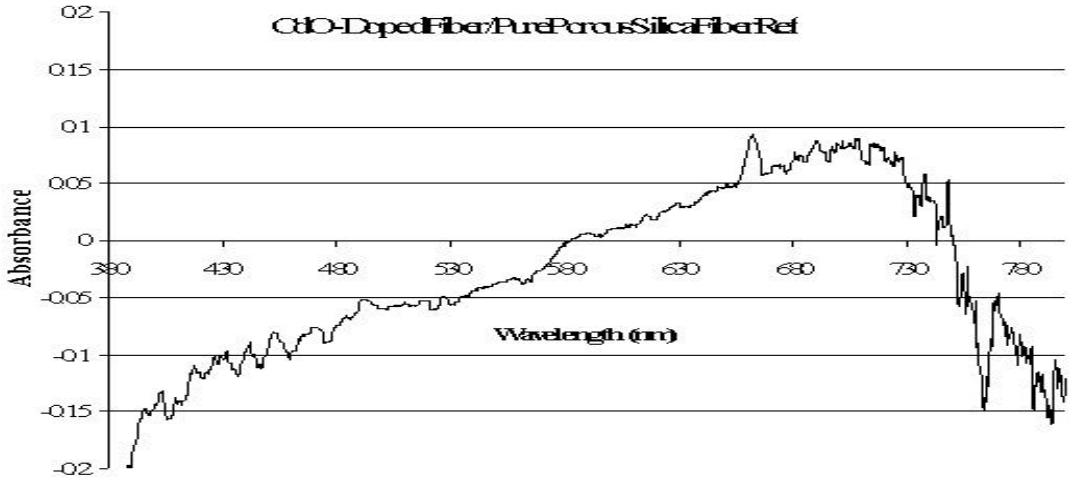

Fig. 3.10.1. An UV/Vis absorption spectrum of the cadmium oxide doped porous silica optical fiber exposed to nitrogen gas at 450 ^{o}C. A short piece (2 cm) of a pure porous silica optical fiber was used as a reference fiber for recording this absorption spectrum.

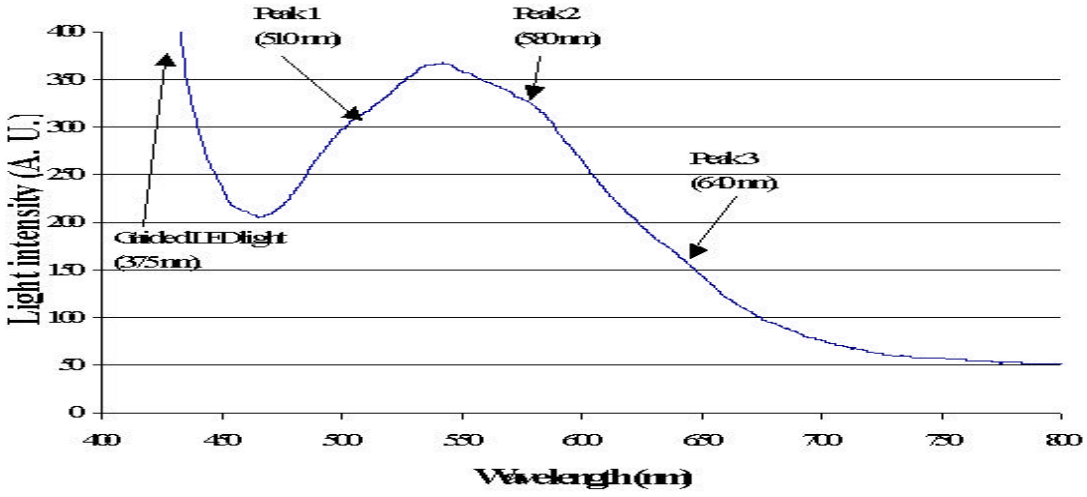

Fig. 3.10.2. An optical transmittance spectrum of a cadmium oxide doped sol-gel silica optical fiber obtained at 450 ^{o}C. Light from the 370 nm LED was fed into one end of the optical fiber and light emerged from the opposite end of the fiber was detected with the optical fiber compatible UV/Vis spectrometer. A second spectrum with peak intensity at around 540 nm is observed in additional to the original LED light (peak intensity at around 370 nm). This second spectrum is the fluorescence signal emitted from the porous silica optical fiber. This fluorescence spectrum is the result of three spectra (peak wavelength at 510 nm, 580 nm and 640 nm, respectively) added together.

F: Optical response of the cadmium oxide doped silica optical fiber on exposure to trace H_2S in a nitrogen gas sample

When a cadmium oxide doped porous silica fiber was exposed to a H_2S containing gas sample, H_2S molecules in the gas sample can diffuse into the porous fiber and react with cadmium oxide doped inside the fiber to form CdS. The reaction of H_2S with metal oxide immobilized inside porous silica materials can occur at room temperature as well as at high temperatures [63-65]. The formed CdS inside the porous silica optical fiber can absorb light and emit fluorescence if excited with an appropriate light source. The UV/Vis optical absorption spectrometric response of the cadmium oxide doped porous silica optical fiber on exposure to trace H_2S in a nitrogen gas sample at 450 ^oC was investigated. It was found that this fiber gives a broad UV/Vis absorption spectrum (Fig. 3.10.3) when the gas sample flowing through the quartz cell was switched from pure nitrogen to a 100 ppmv H_2S containing nitrogen gas sample. The observed absorption spectrum is believed consists from more than one spectrum. The peak absorption wavelength of the main spectrum is around 370 nm, which is believed originates from CdS formed inside the porous silica optical fiber. A second absorption peak at around 510 nm is believed originates from the decrease of fluorescence intensity of the porous silica fiber excited by UV light guided through the fiber. The quench of the porous silica fiber fluorescence by exposure to H_2S gas will be discussed below.

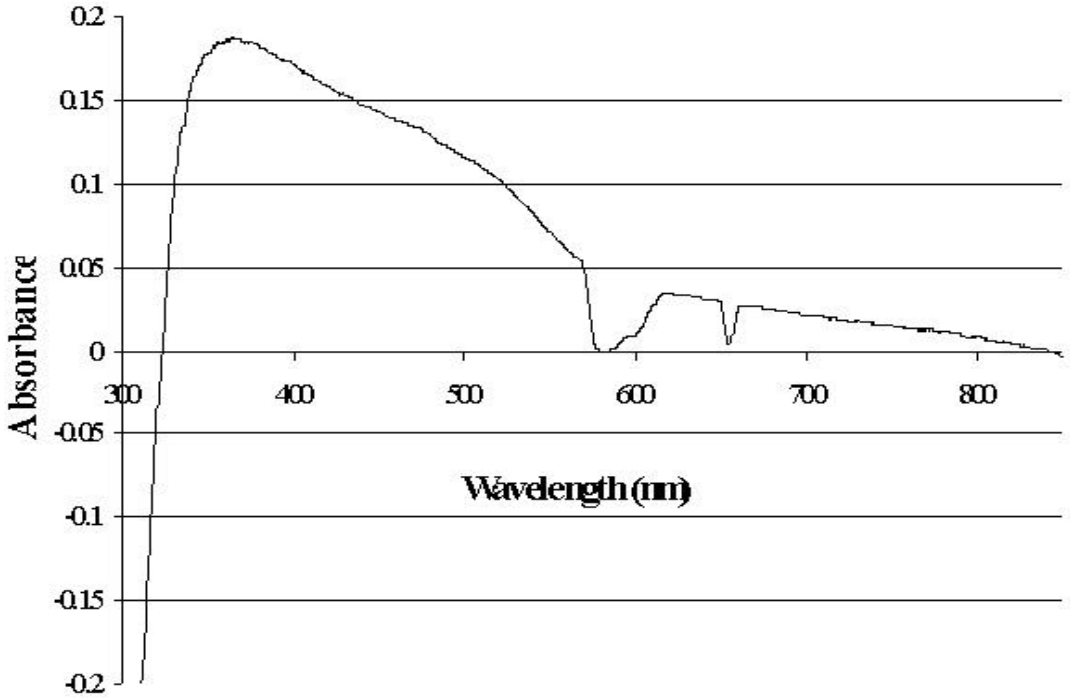

Fig. 3.10.3. An UV/Vis absorption spectrum of the cadmium oxide doped porous silica optical fibers exposed to a nitrogen gas sample containing 100 ppmv H_2S. The temperature of the gas sample was kept at 450 ^oC during the test.

As discussed above, when excited with a 370 UV LED the cadmium oxide doped porous silica optical fiber emits fluorescence with peak emission wavelength at 510 nm,

580 nm and 640 nm. When the fiber was exposed to a H_2S containing gas sample, CdS will be formed inside the nanoprous silica optical fiber. CdS is a compound which emits fluorescence with high quantum efficiency when excited with a UV light source [65,66]. Therefore, it is expected that a significant change of fluorescence property will occur after the doped fiber was exposed to an H_2S containing gas sample. The fluorescence spectra of the doped porous silica optical fiber at 450 ^oC exposed to a pure nitrogen gas sample and a 50 ppm H_2S containing nitrogen gas sample were recorded with the 370 nm LED as an excitation light source. The recorded spectra shown in Fig. 3.10.4 indicate that when the fiber was exposed to a gas sample containing trace H_2S, the fluorescence with peak wavelength at around 510 nm was completely quenched, and the fluorescence spectra with peak wavelength at 580 nm and 640 nm were partially quenched. However, in this high temperature test, the fluorescence signal from the formed CdS inside the fiber was not observed. After the fiber was cooled to room temperature, strong fluorescence signal with peak emission wavelength at 500 nm was observed (Fig. 3.10.5). This is believed the fluorescence spectrum of CdS formed inside the porous silica optical fiber. Obviously, the fluorescence signal of CdS formed inside the porous silica optical fiber was quenched at the high temperature (450 ^oC) environment.

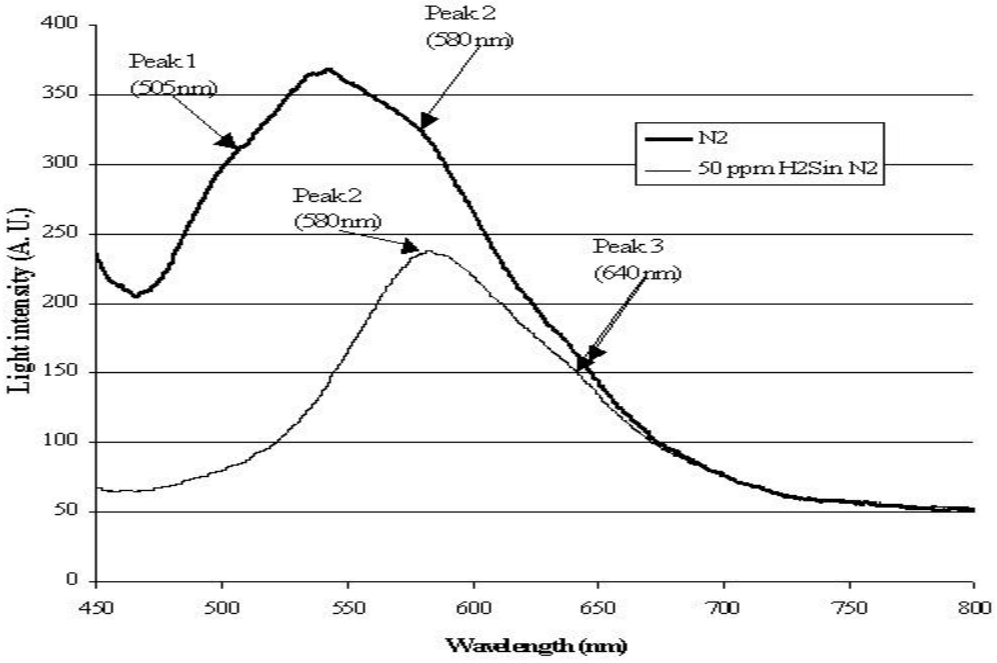

Fig. 3.10.4. The fluorescence spectra of the cadmium oxide doped porous silica optical fiber exposed to a pure nitrogen gas sample and a trace (50 ppmv) H_2S containing nitrogen gas sample at 450 ^oC. With the exposure of the fiber to a 50 ppmv H_2S containing nitrogen gas sample, the first fluorescence spectrum with peak wavelength at 510 nm was completely quenched. The second and third fluorescence spectra with peak wavelength at 580 nm and 640 nm were partially quenched.

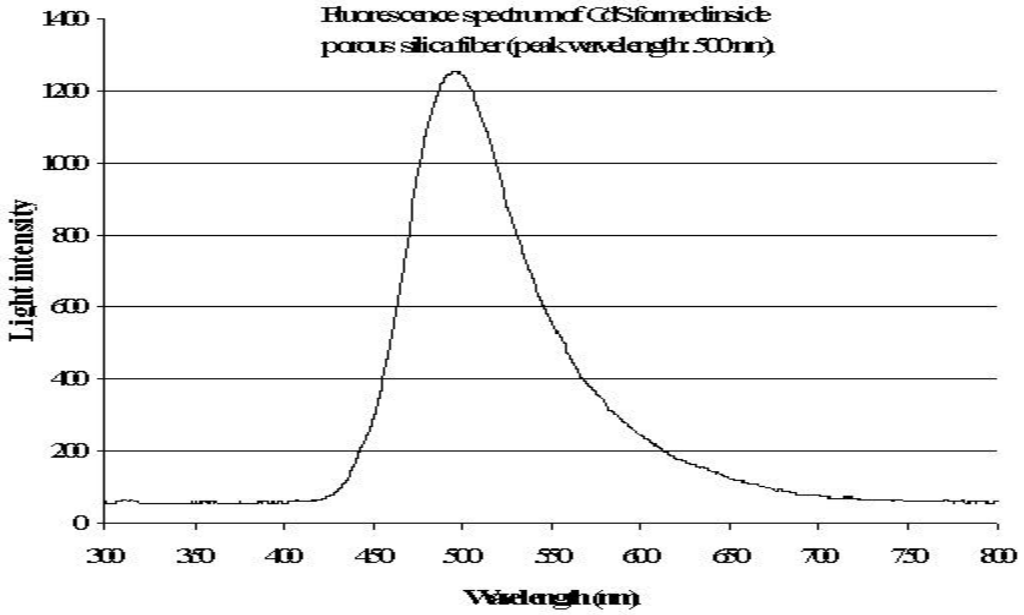

Fig. 3.10.5. A fluorescence spectrum of CdS formed inside the sol-gel silica optical fiber obtained by exciting the fiber at room temperature with the 370 nm LED. The peak wavelength of this CdS fluorescence spectrum is 500 nm.

G: Optical absorption signal of the cadmium oxide doped porous silica optical fiber for continuous monitoring trace H_2S in a high temperature gas sample

The results obtained from above experiments indicate that the exposure of the cadmium oxide doped porous silica optical fiber to trace H_2S in a gas sample causes a significant optical absorption signal with peak absorption wavelength at 370 nm. The exposure of the fiber to trace H_2S in a gas sample also causes the quench of the porous silica fiber fluorescence. The quench of porous silica fluorescence by gas components has been observed in previous researches and sensor techniques have been proposed based on this phenomenon [65,67,68]. However, This Stern-Volmer quenching based sensing technique lacks selectivity for gas sensing [65,68]. Therefore, the fluorescence quench phenomenon was not selected in this work for designing H_2S gas sensor. The formed CdS is highly fluorescent at room temperature. This fluorescence signal can be used for sensing trace H_2S at room temperature, but can cannot be used for continuously monitoring trace H_2S in high temperature gas samples. From these observations the optical absorption signal of the cadmium oxide doped porous silica optical fiber was chosen as a sensing signal for continuously monitoring trace H_2S in a high temperature gas sample.

The optical absorption response of the cadmium oxide doped porous silica optical fiber to CH_4, CO and H_2 in a gas sample was investigated. These gases are the matrix components of gasification-derived fuel gas. It was found that the cadmium oxide doped porous silica optical fiber did not give observable UV/Vis optical absorption signal when exposed to a nitrogen gas sample containing CH_4 (up to 0.5%), CO (up to 1%), H_2 (up to 1%). The fluorescence emission property of this fiber was also not affected by CH_4, CO and H_2 in the nitrogen gas sample in tested concentration range. Gas samples with higher

matrix gas concentrations have not been tested in present work due to safety consideration. From the results obtained from present experiments, it is believed that the optical absorption signal of this cadmium oxide doped porous silica optical fiber can be used for selectively sensing trace H_2S in gasification derived fuel gas.

H: Calibrating the cadmium oxide doped porous silica optical fiber for sensing trace H_2S with fiber optic UV/Vis absorption spectrometry

The optical absorption signal of the cadmium oxide doped porous silica optical fiber exposed to a nitrogen gas sample at 450 ^oC was continuously monitored while trace H_2S was introduced into the gas sample step-by-step with the dynamic gas calibrator. With the increase of H_2S concentration in the gas sample, the absorbance signal increased (Fig. 3.10.6). The relationship of the obtained absorbance signal at 370 nm with the concentration of H_2S in the gas sample follows a linear equation:

$$Abs. = 0.0019\ C_{H_2S}\ (ppmv) + 0.0001 \qquad (3.10.1)$$

The detection limit of this sensor depends on the stability of the light source and the photodetector. With the optical fiber compatible spectrometer as a detector and the DT-100 combo lamp as a light source, an absorbance signal as low as 0.0005 can be detected. The detection limit of this sensor based on this absorbance value is calculated to be 0.26 ppmv.

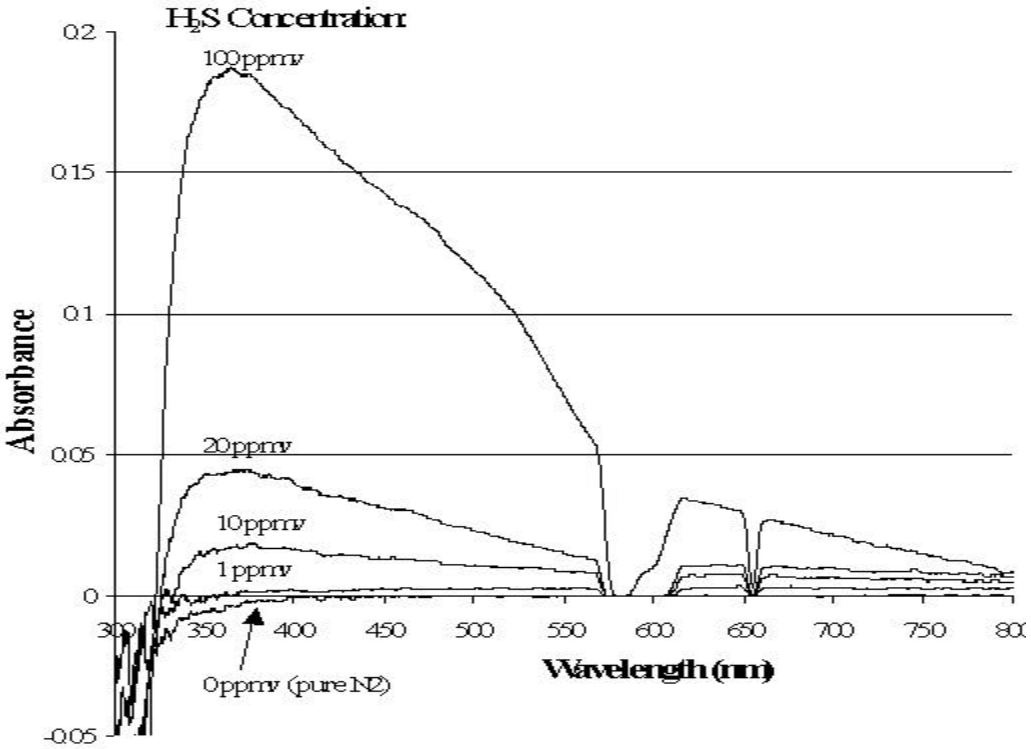

Fig. 3.10.6. UV/Vis optical absorption spectra of the cadmium oxide doped porous silica optical fiber exposed to nitrogen gas samples containing trace H_2S of different concentrations.

The time response of the cadmium oxide doped porous silica optical fiber to trace H_2S in a nitrogen gas sample was recorded. The concentration of H_2S in the gas sample was increased step-by-step and the absorbance signal of the fiber at 370 nm was recorded. The response time of this fiber sensor is more than 30 min for a gas sample containing H_2S in low concentration (ppm level) and shorter than 20 min for the gas sample containing H_2S in higher concentration (100 ppm) (Fig. 3.10.7).

This sensing technique for H_2S detection is not reversible because the reaction of CdO with H_2S to form CdS in the porous silica optical fiber is irreversible. However, this sensor can be re-generated by exposing the used fiber to air at a high temperature. This is a method used to regenerate metal oxide immobilized porous silica H_2S sorbents used for cleaning gasification derived fuel gas. During this exposure process, CdS inside the porous fiber will be oxidized by oxygen in air and cadmium oxide will be formed inside the fiber for use again.

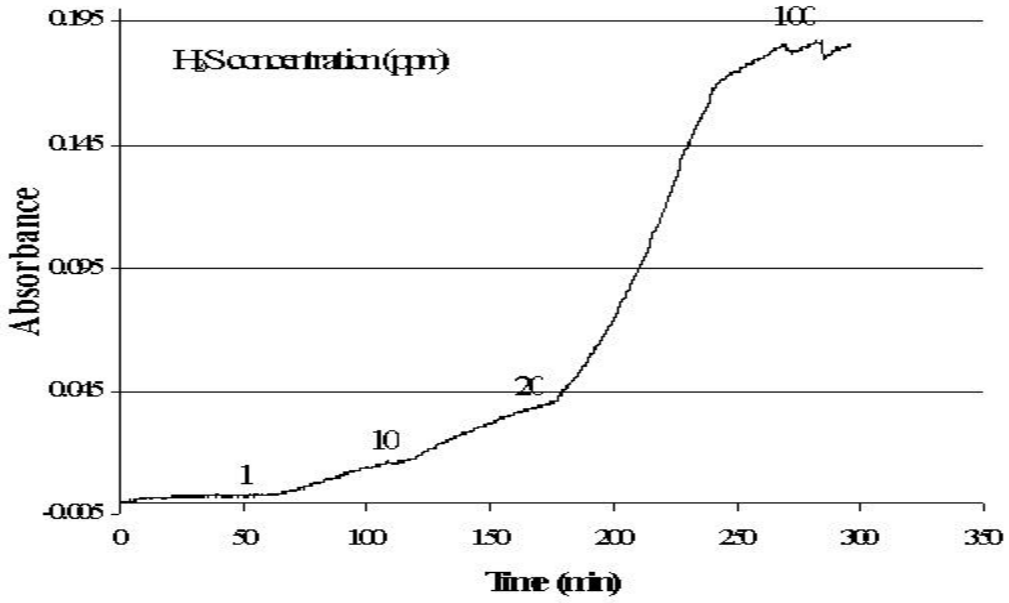

Fig. 3.10.7. Time response of the cadmium oxide doped porous silica optical fiber sensor for monitoring the change of H_2S concentration in a nitrogen gas sample.

I: Conclusion

A cadmium oxide doped porous silica optical fiber has been prepared with a sol-gel technique. The optical properties of the cadmium oxide doped porous silica optical fiber exposed to gas samples containing CH_4, CO, H_2 and trace H_2S were investigated. It was found that the cadmium oxide doped porous silica optical fiber gives an optical absorption signal when exposed to a gas sample containing trace H_2S. The exposure of this doped fiber to CH_4, CO and H_2 does not cause observable optical absorption signal. The optical absorption property of this fiber can be used to continuously monitor trace H_2S down to sub-ppm level in a nitrogen gas sample containing reducing gases. Therefore, it is expected that this sensor can be used as a detector to monitor the breakthrough of a H_2S absorbing column in the process of cleaning gasification derived fuel gas.

3.11. A selective optical fiber hydrogen gas sensor using a porous tin oxide coating on the surface of a silica optical fiber as a transducer

3.11.1. Semiconductor metal oxide membranes as transducers for reducing gas sensing

Semiconductor metal oxides, such as tin oxide, zinc oxide, titanium oxide, zirconium oxide, indium oxide, etc. have long been investigated as sensing materials for monitoring of reducing gas, such as H_2, CO, CH_4 and other hydrocarbons, NH_3, H_2S [69-75]. These materials are usually made in the form of film, which is coated on a substrate, such as a silicon wafer or a glass. Electrodes made of noble metal (gold, platinum) are fabricated in contact with both sides of such a film in order to measure its resistance which is usually in mega Ohm region. Traditionally, the films are insensitive to reducing gas at room temperature. However, if heated to a temperature above 200 ^oC, the resistance of the film changes when exposed to a reducing gas component. The working temperature range for this kind of sensors is usually from 200 ^oC to 400 ^oC. At recent developments, metals and metal oxide have been added to the semiconductor membranes in order to improve the sensitivity, selectivity and response temperature of these solid gas sensors [76-78].

3.11.2. Principle of fiber optic gas sensor using porous semiconductor metal oxide materials as transducers

In order to understand the responsive mechanism of the semiconductor metal oxide materials to reducing gases, sophisticated analytical techniques, including electron microscopy, X-Ray diffraction, FTIR, surface diffuse reflectance spectrometry, UV/Vis absorption spectrometry, NIR spectrometry, have been employed to investigate the microstructure, the nature of chemical bond, the nature of oxygen deficiency, etc [79-81]. Almost all of these analytical techniques were utilized to characterize the materials or investigate the micro structural changes. These investigations were carried out at room temperature before/after the exposure of a material to specific gases, or before/after certain heat treatment procedure. It is difficult to integrate such a sophisticated analytical instrument to investigate a metal oxide film at a sensing environment, which is usually in a corrosive, high temperature environment.

The fiber optic spectroscopic techniques developed in our research program provide us the possibility of investigating the optical spectroscopic properties of a specific semiconductor metal oxide film at high temperature and specific gas environment. The absorption of a reducing gas on the particle surface of a semiconductor metal oxide material can change the oxygen deffecience status, which can be observed through an optical absorption spectrometric method or a fluorescence spectrometric method. If the semiconductor metal oxide material is coated on the surface of an optical fiber, then the change of the optical property can be observed with a fiber optic EW spectrometric method. If the metal oxide is doped inside a porous silica optical fiber, the active core fiber optic spectrometric methods can be used to monitor the absorption process.

3.11.3. An optical fiber H_2S sensor using nanocrystalline SnO_2 coating on an optical fiber core as a transducer

A: Preparing a SnO_2 coated bent optical fiber probe using sol-gel techniques

A bent optical fiber probe using a gold-jacketed silica optical fiber was prepared with a previously reported procedure [44,52]. A tin oxide thin film was coated on the top

of the bent optical fiber probe using a sol-gel method. For synthesizing pure SnO_2 thin films, a pre-cleaned bent optical fiber probe was dipped in the solution of tin-isopropoxide in isopropanol and toluene. After the dip-coating process, the probe was exposed to air for several hours. During this process, tin-isopropoxide on the surface of the bent optical fiber core was hydrolyzed and a tin oxide gel was formed on the surface of the fiber. The gel-coated fiber probe was then inserted into the split tube furnace and dried at 150 °C for 1 h while air was flowed through the tube flow cell. The substrates were dip-coated again using the respective solutions under similar conditions and then dried again at 150 °C for 1 h in air. Finally, the coated probe was calcined at 600 °C in air for 1 h, and then cooled to room temperature inside the furnace. The SEM image of the coated bent optical fiber probes are shown in Figs. 3.11.1, 3.11.2 and 3.11.3.

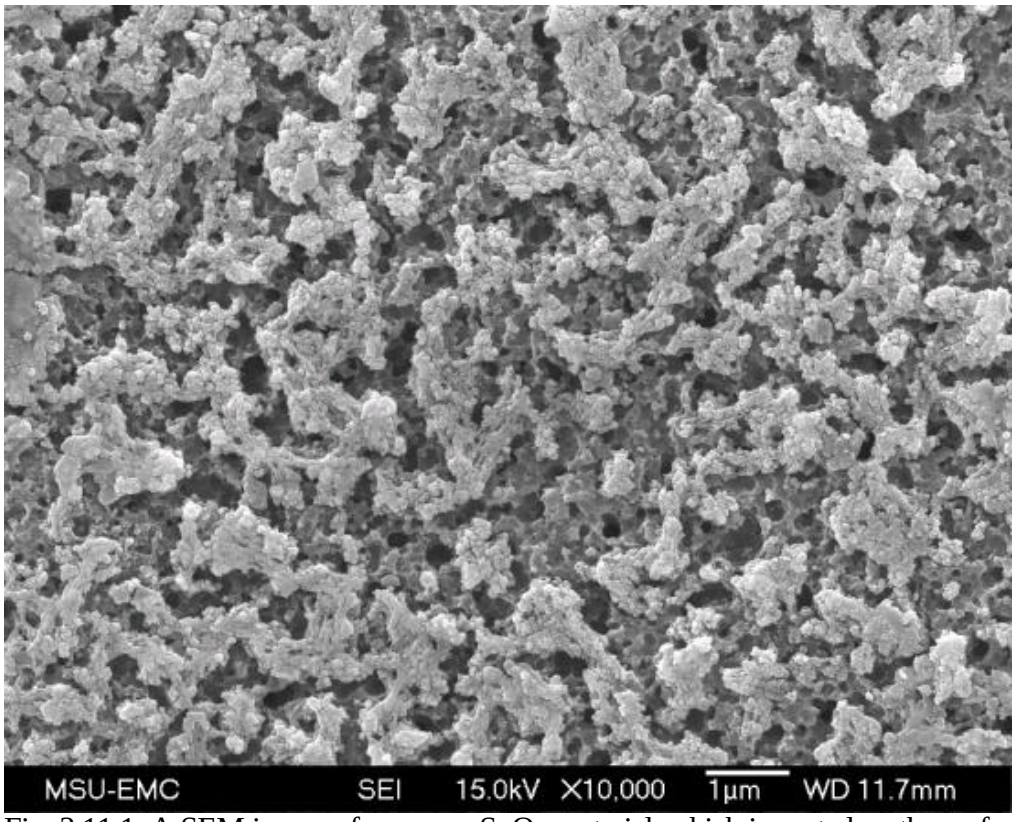

Fig. 3.11.1. A SEM image of a porous SnO_2 material, which is coated on the surface of a bent optical fiber probe. This image shows the porous feature of the material, which is important for gas sensing.

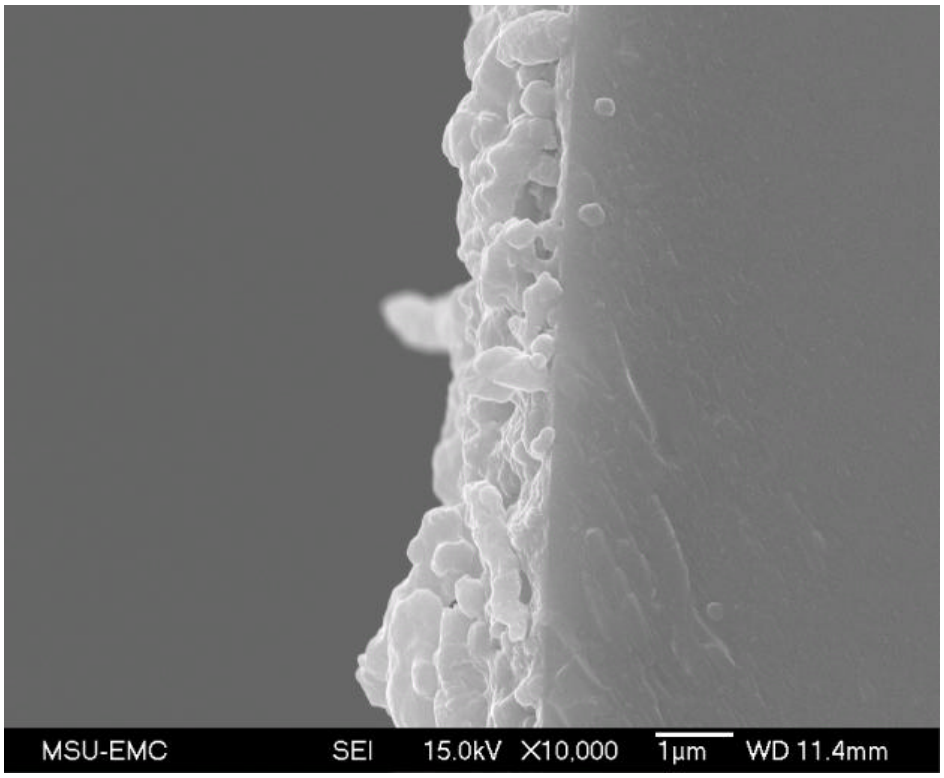

Fig. 3.11.2. A SEM image of a porous SnO_2 material, which is coated on the surface of a bent optical fiber probe. This image shows the thickness of the coating, which is less than 1 µm.

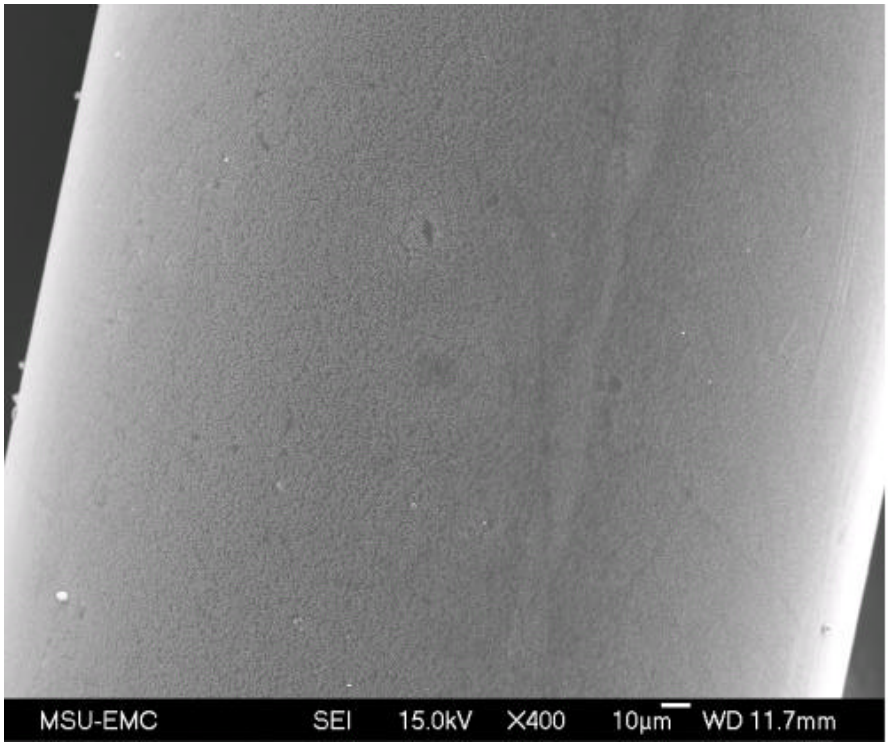

Fig. 3.11.3. A SEM image of a porous SnO_2 material coated optical fiber core.

B: Testing the SnO_2 coated bent optical fiber probe for sensing reducing gases with fiber optic EW absorption spectrometry

The optical properties of the SnO_2 thin film was investigated with an optical fiber EW absorption spectrometric method. The instrument set-up for this investigation is shown in Fig. 2.7. Light from the deuterium/tungsten combo light source was connected to one end of the coated bent optical fiber probe. The second end of the bent optical fiber probe was connected to the optical fiber compatible UV/Vis spectrometer. The coated bent optical fiber probe was deployed inside the quartz gas flow cell which is inserted into the split tube furnace. During the test, the tube furnace was heated to certain temperature and kept at the temperature. A gas sample was flowed through the quartz flow cell and the optical absorption spectrum of the coated optical fiber probe was recorded with the optical fiber compatible spectrometer.

C: Optical absorption spectrum of SnO_2 coating exposed to reducing gas at 600 ^oC

The optical absorption spectrum of the SnO_2 coating on the surface of a bent optical fiber probe exposed to a 1vol% H_2-N_2 gas sample was investigated by using optical fiber evanescent wave absorption spectrometry. In this experiment, the temperature of the furnace was kept at 600 ^oC. Pure N_2 gas was first flowed through the quartz flow cell and light intensity guided through the SnO_2 coated bent optical fiber probe was recorded as reference intensity. A 1vol% H_2-N_2 gas sample was then flowed through the quartz flow cell and the absorption spectrum of the coated optical fiber was recorded. Figure 3.11.4 shows the recorded evanescent wave absorption spectrum in UV/Vis region and NIR region. In the UV/Vis region, an absorption spectrum with peak absorption wavelength at around 320 nm was recorded. In the NIR region, an absorption spectrum with peak absorption wavelength at around 1.7 μm was recorded (Fig. 3.11.5).

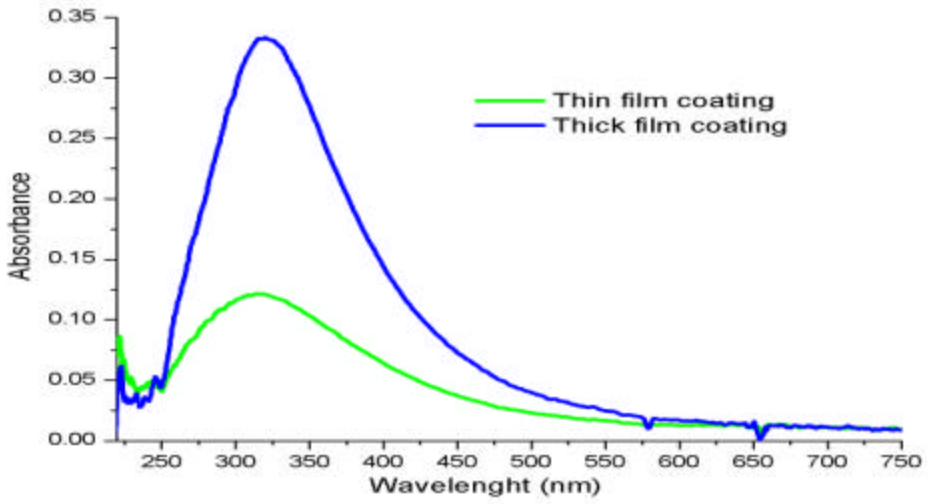

Fig. 3.11.4. Typical UV-Vis absorption spectra of a SnO_2 thin film optical fiber sensor response to a H_2-N_2 flow at 600 °C.

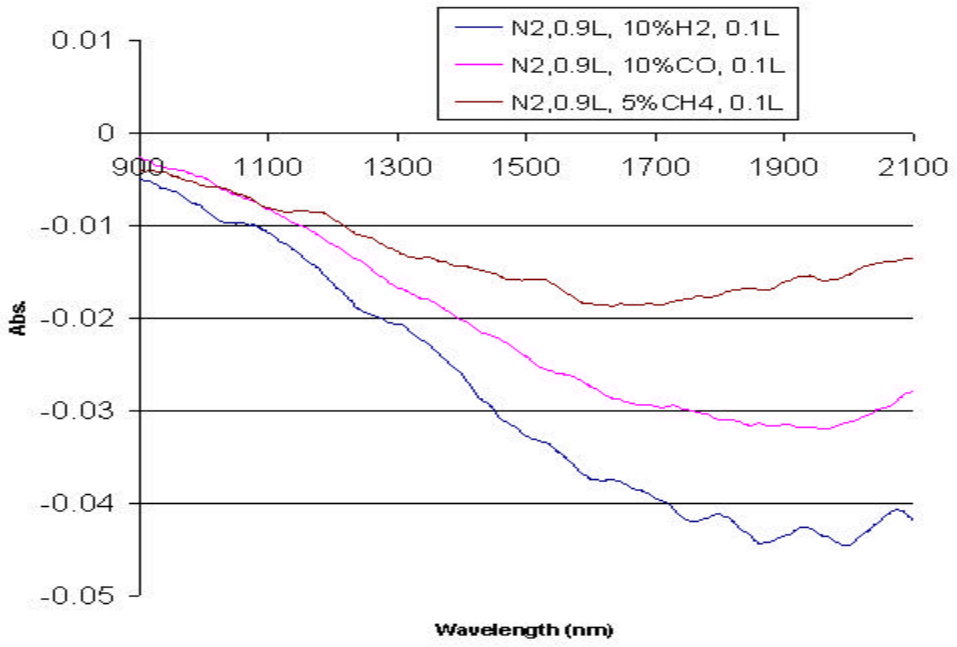

Fig. 3.11.5. NIR absorption spectra of a SnO_2 membrane (thick) coated on a bent optical fiber core exposed to gas samples containing different reducing gas (H_2, CH_4, CO) at 600 ^oC

The observed optical absorbance signal was then associated with a decrease in the surface-adsorbed oxygen-ion concentration on the tin oxide surface during its interaction with H_2. It is well-known that oxygen-ions exist on the surface of semiconductor metal oxide particles [79-81]. The porous surface of the SnO_2 thin film has a high surface area. It has strong tendency to react with H_2 molecules from the gas phase. When hydrogen gas diffused into the porous SnO_2 coating, hydrogen molecules were decomposed on the tin oxide surface to nascent hydrogen atoms, which loose electrons to the conduction band of semiconductor oxide. The generated protons get associated with the surface-adsorbed oxygen ions and hop from one oxygen ion to another. Two adjacent OH groups condense and eliminate H_2O. In the process, net one electron is injected into the conduction band of SnO_2 film and reduces the film's resistance. The chemical reactions involved during the hydrogen sensing are summarized below:

$H_{2(g)}$? $H_{(ads)}+H_{(ads)}$,
$H_{(ads)}+H_{(ads)}$? $2H_{(ads)}^{+}+2e^{-}$,
$2H_{(ads)}^{+}+2O_{(ads)}^{-}$? $2OH_{(ads)}$,
$2OH_{(ads)}$? $H_2O_{(ads)}+O_{(ads)}$,
$O_{(ads)}+e^{-}$? $O_{(ads)}^{-}$,
$H_2O_{(ads)}$? $H_2O_{(g)}+O_{(ads)}$,
The net reaction is:
$H_{2(g)}+O_{(ads)}^{-}$? $H_2O_{(g)}+e^{-}$

The evanescent wave optical absorption spectra of the SnO_2 coated optical fiber probe exposed to nitrogen gas samples containing 5% CH_4, 5% CO were also recorded

using the procedure as described above. Figure 3.11.6 shows the recorded absorption spectra in UV/Vis and NIR regions. In UV/Vis region, no obvious absorption signal was observed when the coated fiber probe was exposed to nitrogen gas samples containing 5% CH_4 or 5% CO. In the NIR region, the probe absorbs light with peak absorption wavelength at 1900 nm when exposed to a 5% CH_4 containing N_2 sample, and also absorbs light with peak absorption wavelength at 1900 nm when the probe was exposed to a 1% CO containing N_2 gas sample (Fig. 3.11.5).

In traditional semiconductor metal oxide membrane sensors, almost all the reducing gases cause the change of resistance of the membrane. These sensors can only detect the existence of reducing gases, but can not discriminate between the gases, and therefore, the sensors lack of selectivity for sensing individual reducing gas. From the recorded evanescent wave absorption spectra in this work, it is clear that the optical absorption spectrum can be used as finger-print to discriminate H_2, CH_4 and CO, and selective sensing of these gases can be achieved.

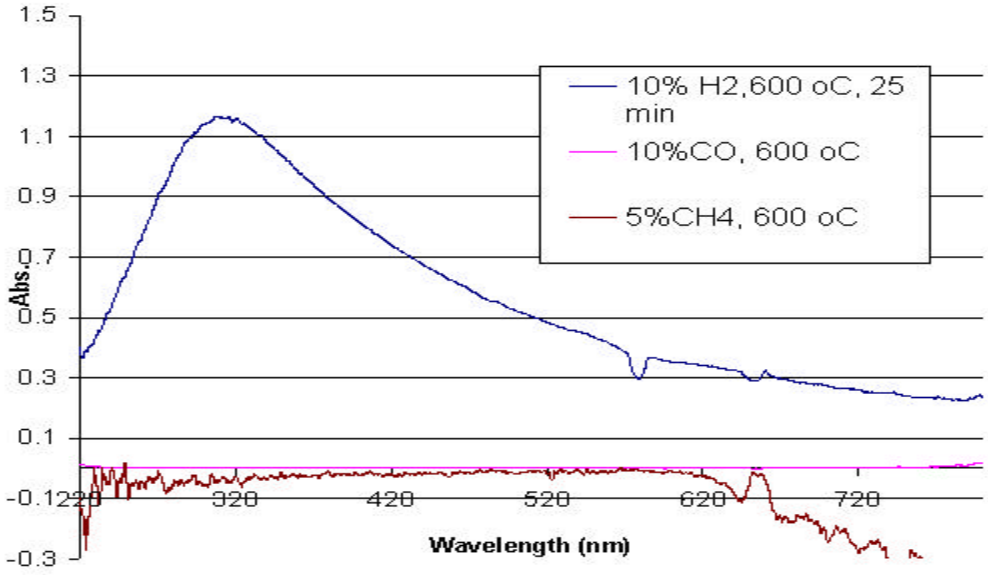

Fig. 3.11.6. Spectroscopic response of a SnO_2 membrane coated on a bent optical fiber core exposed to gas samples containing different reducing gases at 600 ^oC. The spectra indicate that this membrane responses to H_2 in the UV/Vis region, but is insensitive to CH_4 and CO in this wavelength region.

D: Optical absorption spectra of SnO_2 coating exposed to reducing gas at different temperatures

The optical properties of the SnO_2 coating on the optical fiber probe exposed to reducing gas at different temperatures were investigated following the method described above. When a 1vol% H_2-N_2 mixture was used as a sample gas, the SnO_2 coating starts to show absorption signal from ca. 300 ^oC. The intensity of the absorption signal increased with the increase of temperature in the tested range up to 800 ^oC. It is expected that with the increase of temperature more hydrogen molecules diffused into the pores of the SnO_2 coating will be decomposed and more nascent hydrogen atoms are available to

react with surface absorbed oxygen ions. Thus, with the increase of temperature, the absorption signal increased. It was also observed that with the increase of temperature, the peak absorption wavelength of the absorption spectrum has been red-shifted. The peak wavelength shift was considered to be the result of energy level shifting accompanying the increase of temperature.

When the SnO_2 coating on the optical fiber probe was exposed to nitrogen gas samples containing 5% CH_4, optical absorption signal in the UV/Vis region only appeared when the temperature of the gas sample was increased to higher than 800 ^oC (Fig. 3.11.7). The observed absorption spectrum has a peak absorption wavelength very close to that caused by the exposure of the coated probe to a hydrogen-containing nitrogen gas sample. It was believed that the observed absorption signal is caused by hydrogen atoms which are generated from the decomposition of CH_4 at the high temperatures. When the SnO_2 coating on the optical fiber probe was exposed to nitrogen gas samples containing 5% CO, optical absorption signal in the UV/Vis region was not observed even the temperature of the gas sample was increased up to 800 ^oC.

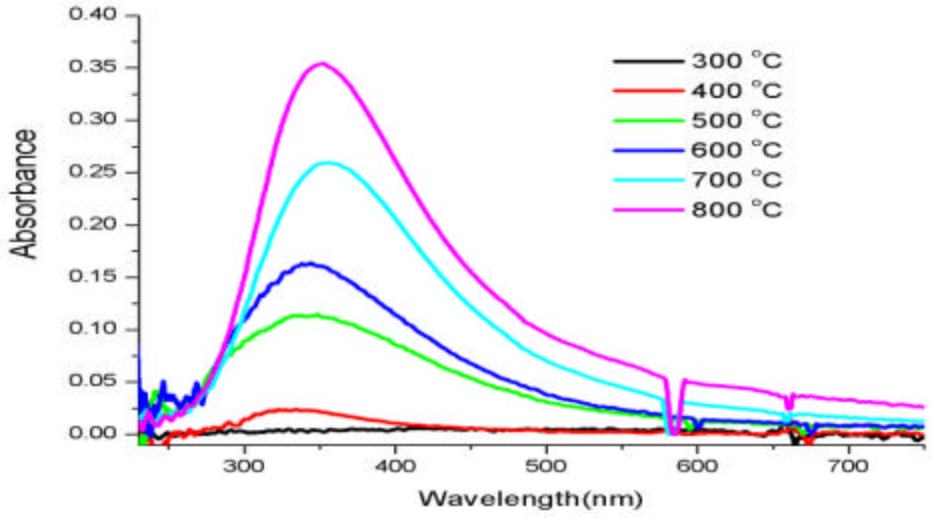

Fix. 3.11.7. UV-Vis absorption spectra of a SnO_2 thin film optical fiber sensor response to a 1vol% H_2-N_2 flow under different temperature.

E: Calibration of the SnO_2 coating on the optical fiber probe for quantitatively sensing H_2 in an inert gas sample

The evanescent wave absorption signal of the SnO_2 coating on the surface of the optical fiber probe in UV/Vis region has been evaluated for quantitatively sensing hydrogen concentration in a nitrogen gas sample. In this test, the 10 vol% hydrogen containing nitrogen gas sample was diluted with pure nitrogen by using the dynamic calibrator and the obtained gas samples was flowed through the quartz cell inside the split tube furnace. The temperature of the furnace was kept at 600 ^oC. The obtained absorption spectra of the probe exposed to nitrogen gas samples containing hydrogen of different concentrations are shown in Fig. 3.11.8. With the increase of hydrogen concentration in the gas sample, the absorption signal increased. The relationship of the

absorbance signal with the concentration of hydrogen in the nitrogen sample can be described by follow equation:

$$Abs. = 0.082Ln(C_{H2}) + 0.145 \qquad (3.11.1)$$

This calibration curve follows a Langmuir adsorption isotherm, which indicates the absorption signal is originated from the reaction of oxygen ions on the surface of the pores with hydrogen absorbed onto the walls of the porous structure in the coating.

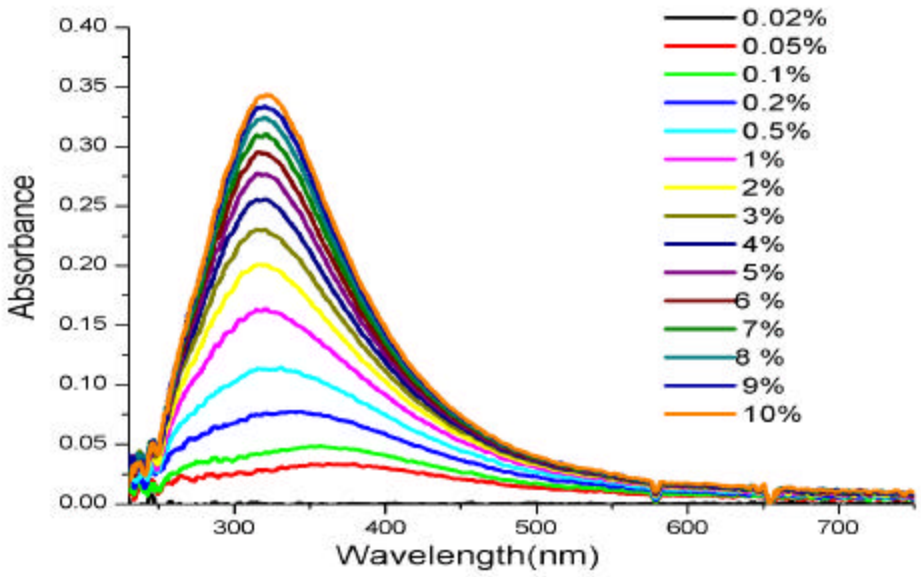

Fig. 3.11.8. UV-Vis absorption spectra of a SnO_2 thin film optical fiber sensor response to H_2-N_2 flows with different H_2 concentration at 600 °C.

F: Time response of the SnO_2 coated optical fiber probe to the change of hydrogen concentration in a gas sample

The time response of the SnO_2 coating on the bent optical fiber probe for sensing H_2 in a nitrogen gas sample was tested. In this test, the source gas sample was switched from pure N_2 to 1vol% H_2-N_2 mixture and the evanescent wave optical absorption signal of the SnO_2 coated bent optical fiber probe deployed inside the quartz gas flow cell was continuously monitored. The recorded result is presented in Fig. 3.11.9. As shown in Fig. 3.11.9, under the experimental conditions used in this study, the absorption signal reaches the steady-state signal intensity within 1 min. The volume of the quartz flow cell used n this work is 0.24 L. The flow rate of the gas sample is 1 L/min. The change of hydrogen concentration in the flow cell from zero (pure nitrogen) to 1% needs a time of around 1 minute under the experimental conditions used in this work. Therefore, it is believed that the response time of the SnO_2 coating for gas sensing should be within seconds.

The response time of this SnO_2 coating for sensing H_2 is faster compared with response time of some reported semiconductor metal oxide membrane based sensors [82].

It was believed that the capability of using a very thin SnO_2 coating in this work is responsible of this fast response of this sensing technique. In optical fiber evanescent wave absorption spectrometry, the penetrate depth of evanescent wave is comparable to the wavelength of the light guided through the fiber. Therefore, it is possible to using a coating with thickness in sub-micrometer as a sensing membrane.

When the sample gas was switched from 1 vol% H_2-N_2 to pure nitrogen, the optical absorption signal decreased with time. Figure 3.11.10 shows the recorded changes of the absorbance signal. It takes about 20 minutes for the absorption signal decreased to the baseline after the gas sample was switched to pure nitrogen. If the gas sample was switched to compressed air, the absorption signal decreased quickly (about 5 minutes) to the baseline. These results also suggest that the change of surface-adsorbed oxygen-ion concentration is responsible for the probe to sense H_2 gas.

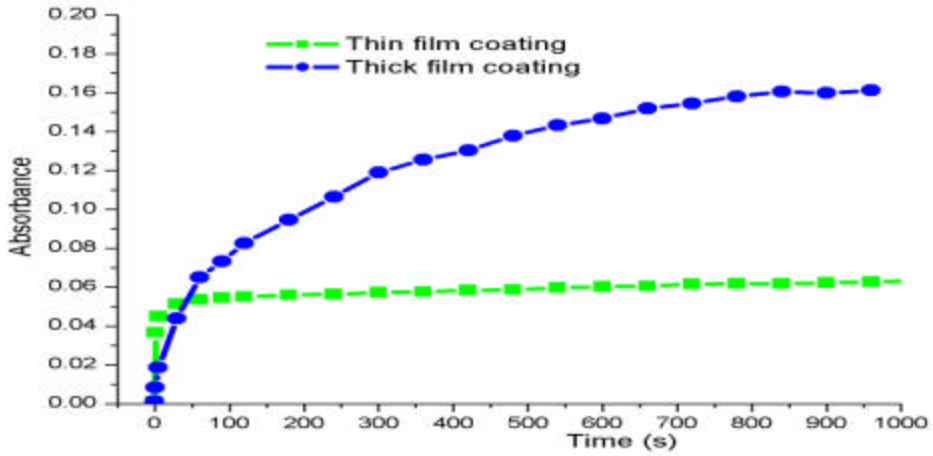

Fig. 3.11.9. Time response of the absorbance of a SnO_2 thin film optical fiber sensor to a 1 vol % H_2-N_2 flow at a wavelength of 320 nm under 600 °C.

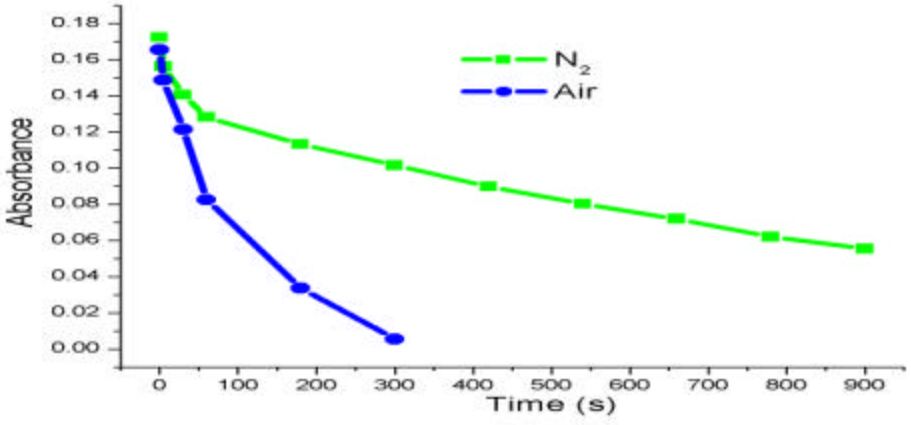

Fig. 3.11.10. UV-Vis absorption spectra of a SnO_2 thin film optical fiber sensor recovery response from 1 % vol H_2-N_2 flow to a (a) N_2 flow and (b) air flow at 600 °C.

G: Advantages of semiconductor metal oxide fiber optic spectrometric methods for reducing gas sensing

The advantages of the fiber optic sensing technique developed in this work include:

1. High sensitivity (ppm level detection).
2. Applicable for high temperature gas sensing (up to 900 ^{o}C).
3. Selective sensing (can selectively sensing H_2 in the existence of other reducing gases).
4. If a catalyst is incorporated into the porous material, it is possible to develop selective multi-gas components sensor.
5. Fast response (within seconds level).
6. Applicable for corrosive gas monitoring.
7. Immune to electromagnetic noise and avoided potential electric discharge ignited explosion.

4. Conclusion

The objective of this proposed project is developing OFCS for on-line, real time monitoring the concentration of gases in IGCC processes in order to control chemical reactions in IGCC. The proposed objectives of this project include:

1. Develop techniques for making sensing agent doped sol-gel materials.
2. Investigate the microstructure and optical properties of sol-gel derived materials.
3. Study the reaction of NH_3 with transitional metal ions doped in a PSOF at high temperature, and design a fiber optic sensor for monitoring NH_3 in IGCC process.
4. Design and test an optical fiber H_2S sensor using zinc ions doped sol-gel material as a transducer

During this reporting period, sol-gel techniques have been developed for preparing porous silica and semiconductor metal oxide materials. In addition, nanometer particles of noble metals have been prepared with micelle/reversed micelle techniques. Nanocrystalline semiconductor metal oxide materials have also been prepared with sol-gel techniques. Metal ions, metal oxides and nanocrystalline semiconductor metal oxides have been immobilized into porous silica matrials via doping a silica sol solution with metal salt solution or co-hydrolyzing a metal alkyloxide to obtain a mixed sol solution. Nanometer metal particles have been immobilized into porous silica through the combination of a sol-gel technique with micelle/reversed micelle techniques. One of our patented techniques has been employed for fabrication of porous silica fibers for designing fiber optic sensors.

The prepared materials have been investigated with electron microscopes. SEM has been employed to observe the microstructure and morphology of sol-gel derived porous silica materials, sol-gel derived semiconductor metal oxides, the coating of porous silica materials and semiconductor metal oxide on the surface of an optical fiber, and silica optical fibers. TEM has been employed to observe the microstructure and morphology of nanometer metal particles and measure the distribution of particle size.

The optical properties of the prepared porous materials have been investigated with fiber optic spectrometric methods. Active core fiber optic spectrometry has been employed to investigate the optical properties of sol-gel derived porous silica optical fibers. Fiber optic EW absorption spectrometry has been employed to investigate the optical properties of the porous materials as coatings on the surface of silica optical fibers. The optical absorption and fluorescence emission properties of these materials in the wavelength region from 200 nm to 2.1 μm have been investigated with the fiber optic spectrometric techniques. The optical properties of these materials have been investigated both at ambient temperature and high temperatures. These materials have been exposed to gas samples of different compositions at different temperatures, and the response of these materials to different gas composition at high temperature has been investigated.

Fiber optic sensor techniques have been developed based on the comprehension of the microstructure and optical properties of these materials exposed to gas samples of varied composition at different temperatures. Fiber optic temperature sensor techniques using sol-gel derived refractive thermochromic materials as transducers can be used for monitoring up to 100 oC in corrosive gas environment. Gas sensors developed in this project include a fiber optic ammonia sensor using silver nanometer particles immobilized porous silica material for monitoring trace ammonia at ambient temperature down to 61 ppb, a CuCl2 doped porous silica optical fiber sensor for monitoring trace

ammonia at high temperature down to 0.3 ppm, a CdO doped porous silica optical fiber sensor for monitoring trace hydrogen sulfide at high temperature down to sub-ppm level, and a SnO2 coating based fiber optic sensor for selectively monitoring hydrogen gas at high temperature down to ppm. All these sensors are reversible, can be used for continuous monitoring industrial processes. The sensors for high temperature gas sensing are corrosive resistant, applicable in high temperature corrosive gas environment encountered in IGCC processes.

From the accomplishment of this project, it is clear that the proposed goal of this project has been achieved during this reporting period. In addition to the original goal, sensing techniques for temperature monitoring in corrosive gas environment and a selective hydrogen gas sensing technique has also been developed in this project. Moreover, based on the foundation knowledge built up in this project, sensor technologies for monitoring other gas components exist in coal-derived syngas can be developed. For example, the sensor technique based on sol-gel derived nanocrystalline semiconductor metal oxide material can be developed for sensing other reducing gases to monitor syngas cleaning processes. Further, the fiber optic spectrometric techniques developed in this project are also useful in investigating the catalyzed high temperature chemical reactions used syngas reforming and cleaning.

5. Publication of papers supported by this project

1. S. Tao, "Fiber optic sensors using sol-gel derived nanomaterials for gas sensing" in "Optical Fibers Research Advances", F. Columbus, ed., Nova Science Publishers, Inc., in press.
2. Q. Yan and S. Tao, "Optical fiber evanescent wave spectrometry of a nanocrystaline tin oxide thin film for selective hydrogen sensing in high temperature gas samples", in preparation for publication on J. Am. Chem Soc..
3. S. Tao and T.V.S. Sarma, "High sensitivity gas sensor using photonic crystal fiber", in preparation for publication on Opt. Lett.
4. T. V. S. Sarma and S. Tao, "An active core fiber optic sensor for detecting trace H_2S at high temperature using a cadmium oxide doped porous silica optical fiber as a transducer", submitted to Sens. & Actuators, B: Chem., for publication
5. Shiquan Tao, Joseph C. Fanguy and T. V. S. Sarma, **"**An optical fiber chemical sensor for monitoring trace ammonia in high temperature gas samples with a $CuCl_2$-doped porous silica optical fiber as a transducer", Submitted to Analyst for publication.
6. H. Guo and S. Tao, "An active core fiber optic temperature sensor using an Eu(III) doped sol-gel silica fiber as a temperature indicator", *IEEE Sensor Letters*, in press.
7. H. Guo and S. Tao, "Sol-gel synthesis of palladium doped silica nanocomposite fiber using Triton X-100 micelle template and the application for hydrogen gas sensing", *IEEE Sensor Journal*, in press.
8. H. Guo and S. Tao, "Silver nanoparticles doped silicate nanocomposites coated on an optical fiber for ammonia sensing", *Sens. & Actuators, B: Chem*., in press.
9. S. Tao and A. Jayaprakash, "A fiber optic temperature sensor with an epoxy-glue membrane as a temperature indicator", *Sens & Actuators, B: Chem*., **B119**, 615 (2006).
10. S. Tao, X. Hu and Q. Yang, "A fiber optic sensor for in situ real-time monitoring H2O2 in a PEM fuel cell during fuel cell operation", *Proceedings of 22nd International Pittsburgh Coal Conference*, 178/1-178/14, Sept. 12-14, 2005, Pittsburgh.
11. J. Fanguy and S. Tao, "A highly sensitive sol-gel silica optical fiber sensor for monitoring of trace ammonia in high temperature gas samples", *Proceedings of 22nd International Pittsburgh Coal Conference*, 208/1-208/18, Sept. 12-14, 2005, Pittsburgh.
12. S. Tao, J. C. Fanguy, X. Hu and Q. Yan, "Fiber optic sensors for in situ, real time monitoring PEM fuel cell operation", *Proceedings of Third International Conference on Fuel Cell Science, Engineering and Technology*, 231-234, Ypsilanti, MI, May 23-25, 2005 (2005).

Reference

1. S. Tao, C. B. Winstead, J. P. Singh and R. Jindal, *Opt. Lett.*, **27**, 1382 (2002).
2. S. Tao, C. B. Winstead, R. Jindal and J. P. Singh, *IEEE Sensors Journal*, **4**, 322 (2004).
3. S. Tao, C. B. Winstead, H. Xian and S. Krunal, *J. Environ. Monitor*. **4**, 815 (2002).
4. S. Tao, S-F, Gong, L. Xu and J. C. Fanguy, *Analyst*, **129**, 342 (2004).
5. S. Tao, "Fiber optic chemical sensors for environmental monitoring", in "Encyclopedia of Sensors", C. A. Grimes, E. C. Dickey and M. V. Pishko, eds., **Vol. 3**, 467, American Scientific Publishers, Stevenson Ranch, CA, 2006.
6. W. R. Seitz, *Anal. Chem*., **56**, 16A (1984).
7. K. T. V. Gatan and B. T. Meggitt, eds., "Optical fiber sensor technology, volume 4: chemical and environmental sensing", Kluwer Academic Publishers, Dordrecht, The Netherlands, (1999).
8. B. J. Scott, G. Wirnsberger and G. D. Stucky, *Chem. Mater*., **13**, 3140 (2001).
9. L. L. Hench and J. K. West, *Chem. Rev*., **90**, 33 (1990).
10. T. J. Barton, et al., Chem. Mater., 11, 2633 (1999).
11. C. J. Brinker and G. W. Scherer, eds., "Sol-Gel Science: The Physics and Chemistry of Sol-Gel Processing", Academic Press, Inc., New York, 1990.
12. L. M. Liz-Marzan, M. Giersig and P. Mulvaney, *Langmuir*, **12**, 4329 (1996).
13. T. Li, J. Moon, A. A. Morrone, J. J. Mecholsky, D. R. Talham and J. H. Adair, *Langmuir*, **15**, 4328 (1999).
14. D-S. Bae, K-S. Han and J. H. Adair, *J. Mater. Chem*., **10**, 1039 (2002).
15. I. Lisiecki, *J. Phys. Chem. B*, **109**, 12231 (2005).
16. Y. C. Kim, S. Banerji, J. F. Masson, W. Peng and K. S. Booksh, *Analyst*, **130**, 838-843 (2005).
17. Zhang, F. Phillipp, G. W. Meng, L. D. Zhang and C. H. Ye, *J. Appl. Phys*., **88**, 2169 (2000).
18. Y. Posada, L. F. Vallejo, L. San Miguel, O. Resto and I. Balberg, *J. Appl. Phys*., **99**, 114313/1 (2006).
19. G. Di Francia, M. Della Noce, V. La Ferrara, L. Lancellotti, P. Morvillo and L. Quercia, *Mater. Sci. Tech*., **18**, 767 (2002).
20. X. Zhang, C. Cheng, H. Guo, W. Huang, T. Polenova, L. C. Francesconi, D. L. Akins, "Optical spectra of a novel polyoxometalate occluded within modified MCM-41," *J. Phys. Chem. B*, **109**, 19156 (2005).
21. W. Fulkerson, R. R. Judkins and M. K. Sanghvi, *Science American*, Sept., 1990, 129.
22. M. M. Joshi and S. Lee, *Energy Sources*, **18**, 537 (1996).
23. T. D. McGee, (Ed.), "Principles and Methods of Temperature Measurement", John Wiley & Sons, New York, 1988.
24. P. R. N. Childs, (Ed.), "Practical Temperature Measurement", Butterworth-Heinemann, Oxford, 2002.
25. J. Jung, H. Nam, B. Lee, J. O. Byun and N. S. Kim, *Appl. Opt*., **38**, 2752 (1999).
26. X. C. Li, F. Prinz and J. Seim, *Smart Mater. Struct*., **10**, 575 (2001).
27. S. C. Kaddu, S. F. Collins and D. J. Booth, *Meas. Sci. Technol*., **10**, 416 (1999).

28. M. Ling and H. Li, *Sens. & Actuators, B; Chem*., **B12**, 53 (1993),
29. S. A. Wade, S. F. Collins and G. W. Baxter, *Appl. Phys. Rev*., **94**, 4743 (2003).
30. S. W. Allison and G. T. Gillies, *Rev. Sci. Instruments*, **68**, 2615 (1997).
31. W. H. Fonger and C. W. Struck, *J. Chem. Phys*., **52**, 6364 (1970).
32. T. Sun, Z. Y. Zhang, K. T. V. Grattan, A. W. Palmer and S. C. Collins, *Rev. Sci. Instrum*., **68**, 3442 (1997).
33. S. Tao and A. Jayaprakash, *Sens. & Actuators, B: Chem*., **B119**, 615 (2006).
34. "Fuel Cell Handbook", 6th edition, EG&G Technical Services, Inc., 2002, p.169.
35. J. E. Roehl, *Appl. Spectrosc. Rev*., **26**, 1 (1991).
36. R. D. Sacks, M. L. Nowak and H. L. Smith, *Proceedings of the Annual ISA Analysis Division Symposium*, **29**, 133 (1996).
37. Z. Wang, J. Wang, H. Richter, J. B. Howard, J. Carson and Y. A. Yiannis, *Energy & Fuels*, **17**, 999 (2003).
38. M. E. Webber, D. S. Baer and R. K. Hanson, *Appl. Opt*., **40**, 2031 (2001).
39. A. Schmohl, A. Miklos, P. Hess, *Appl. Opt*., **41**, 1815 (2002).
40. J. A. Neuman, T. B. Ryerson, L. G. Huey, R. Jakoubek, J. B. Nowak, C. Simons and F. C. Fehsenfeld, *Environ. Sci. and Technol*., **37**, 2975 (2003).
41. O. Spector and E. Jacobson, *Proceedings of SPIE*., vol. **3853**, 233 (1999).
42. J. Shi, R-X. Yan, Y-F. Zhu and X-R. Zhang, *Talanta*, **61**, 157 (2003).
43. K. Sakai, M. Sakada and Y. Takata, "*Instrumental Environmental Analysis*", 5th edn., Maruzen Publisher, Tokyo, 1995.
44. S. Tao, J. C. Fanguy and L. Xu, *Sens. & Actiators B: Chem*., **B115**, 158 (2006).
45. H. Guo and S. Tao, *Sens. & Actiators B: Chem*., in press.
46. C. G. Enke, eds., *The Art & Science of Analytical Chemistry*, 2nd edn., John Wiley & Sons, Inc., 2000.
47. K. L. Cheng, *Anal. Chem*., **34**, (1392) 1962.
48. R. C. Weast, M. J. Astle and W. H. Beyer, ed., *CRC Handbook of Chemistry and Physics*, 65th edn., CRC Press, Inc., Boca Raton, FL, 1984.
49. S. Tao and T. Kumamaru, *Anal. Proc*., **32**, 371 (1995).
50. S. Tao and T. Kumamaru, Appl. Spectrosc., **50**, 785 (1996).
51. S. Tao and T. Kumamaru, *J. Anal. At. Spectrom*., **11**, 111 (1996).
52. L. Xu, J. C. Fanguy, K. Soni and S. Tao, *Opt. Lett*., **29**, 1191 (2004).
53. S. Bharathi, N. Fishelson, O. Lev, *Langmuir*, **15**, 1929 (1999).
54. R. W. Steven, T. H. Gardner, D. Shekhawat, D. A. Berry and A. D. Freed, *Proceedings of Annual Intern. Pittsburgh Coal Conference*, 22nd, 247/1-247/9 (2005).
55. R. Ben-Slimane and M. T. Hepworth, *Energy & Fuels*, **8**, 1175 (1994).
56. A. Safavi, B. Haghighi and F. Peiravian, *Anal. Lett*., **36**, 479 (2003).
57. E. S. Larsen, W. W. Hong and M. L. Spartz, *Appl. Spectrosc*., **51**, 1656 (1997).
58. R. L. Benner and D. H. Stedman, *Anal. Chem*., **61**, 1268 (1989).
59. H. Tang, P. Heaton, B. Brassard and J. Dunbar, *American Laboratory*, **29**, 26 (1997).
60. C. Wang, X. Chu and M. Wu, *Sens. Actuators, B: Chem*., **B113**, 320 (2006).
61. M. Ando, S. Suto, T. Suzuki, T. Tsuchida, C. Nakayama, N. Miura and N. Yamazoe, *Chem. Lett*., **2**, 335 (1994).
62. Y. Chun, S. Zhao, P. Wei and J. Lu, *Sens. Actuators, B: Chem*., **14**, 519 (1993).

63. J. Abbasian and R. B. Slimane, *Ind. Eng. Chem. Res*., **37**, 2775 (1998).
64. K. C. Kwon, E. R. Crowe and S. K. Gangwal, *Sep. Sci. Tech*., **32**, 775 (1997).
65. T. Fujii, N. Tanaka, H. Tai, S. Obara and A. B. Ellis, *Bull. Chem. Soc. Jpn*., **73**, 809 (2000).
66. G. C. Lisensky, G. J. Meyer and A. B. Ellis, *Anal. Chem*., **66**, 2531 (1988).
67. G. Di Francia, M. Della Noce, V. La Ferrara, L. Lancellotti, P. Morvillo and L. Quercia, *Mater. Sci. Tech*., **18**, 767 (2002).
68. S. Ashutosh and O. S. Wolfbeis, *Proceedings of SPIE, The international Society for Optical Engineering*, **990**, 116 (1988).
69. W. H. Brattain and J. Bardeen, *Bell System Tech. J.*, **32**, 1 (1953).
70. N. Taguchi, "Gas detection device", British Patent# 1280809, 1970.
71. G. Korotcenkov, *Sens & Actuators, B: Chem*., **B107**, 209 (2005).
72. F. Reti, G. Kiss and I. V. Perczel, *Sens & Mater*., **16**, 53 (2004).
73. O. K. Varghese and C. A. Grimes, *J. Nanosci. Nanotech*., **3**, 277 (2003).
74. Y. Matsuura, *Chem. Sens*., **17**, 42 (2001).
75. H. Meixner, J. Gerblinger, U. Lampe and M. Fleischer, *Sens. & Actuators, B: Chem.*, **B23**, 119 (1995).
76. M. Ivanovskaya and P. Bogdanov, *Sens. & Actuators, B: Chem*., **B77**, 264 (2001).
77. C. Wang, X. Wang, B. Xu, J. Zhao, B. Mai, P. Peng, G. Sheng and J. Fu, *J. Photochem. Photobiology A: Chem.*, **168**, 47 (2004).
78. M. Okuya, K. Shiozaki, N. Horikawa, T. Kosugi, G. R. A. Kumara, J. Madarasz, S. Kaneko and G. Pokol, *Solid State Ionics*, **172**, 527 (2004).
79. M. Bhagwat, P. Shah and V. Ramaswamy, *Mater. Lett*., **57**, 1604 (2003).
80. A. Chiorino, G. Ghiotti, F. Prinetto, M. C. Carotta, G. Martinelli and M. Merli, *Sens. & Actuators, B: Chem*., **B44**, 474 (1997).
81. G. Ghiotti, A. Chiorino, W. Pan and L. Marchese, *Sens. & Actuators, B: Chem*., **B7**, 691 (1992).
82. D. P. Mann, T. Paraskeva, K. F. E. Pratt, I. P. Parkin and D. E. Williams, *Meas. Sci. Technol*, **16**, 1193 (2005).